運輸省港湾技術研究所

港湾技術研究所報告

REPORT OF THE PORT AND HARBOUR RESEARCH INSTITUTE

MINISTRY OF TRANSPORT

VOL. 25 NO. 3 SEPT. 1986

NAGASE, YOKOSUKA, JAPAN

港湾技術研究所報告 (REPORT OF P.H.R.I.)

第25巻　第3号 (Vol. 25, No. 3), 1986年9月 (Sept. 1986)

目　　次 (CONTENTS)

REPORT OF THE PORT AND
HARBOUR RESEARCH INSTITUTE
Vol. 25, No. 3 (Sept. 1986)

1. Strength and Deformation of Beam-to-Column Joints for Offshore Concrete Structures

Osamu KIYOMIYA*
Hiroshi YOKOTA**
Toshiyuki YOKOI***

Synopsis

Prestressed precast concrete members are being introduced to offshore structures. When they are assembled on the fabrication yard or the construction site to form an overall structure, the joints among precast members are introduced in the structure. For land concrete structures such as buildings and bridges, many connecting methods have been proposed. However, the connecting methods proposed for the offshore structures are not so many as those for land ones.

The concrete members and joints in the offshore structures are subjected to strong wave forces repeatedly in horizontal and vertical directions and are exposed to severe corrosive environments. Some connecting methods for the land structures cannot be applied to the offshore structures in viewpoint of the force properties and the corrosion of steel bars.

Five kinds of the joints between a beam and a column which have the possibility of the application to the offshore structures are selected. These joints are the monolithic joint, the cast-in-place concrete joint, the adhesive joint, the haunch joint, and the insertion joint. Static loading tests on the specimens were carried out to study their strength and crack properties. The structural design calculations by the limit state design methods (JSCE in 1983 and CEB-FIP in 1978) were made and compared with the test results to examine the applicability of the design methods to offshore structures.

This report describes the results of the loading test and the comparison of the experimental results with the calculated ones obtained by the limit state design method. The following main results were obtained by this study:

1) The flexural collapse was dominant in each specimen. The ultimate strengths of the cast-in-place concrete joint, the haunch joint, and the insertion joint were almost the same as that of the monolithic joint. The ultimate strength of the adhesive joint was considerably lower than those of the others.
2) In all the specimens, flexural cracks appeared at the joints due to the loading. However, crack patterns differed among the specimens. The maximum crack width in the adhesive joint was larger than those in the other joints at a certain loading stage. The application of the adhesive joint to the offshore structures needs careful consideration on durability of materials such as concrete and steel.
3) As to the ultimate strength and the crack width, the formulae presented in the limit state design method gave the safe side values for the five kinds of the joint.

* Chief of Subaqueous Tunnels and Pipelines Laboratory, Structures Division
** Senior Research Engineer, Structures Division
*** Director, Structures Division

港湾技術研究所報告
第25巻第3号(1986. 9)

1. 海洋構造物におけるコンクリート柱・はり接合部の耐力・変形性状

清宮　理*・横田　弘**・横井　聡之***

要　旨

海洋空間あるいは海洋資源を有効に利用するため各種の海洋構造物の建設が積極的に計画・実施されている。海洋環境下での施工の迅速性，容易性，建設費の低減等の観点から，陸上で製作したプレキャスト部材を現地で接合して海洋構造物を建設する工法の採用が考えられる。プレキャスト部材を用いた構造物は，部材同志の接合部が存在する。海洋環境下で強大な波浪外力を繰り返し受け，かつ鉄筋等の鋼材の腐食の発生・進行にとり非常に厳しい条件下に建設されるコンクリート製海洋構造物では，接合方法の選定には十分に注意を払う必要がある。

本研究は，海洋環境下で採用可能な柱・はり接合方法を構造力学的に調べ，かつ限界状態設計法（土木学会・限界状態設計法指針（案）に示される終局耐力の提案式及び CEB-FIP・Model Code（1978年）に示されるひびわれ幅に関する提案式）の接合部への適用性を調べるために実施したものである。研究の対象とした柱・はり接合方法の種類は，一体接合構造，場所打ち接合構造，接着剤接合構造，ハンチ接合構造及び差込み接合構造の5種類である。これらの接合構造を対象に供試体を16体製作し，静的載荷実験を実施した。実験では，供試体を逆T字型に固定し，柱部材の上端に油圧ジャッキを用いて水平方向に載荷した。

本報告では，これらの実験結果及び接合構造の力学性状について述べた。また，前述の設計法での計算値と実験結果との比較・検討を行った。

本報告での主要な結論は，以下のとおりである。

① 載荷実験では，各接合構造とも曲げ破壊が卓越した。終局耐力に関して，接着剤接合構造を除く各接合構造間では，大きな差はなかった。接着剤接合構造の終局耐力は，他の構造よりも小さい値であった。

② ひびわれは，いずれの接合構造でも曲げひびわれが卓越したが，終局に至るまでのひびわれの進展過程は，各接合構造間で異なっていた。

③ 終局耐力及びひびわれ幅に関して，今回のいずれの供試体でも，前述の限界状態設計法に示される式による計算値よりも実験値のほうが小さいか，ほぼ同程度であった。

* 構造部　沈埋構造研究室長
** 構造部　主任研究官（複合構造担当）
*** 構造部長

CONTENTS

1. Introduction

Many types of offshore structures made of reinforced or prestressed concrete have been constructed in order to utilize the offshore space and exploit natural resources in the offshore regions. Offshore concrete platforms, sea walls of man-made islands, and breakwaters can be cited as examples. In constructing the concrete structures in the offshore regions, execution work is performed under severe marine environments such as waves, winds, and tidal currents. Therefore, rapid and reliable execution work is demanded at the construction site in the offshore regions. To cope with the demand, the prefabrication method is one of the most effective and practical methods. Structural members are manufactured at factories or yards on the land, and then they are put together. In such structures, there exist the joints among members.

The concrete members and the joints in offshore structures are subjected to strong wave forces due to storms repeatedly, and are exposed to severe environments that can cause corrosion to embedded steel bars and deterioration to concrete. Some kinds of joints in the land structures such as buildings and bridges may not be applied to the offshore structures because natural environments in the offshore are much severer than those on the land. Therefore, the joints in the offshore structures must be judged their adequacy, and the procedure to design these joints must be examined and established.

There are many kinds of joints as to types of connected members; beam-to-column, wall-to-wall, floor-to-wall, etc. In this study, the joint between a beam and a column was taken up. Five kinds of the joints which were considered to be applicable to the offshore structures were selected. Static loading tests were carried out on the specimens to clarify their mechanical properties: ultimate strength, crack formation and so on. The calculation of the ultimate strength and the crack width was also carried out by the limit state design method to clarify the applicability of the design method to the joints in the offshore structures. Then the calculated results were compared with the test results.

The research program on the joint in offshore structures consists of the following three work: the static strength and crack formations of the joints when flexure forces are applied, the fatigue strength, and the strength of the joints when both flexure and axial forces are applied simultaneously. This paper describes only the results of the first work, that is, the mechanical behaviors of the joints under the static loads. The authors are carrying out the fatigue loading tests and the two-directional loading tests. The results of those tests will be published in the near future.

2. Outline of Joints

2.1 Joints in Land Structures

A joint connects structural members such as beams, columns, walls, and floors each other. The joint is one on the most important parts in land structures such as buildings and bridges made of concrete members. Many kinds of connecting methods have been proposed and used particularly in buildings [1]. The examples of the joints used in buildings are shown in Fig. 1. The joints are divided into four categories in respect to the connecting methods as follows:

(a) Cast-in-place concrete joints

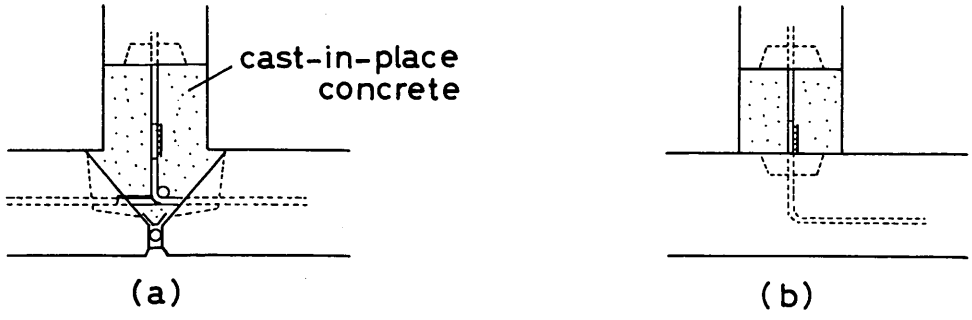

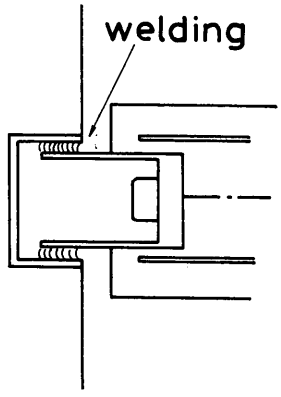

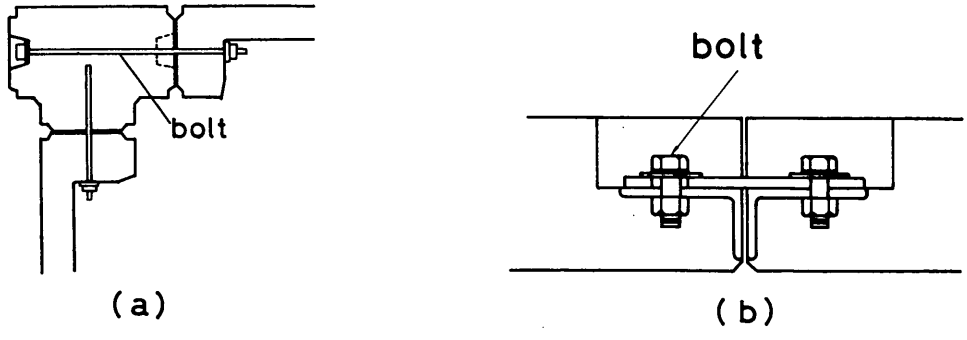

Fig. 1 Examples of joints [2, 3]

(b) Welded joints
(c) Mechanical joints
(d) Monolithic joints

The cast-in-place concrete joints are called wet joints. Members are connected at the cast-in-place concrete region where bars are jutted out and spliced. As for the welded joints, members are connected by welding of steels as the joint part. As for the mechanical joints, members are connected by bolts or other mechanical ties. The welded joint and the mechanical joint are called collectively the dry joint. The monolithic joints are made by casting of concrete into connected members at the same time without any connecting devices from (a) to (c) as mentioned above. Taking the following items into account, these joints in land structures must be designed:

(a) Dimension and purposes of structures
(b) Properties and kinds of forces which should be transmitted through the joint.
(c) The accuracy of precast concrete members
(d) Work at the site: availability of construction machines, natural conditions, construction periods, and so on

2.2 Joints in Offshore Structures

The following fundamental items should be considered in designing joints in offshore structures:

(a) Strength and deformation of the joint
(b) Crack formation and crack width at the joint
(c) Corrosion of embedded bars and steel
(d) Deterioration of concrete
(e) Fatigue properties of the joints for wave forces
(f) Execution methods of the joints
(g) Details of the bar arrangement and the haunch

To know the crack formation is important in offshore structures. Excessive cracks do great damage to the structures. For example, the corrosion of reinforcing bars, the degradation of concrete surfaces, and the degradation of the watertightness are associated with the formation of cracks. Thus, in the examination of the serviceability limit state, it is required to calculate crack width which is a function of the induced bar stress due to the permanent load, the concrete cover, and so on, and therefore, the crack width should be smaller than the allowable value.

In offshore structure, the three exposure conditions are considered, that is, the atmospheric zone, the splash zone, and the submerged zone [4]. In "Technical Standard for Port and Harbour Facilities in Japan (1980)" [5], the minimum concrete covers for embedded reinforcement are specified as 7 cm in cases of directly contact with sea water, being washed by sea water, and exposed to severe sea wind, and as 5 cm in other cases. The concrete cover is related to the crack width at the concrete surface. The above values of the concrete cover are set to restrict the crack width below 0.2 mm in the splash zone.

2.3 Selected Connecting Methods

Five types of joints were selected in this study, which could be classified into the cast-in-place concrete joint and the mechanical joint described in **2.1.** The welded joint was not selected in this study because the welding work is considered to be very difficult at the site in the offshore regions. The selected joints are shown in Fig. 2.

(a) Monolithic joint

The joint in the monolithic structure is formed at the intersectiom of a beam and a column. Both members are reinforced by steel bars monolithically, then concrete is

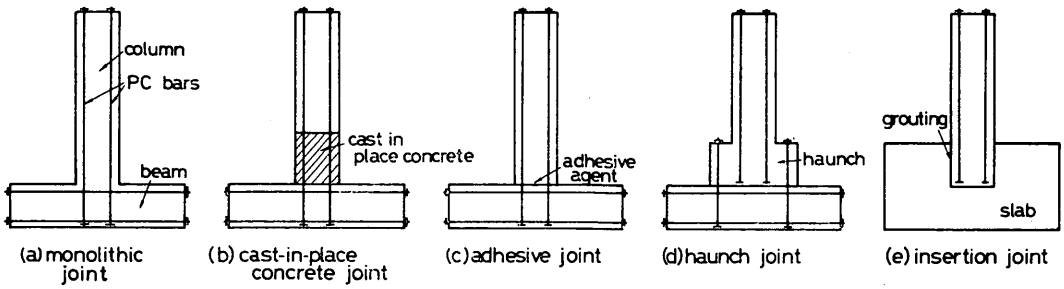

Fig. 2 Outline of connecting methods

cast at the same time.

(b) Cast-in-place concrete joint

This joint connects precast concrete members by means of cast-in-place concrete and splice joints of reinforcing bars. Reinforcing bars jutted out from the precast members are spliced to satisfy the specified lap length. Afterwards, concrete is cast between the precast members. The shrinkage compensating concrete is normally used at the joint region.

(c) Adhesive joint

The two precast members are connected by the adhesive agent at the intersection and prestressing tendons. The peculiarity of this joint is that no reinforcing bars pass through the intersection of members. The cohesive forces of the agent transmit the induced forces without reinforcing bars. Moreover, the adhesive agent is also expected to provide watertightness at the joint.

(d) Haunch joint

The end of the column which is to be connected to another member is widened to form the haunch where PC tendons will be located. Prestressing forces are applied for connecting precast members. The adhesive agent is additionally applied at the joint face so as to make the strength higher and to provide the watertightness.

(e) Insertion joint

This joint is often seen as the slab-to-column joint rather than the beam-to-column joint. The column is inserted into the hole of the slab or the square notch of the beam. The void of the two members is filled with shrinkage compensating cement paste or mortar.

These five types of joints can be applied to reinforced and/or prestressed concrete offshore structures. In the prestressed concrete structures in the marine environment, the bonded prestressing members have generally been adopted. The unbonded members are not generally used there because of the corrosion of prestressing tendons, etc. In the future, the unbonded members, however, will be used in upper part of the offshore structures above sea level when the protection method for the tendon from corrosion is established.

3. Description of Experimental Work

3.1 Test Specimen

Sixteen test specimens were manufactured corresponding to the five types of joint as shown in Fig. 2. Each specimen consisted of a column and a beam (in case of a

slab). The intersection of the two members will be referred as a joint region. Each specimen had its own unique joint and the arrangement of reinforcement.

The column was 30 cm in width, 30 cm in thickness, and 140 cm in height. The beam was 30 cm in width, 50 cm in thickness, and 200 cm in length. Each specimen has a designation code like "M-R-16." The first letter stands for the connecting methods adopted, that is, M for the monolithic joint, C for the cast-in-place joint. A for the adhesive joint, H for the haunch joint, and I for the insertion joint. The second letter stands for reinforced (R) or prestressed (PB or PU) concrete members. PB stands for the bonded PC member and PU stands for the unbonded PC member. The numerical number in the last represents the reinforcement ratio of the column, that is, 16 and 23 stand for 0.16% and 0.23%, respectively. Specifications of all the specimens are summarized in Table 1. The details of bar arrangements of M-PU and M-PB are

Table 1 Specifications of the column in the specimens

specimen	$b \times h$ (cm)	reinforcement	reinforcement ratio (%)	PC bar	spacing *2) of hoop (cm)	hoop reinforcement ratio (%)	σ_{pe} (kgf/cm^2)	f'_{cd} (kgf/cm^2)
M- R -16	30×30	4-D10	0.16	—	5	0.42	—	240
M- R -32	30×30	12-D10	0.32	—	5	0.42	—	240
M-P U-16	30×30	4-D10	0.16	2-ϕ17	15	0.40	20	350
M-P U-32	30×30	12-D10	0.32	2-ϕ23	15	0.14	40	350
M-P B-16	30×30	4-D10	0.16	2-ϕ17	15	0.14	20	350
M-P B-32	30×30	12-D10	0.32	2-ϕ23	15	0.14	40	350
C- R -16	30×30	4-D10	0.16	—	5	0.42	—	240
C- R -32	30×30	12-D10	0.32	—	5	0.42	—	240
C-P B-16	30×30	4-D10	0.16	2-ϕ17	15*3) 12	0.14 0.17	20	350
C-P B-32	30×30	12-D10	0.32	2-ϕ23	15*3) 12	0.14 0.17	40	350
A-P B-16	30×30	4-D10	0.16*1)	2-ϕ17	15	0.14	20	350
A-P B-32	30×30	12-D10	0.32*1)	2-ϕ23	15	0.14	40	350
H-P B-16*4)	30×30	4-D10	0.16	2-ϕ17	15	0.14	20	350
	60×30	4-D10	0.16*1)	2-ϕ17 2-ϕ23	15	0.14	20	350
H-P B-32*4)	30×30	12-D10	0.32	2-ϕ23	15	0.14	40	350
	60×30	12-D10	0.32*1)	2-ϕ23 2-ϕ32	15	0.14	40	350
I-P B-16	30×30	4-D10	0.16	2-ϕ17	15	0.14	20	350
I-P B-32	30×30	12-D10	0.32	2-ϕ23	15	0.14	40	350

*1) Reinforcement ratio was zero at the joint face.
*2) The diameter of the hoop was 6mm.
*3) The lower value was that in the cast-in-place region.
*4) The lower line shows those of the haunch.

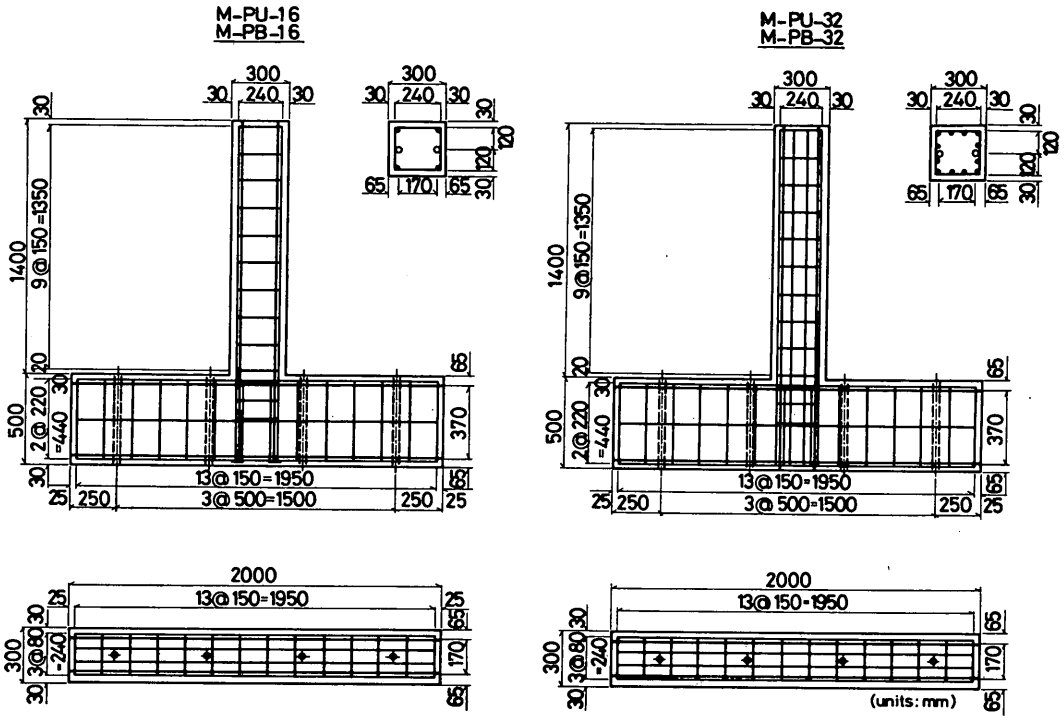

Fig. 3 Details of the specimens (M-PU and M-PB)

shown in Fig. 3. Those of the other specimens are presented in **Appendix A.**

The specimens designated as M-R were the monolithic reinforced concrete ones. Concrete was cast into the beam and the column at the same time. M-PB and M-PU were monolithic prestressed concrete specimens. Two prestressing bars were inserted into sheaths arranged through the joint face. Prestressing forces were introduced by a jack at the age of about one week. For the bonded PC specimens, each prestressing bar was bonded to its surrounding concrete by grouting into the void between a prestressing bar and its sheath. On the other hand, for the unbonded ones, the grouting was not performed. In C-R and C-PB, the beam and the column were connected with cast-in-place concrete. Reinforcing bars jutted out from the precast column and the precast beam were spliced. The lap length of reinforcing bars was approximately 25 cm. The joint region, the cast-in-place region in this case, was 30 cm in height from the intersection of both members. In A-PB, the beam and the column were connected with adhesive agents. Furthermore, prestressing forces were introduced to connect both members tightly. H-PB had a haunch which made the area of the joint faces larger. The adhesive agent was also applied at the joint surface. The haunch was 30 cm in width, 60 cm in thickness, and 30 cm in height. I-PB had the insertion joint. This joint was formed by inserting the column into the slab, and then by filling the space between the two members with expansive cement paste. The slab was 90 cm in width, 150 cm in length, and 80 cm in thickness.

3.2 Material Properties

The materials used for concrete were as follows:

(a) Cement

High early strength portland cement conformed to JIS R 5210 was used. Table 2 gives the physical and chemical properties of the cement.

Table 2 Properties of the cement

specific gravity	fineness		setting			soundness
	Blaine (cm^2/g)	88μm residual (%)	water (%)	initial (h-min)	final (h-min)	
3.12	4210	0.2	29.9	2-04	3-10	good

flow	flexural strength (kgf/cm^2)				compressive strength (kgf/cm^2)			
	1 day	3 days	7 days	28 days	1 day	3 days	7 days	28 days
246	35	51	67	81	129	250	347	471

chemical composition (%)								
ig. loss	insol.	SiO_2	Al_2O_3	Fe_2O_3	CaO	MgO	SO_3	total
1.0	0.1	21.0	5.0	2.7	65.8	1.4	2.6	99.6

(b) Aggregate

Crashed stone and sand produced at Hachioji located west of Tokyo was used. The maximum size of the aggregate was set at 10 mm because of the dimension of the specimen and the congested reinforcement. Table 3 gives the properties of the aggregate.

Table 3 Properties of the aggregate

	specific gravity	bulk density (kg/m^3)	finess modulus	absorption (%)	88μm sieve test (%)	soundness (%)
coarse	2.66	—	—	0.81	—	—
fine	2.16	1712	3.12	1.54	3.15	0.5

(c) Admixture

The air entraining and water reducing agent was used. Its quantity was 0.25% of the weight of cement. The expansive admixture was additionally used for shrinkage compensating concrete which was cast into the joint region in the cast-in-place concrete joint. Its weight per unit volume of concrete was 60 kgf/m^3.

The qualities of reinforcing and prestressing bars embedded in the specimens are as follows:

(a) Reinforcing bar

Steel reinforcing bars conformed to JIS D 3112 SD 35 were used. The diameter

Table 4 Mechanical properties of reinforcing bars

diameter (mm)	surface type	yield strength (kgf/cm^2)	tensile strength (kgf/cm^2)	elongation (%)
6	deformed	3750	5420	26.3
10	deformed	3920	5560	23.2
13	deformed	3750	5560	23.5

was 10 mm for the column reinforcement, 13 mm for the beam reinforcement, and 6 mm for the hoop reinforcement and for others. Their mechanical properties are presented in Table 4.

(b) Prestressing bar

Prestressing bars conformed to JIS G 3109 Type A-1 (SBPR 85/95) were used for the PC specimens. The prestressing bars of 17 mm in diameter were arranged in the column with the lower reinforcement ratio (0.16%). Those of 23 mm in diameter were arranged there with the higher reinforcement ratio (0.32%). In the haunch region, those of 23 mm (for H-PB-16) and 32 mm (for H-PB-32) in diameter were used to connect both members. Moreover, those of 23 mm in diameter were arranged in the beam. Table 5 gives mechanical properties of each prestressing bar.

The adhesive agent (epoxy resin) was applied to the joint faces of the adhesive joint specimens and the haunch joint specimens.

Table 5 Mechanical properties of prestressing bars

diameter (mm)	surface type	specimen *1)	yield strength (kgf/cm^2)	tensile strength (kgf/cm^2)	modulus of elasticity ($\times 10^6 kgf/cm^2$)	elongation (%)
17	round	M, C, A, H, I-PB-16	9100	10000	2.04	11
17	round	M-PU-16	9100	10000	2.03	11
23	round	M, C, A, H, I-PB-32, H-PB-16	8700	9600	2.04	9
23	round	M-PU-32	8800	9700	2.03	10
32	round	H-PB-32	9500	10500	2.04	12

*1) presented in the column. ϕ17 prestressing bars were used in the beam.

3.3 Fabrication

Specified characteristics of concrete such as compressive strength, slump, and air content are listed in Table 6. Design concrete strength was 240 kgf/cm^2 for the RC specimens and 350 kgf/cm^2 for the PC specimens. The mix proportions of concrete given in Table 6 were determined to satisfy the specified characteristics.

Concrete was mixed in a batching plant, and then cast into a form and compacted with rod type vibrators. Slump, air content, and initial temperature of concrete were measured before casting, so as to confirm the fulfillment of the specified characteristics. Table 7 presents the properties of the concrete at the time of casting, and the compressive strength at the age of 28 days.

In the cast-in-place concrete joint specimens, concrete was cast at the same time into the beam and the column except for the joint region between the two members. Then after about one week from the preceding concrete casting, shrinkage compensating concrete was cast at the joint region. At that time, the chipping was carried out so as to remove laitance and inferior aggregates at the both joint surfaces.

Table 6 Specified mix for the concrete

type of specimen	specified concrete strength (kgf/cm^2)	slump (cm)	maximum size of aggregate (mm)	air content (%)	water-cement ratio (%)	fine agg. ratio (%)	weight of materials (kgf/m^3)				water reducing agent (l/m^3)
							water	cement	fine agg.	coarse agg.	
PC	350	8±2.5	10	5±1	60	50	170	283	900	916	2.83
RC	240	8±2.5	10	5±1	74	52.8	174	235	965	879	2.35

Table 7 Properties of the concrete

No.	slump (cm)	air content (%)	concrete temperature (°C)	compressive strength at 28 days (kgf/cm²)
M- R -16	4.5	5.2	11	283
M- R -32	4.5	5.2	11	283
M-P U-16	7.2	4.3	9	330
M-P U-32	7.2	4.3	9	330
M-P B-16	7.2	4.3	9	330
M-P B-32	7.2	4.3	9	330
C- R -16	4.5	5.2	11	283
C- R -32	4.5	5.2	11	283
C-P B-16	5.4	3.8	11	385
C-P B-32	5.4	3.8	11	385
A-P B-16	5.6	3.6	12	331
A-P B-32	5.4	3.8	11	385
H-P B-16	5.6	3.6	12	331
H-P B-32	6.0	4.7	20	319
I-P B-16	5.6	3.6	12	331
I-P B-32	7.0	4.4	12	326

Table 8 Mix proportion of the grouting cement paste

cement (kgf)	water (kgf)	warer-cement ratio	water reducing agent (gf)	aluminum powder (gf)
40	18	0.45	100	3

Prestressing force was introduced in the PC specimens in accordance with the JSCE Standard for Prestressed Concrete [6]. In order to guarantee the effective prestress value (20 kgf/cm² for the lower reinforcement ratio specimens or 40 kgf/cm² for the higher ones) at the time of the loading test, due consideration was given to various factors leading to the loss of prestress [7] for the determination of the initial prestressing forces. Cement paste grouting was performed immediately after the introduction of prestressing forces. The mix proportion of the cement paste for grout-

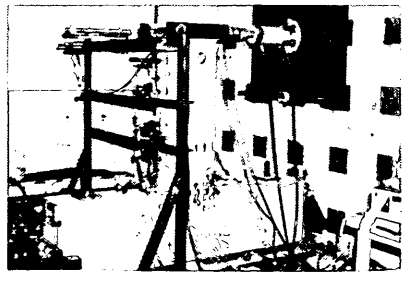

Fig. 4 Testing setup

Fig. 5 Testing setup

ing is listed in Table 8.

For the insertion joint specimens, the cement paste which had the same quality as that used for PC-grouting was filled into the void between the column and the slab.

3.4 Test Procedures and Instrumentation

The loading test was conducted on the test bed at the Port and Harbour Research

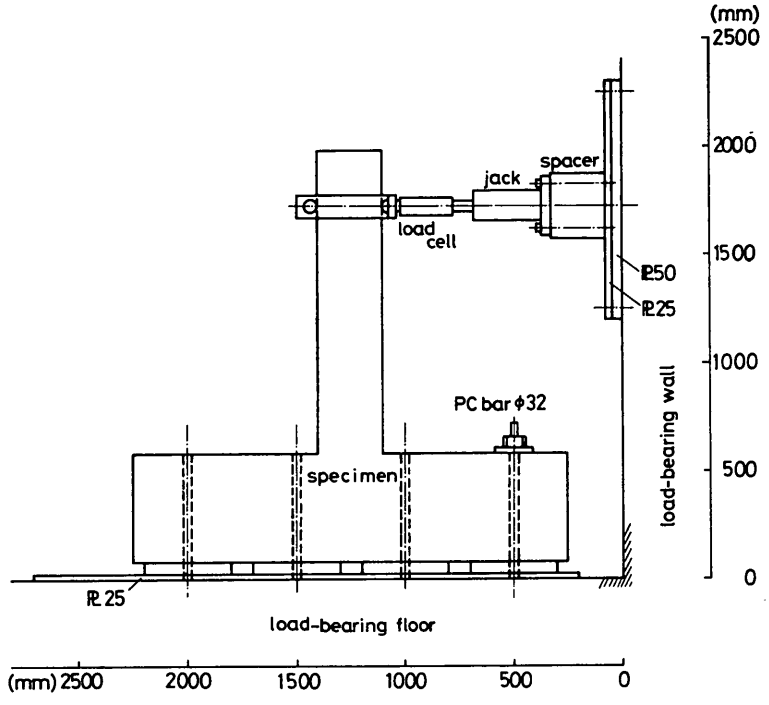

Fig. 6 Schematic diagram of loading arrangements

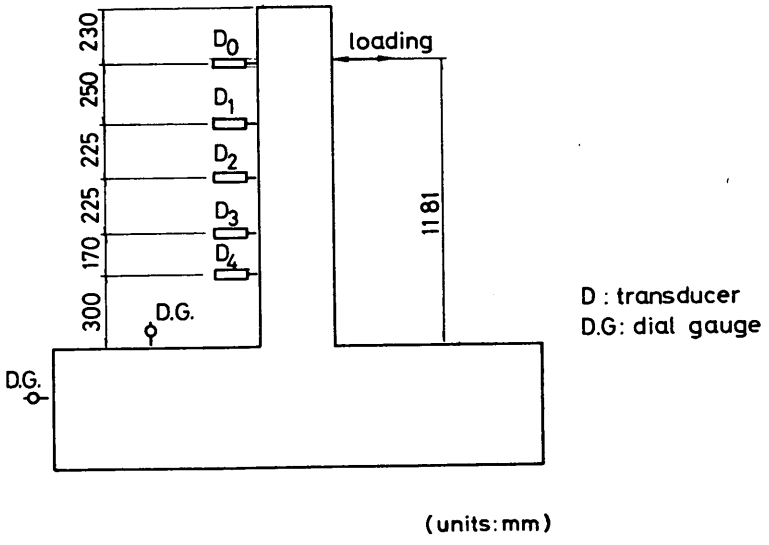

Fig. 7 Location of displacement transducers

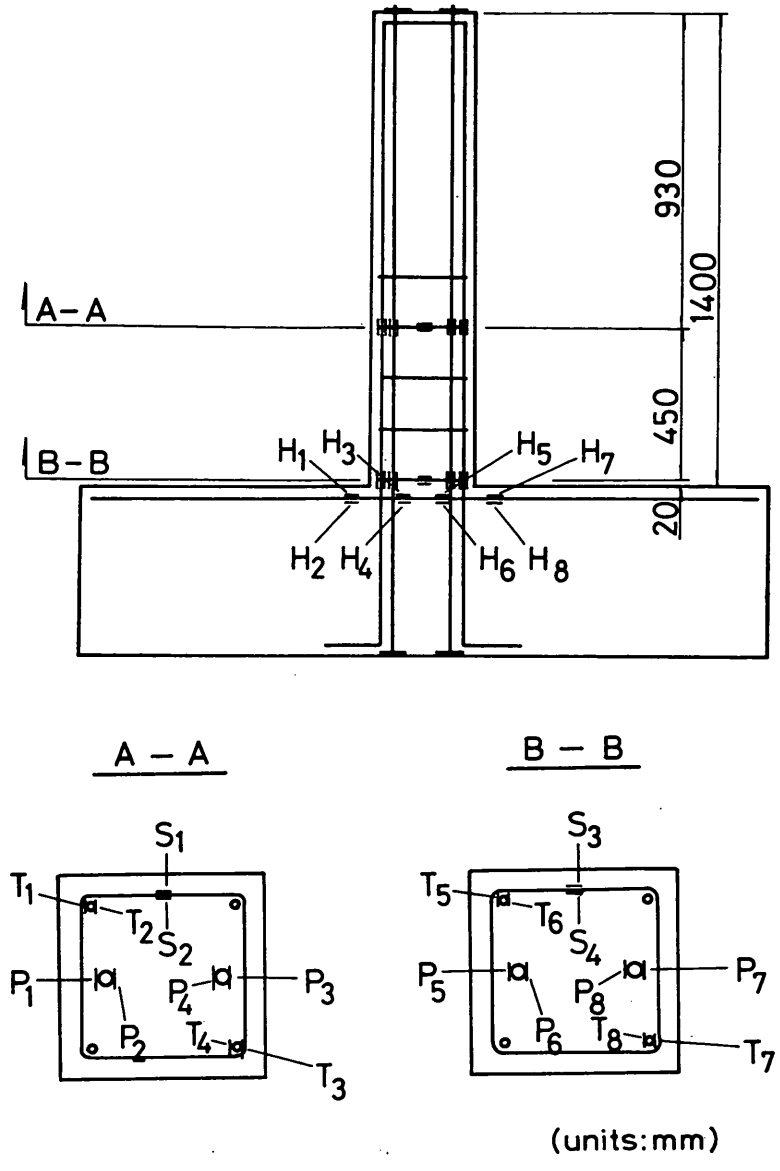

Fig. 8 Location of strain gauges in steel bars (M-PU, M-PB, C-PB, and A-PB)

Institute. The test specimen was fixed onto the floor with four prestressing bars of 32 mm in diameter which passed through the specimens. Figures 4 and 5 show the test setup.

Concentrated lateral load was applied at the point of 20 cm distance below the top of the column as shown in Fig. 6, with a hydraulic jack of 50 tf in capacity and 200 mm in stroke. Consequently, the joint region was subjected to flexural moment and the shear force.

All the specimens were loaded to failure under the following loading programs: Up to the first yield of reinforcing bars, the load was monotonically increased by an increment of about 0.5 or 1.0 tf. When the first yield was confirmed in the measure-

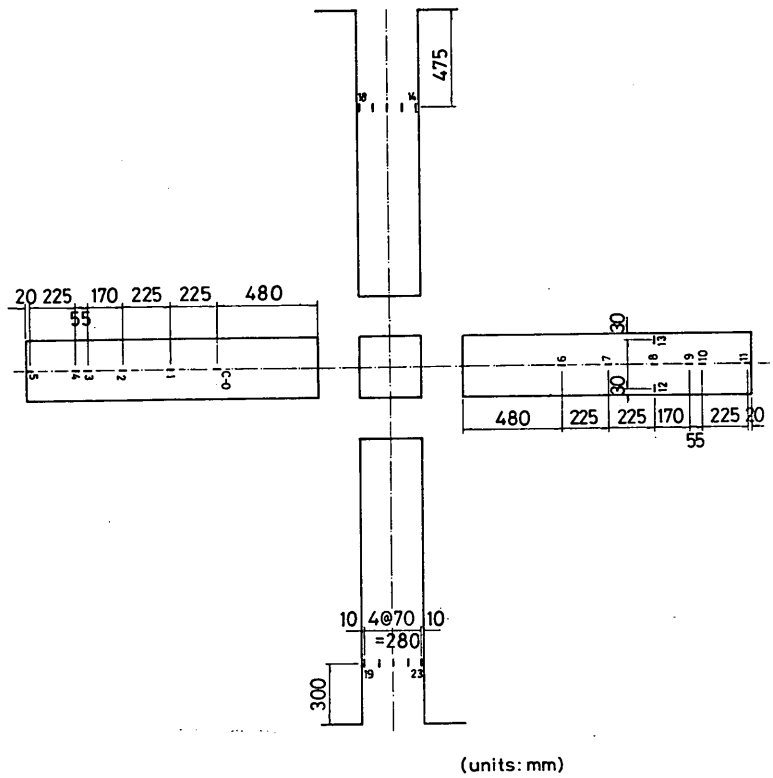

Fig. 9 Location of strain gauges on the concrete surface (M-R, M-PU, M-PB, C-R, C-PB, and A-PB)

ment, the applied load was released (unloaded). After that, the loading-unloading repetition was controlled by the measured deflection at the loading point. Namely, the maximum deflection at ith loading step was set equal to $i \cdot \delta_y$, where δ_y denotes the deflection at the first yield. The applied load was supposed to be wave forces which acted on real offshore structures, but dynamic effects of wave forces were not considered in this study. Moreover, the vertical load was not applied which corresponded to the weight of superstructures, uplift forces due to waves, and the rotation of structures due to waves.

In the experiment, applied load, deflection, strain of concrete and reinforcing and prestressing bars, and crack widths were measured. The applied load was measured with a load cell attached at the tip of the jack. The deflection of the test specimen was measured with displacement transducers of 50 mm in stroke. The strains in concrete and bars were measured with electrical resistant strain gauges attached onto the respective surfaces. The gauge length was 3 mm for reinforcing and prestressing bars, and 30 mm for concrete. Two strain gauges in pairs were attached at each measuring point on the bars, and the strain of bars was defined as the average value of these measured strains. The locations of displacement transducers are shown in Fig. 7. In the test of the insertion joint, displacement transducer D 4 was not installed. The locations of strain gauges installed in the M-PU, M-PB, C-PB, and A-PB are shown in Figs. 8 and 9. The locations of the other specimens are presented in

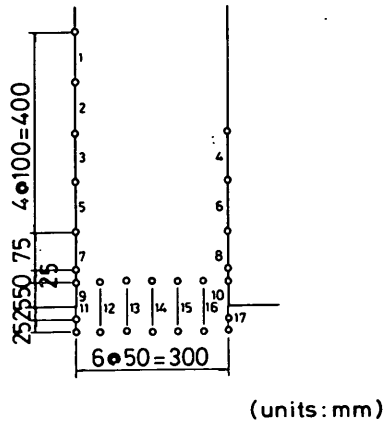

Fig. 10 Location of the contact points

Appendix B.

Contact points were attached on the one-side of the test specimen in order to measure crack widths as shown in Fig. 10. The interval of contact points was about 100 mm. Locations of cracks and their developments were measured and sketched by visual inspection.

All the measurements were performed at each loading step except for the crack width. The crack width was measured at the maximum load applied in each loading cycle for the sake of reducing the measuring time because of avoiding the influence by the creep and relaxation infection.

4. Experimental Results and Consideration

4.1 General

Results and consideration from the experiment on the sixteen specimens are presented and discussed. Specifically, applied loads or moments at the first crack, at the first yield, and at the ultimate, deflection at the loading point, cracks occurred on the concrete surface, strains in bars and concrete, and energy absorptions are discussed in detail.

The applied flexural moment calculated from the applied loads and the deflection of the column are summarized in Table 9. The moment was calculated by multiplying the applied load by the loading-span. The loading-span was defined as the distance between the loading point and the joint surface for M, C, A, and I specimens, and that between the loading point and the top section of the haunch for H specimens. The ultimate flexural moment (M_u) was defined as the maximum value of the applied moment. The first yield moment (M_y) is the value when strain of bars reached the yield one which was defined as the yield strength divided by the modulus of elasticity. Moreover, the cracking moment (M_c) is the value at which a crack was initiated on the concrete surface. Furthermore, the deflections at the first yield (δ_y) and at the ultimate (δ_u) were measured at the loading point in the respective loading steps. The value of μ was defined as the ratio of δ_u to δ_y, that is, the ductility factor at the ultimate. The ductility factor at the ultimate is an index of the toughness of the member.

Table 9 Summary of the experimental results

specimen	testing age (d)	f'_c (kgf/cm²)	f_{ct} (kgf/cm²)	M_c (×10⁵kgf•cm)	M_y (×10⁵kgf•cm)	M_u (×10⁵kgf•cm)	δ_y (mm)	δ_u (mm)	μ
M- R -16	49	295	40.8	1.18	1.61	2.60	2.47	23.58	9.55
M- R -32	53	295	40.8	1.77	3.29	5.08	4.72	17.27	3.66
M-P U-16	37	375	48.7	2.95	3.52	5.91	3.28	21.33	6.50
M-P U-32	34	375	48.7	3.54	6.57	12.40	4.60**	21.50**	4.67
M-P B-16	47	375	48.7	2.95	4.30	5.91	3.57	11.42	3.20
M-P B-32	43	375	48.7	3.54	7.68	11.81	8.29	30.91	3.73
C- R -16	60	295	40.8	0.59	1.51	2.01	5.18	27.57	5.32
C- R -32	56	295	40.8	1.77	4.03	5.31	5.54	20.68	3.73
C-P B-16	62	340	46.8	1.77	4.81	7.09	4.29	19.13	4.46
C-P B-32	59	340	46.8	3.54	8.82	12.88	7.33	21.31	2.91
A-P B-16	79	367	49.4	2.36	— *	4.13	—	12.29	—
A-P B-32	66	340	46.8	4.72	— *	6.50	—	12.99	—
H-P B-16	83	367	49.4	2.64	4.69	6.61	3.46	8.75	2.53
H-P B-32	42	335	47.6	2.64	8.46	11.89	6.25	22.98	3.68
I-P B-16	89	363	45.2	3.08	4.22	6.96	2.56	19.13	7.47
I-P B-32	80	417	44.4	3.52	7.55	12.33	4.42	17.79	4.02

*) Reinforcing bar did not yield.
**) The values were measured at D-1 shown in Fig. 16.

Compressive and flexural strengths of concrete (f_c' and f_{ct}) at the loading test were measured through the preliminary tests. Cylindrical specimens of ϕ 10×20 cm conformed to JIS A 1108 and prism specimens of 10×10×40 cm conformed to JIS A 1106 were applied to the respective tests.

The outline of the fracture mechanism of the specimens could be summarized as follows [8, 9] :

(a) All the specimens showed the flexural failures. The shear failure was not dominantly observed.
(b) The buckling failure or tensile fracture of the longitudinal reinforcing bars and prestressing ones did not occur at the joint.
(c) The column did not penetrate into the beam. The longitudinal reinforcing bars did not come out from the beam.
(d) The fracture concentrated at nearby the joint. In the haunch joint specimens, it occurred also at the upper section of the haunch. The beam did not collapse in all the specimens.
(e) The anchors of prestressing bars were not broken.

4.2 Strength and Deflection

Measured load-deflection curves are shown in **Appendix C.** Since the loading-span was different among the specimens, the load-deflection curves were modified to the flexural moment-curvature curves for the sake of the comparison. In the haunch joint specimens, the loading-span was defined as the distance between the loading point and the upper section of the haunch. The envelopes obtained from the flexural moment-curvature curves are shown in Figs. 11 through 14. The applied flexural moments were obtained by the applied load multiplied by the loading-span. The curvature was calculated from the measured strain of bars and concrete in the vicinity of the joint face.

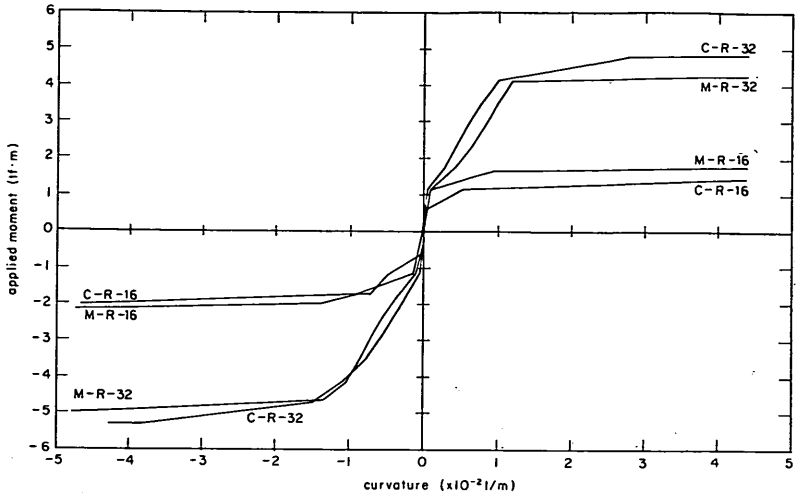

Fig. 11 Moment vs. curvature relationship (M-R and C-R)

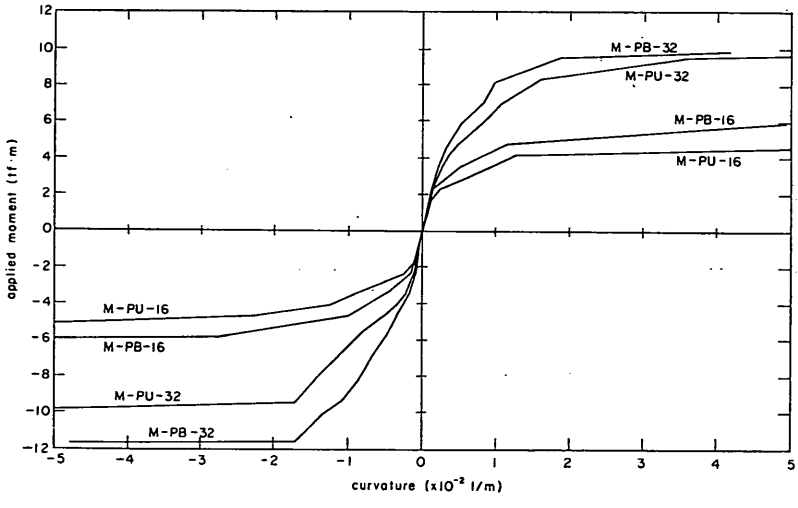

Fig. 12 Moment vs. curvature relationship (M-PU and M-PB)

The ultimate load or the ultimate flexural moment will be discussed. The ultimate flexural moment of M-R-16 (monolithic reinforced concrete) was larger than that of C-R-16, but those of the other monolithic specimens were smaller than those of the connected ones. The existence of splice joints of bars and the variation of concrete strength could cause the difference among their ultimate moments. Those of the adhesive joint specimens were 50 through 70% of those of the monolithic specimens, because no reinforcing bar passed through the joint. Furthermore, there are little differences among ultimate moments of the haunch joint, the insertion joint, and the PC monolithic joints. Flexural properties of the haunch joint was almost the same as that of the monolithic joint. The ultimate flexural moments of the bonded PC specimens and the unbonded ones were almost the same, and then there is not an important primary factor to the ultimate moment whether the PC bar is bonded or not in this

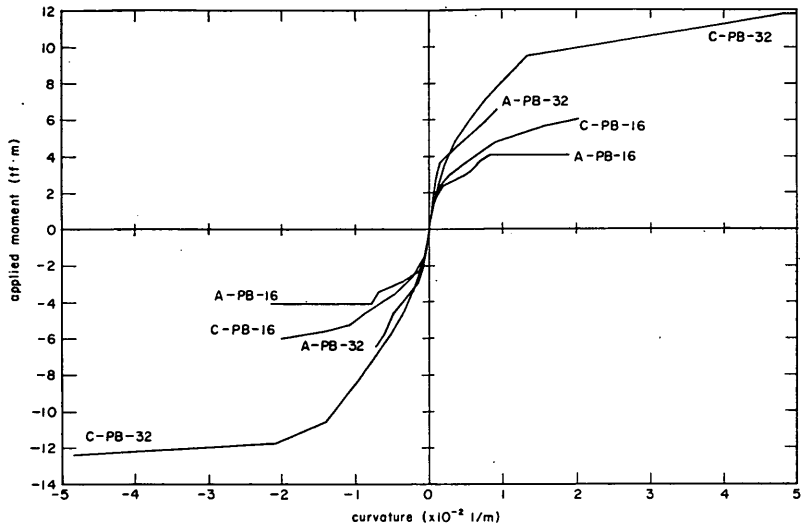

Fig. 13 Moment vs. curvature relationship (C-PB and A-PB)

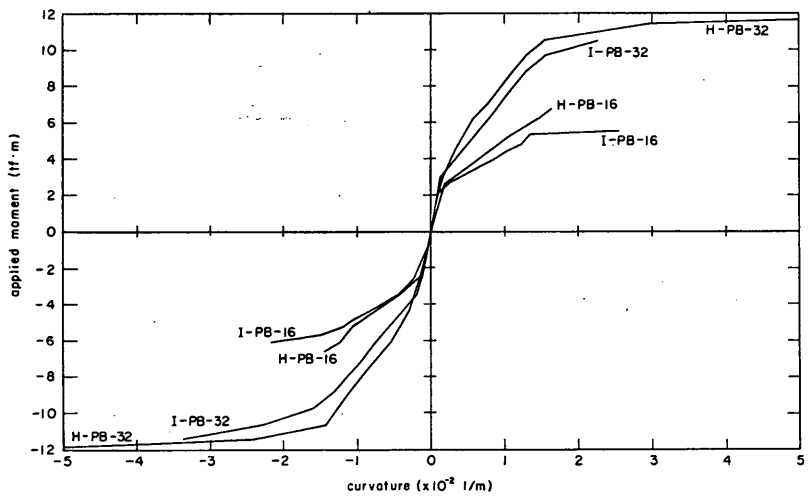

Fig. 14 Moment vs. curvature relationship (H-PB and I-PB)

loading test.

The capability of deflection or rotation about the joint can be examined by the curvature and the ductility factor. There were no differences of the curvature at the joint among the RC specimens. The bonded PC specimen provided less or almost the same curvature than the unbonded one. The curvature at the joint of the adhesive joint was the smallest. That of the insertion joint was the second smallest, and those of the other specimens were almost the same.

The ductility factor at the ultimate is listed in Table 9. The values ranged from 3 to 10. It could be said that the connected specimens had enough ductilities [10].

The deflected shapes along the height of the column are shown in Figs. 15 (M-PB) and 16 (H-PB). Those of the other specimens are presented in **Appendix D.**

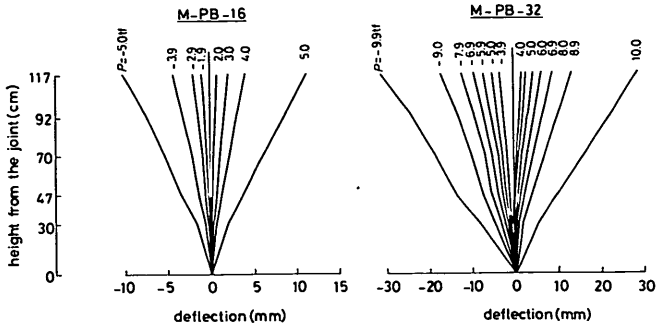

Fig. 15 Deflected shapes (M-PB)

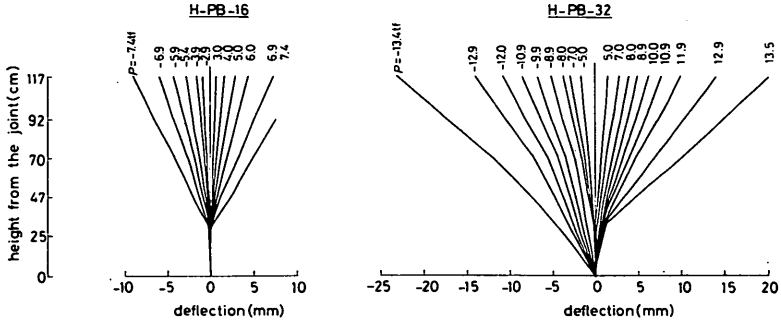

Fig. 16 Deflected shapes (H-PB)

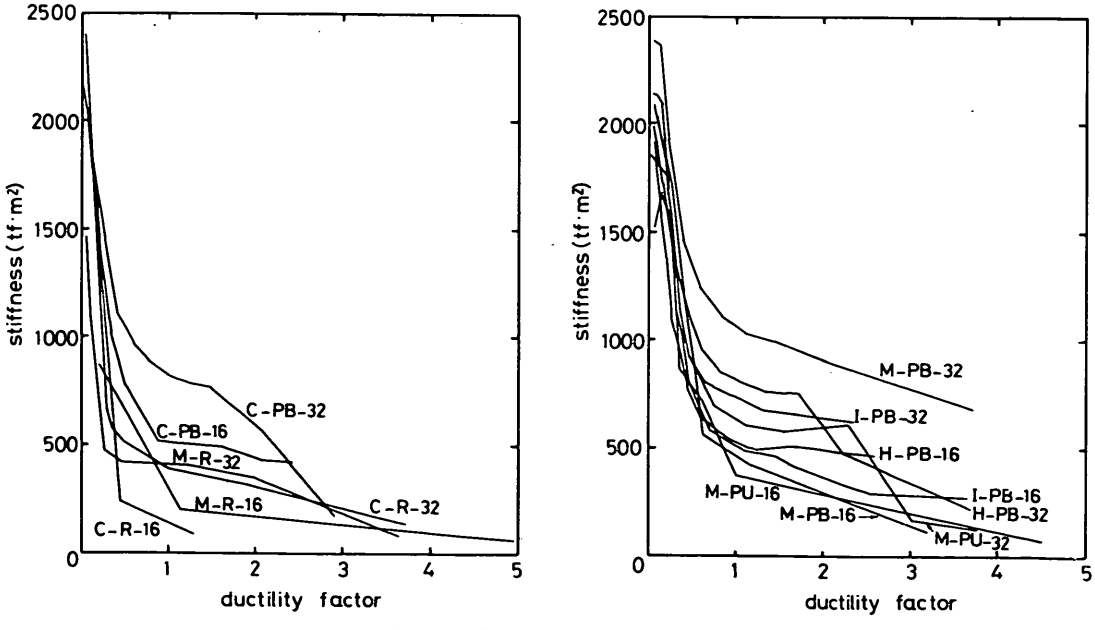

Fig. 17 Stiffness deterioration

The deflected shape was almost linear, and no deflection was measured at the joint section. In other words, penetration of the column into the beam and the horizontal displacement of the column at the joint were not observed. The haunch joint specimens showed little deflection in the haunch region up to the first yield. Afterwards, the deflection at the joint of H-PB-16 was little up to the ultimate, but that of H-PB-32 was significantly observed.

Figure 17 shows the stiffness degradation. The stiffness of the specimen could be obtained by the following equation:

$$K_i = M_i/\phi_i \qquad \cdots\cdots\cdots\cdots(1)$$

where, K_i: average stiffness
M_i: applied bending moment
ϕ_i: measured curvature
i: ith loading cycle

Since reinforcing bars did not yield in the adhesive joint specimens, their results were not shown in these figures.

The stiffness on all the specimens decreased significantly even before the first yield. Furthermore, the specimens showed almost the same degraded stiffness regardless of joint types. However, there was a little difference of the stiffness degradation between the bonded and the unbonded PC specimens.

4.3 Crack Formation

Figures 18 through 25 show crack formations observed on each column. The numerical numbers in these figures show the applied load corresponding to the crack development. In general, only flexural cracks were formed in the specimens with the lower reinforcement ratio, and on the other hand in the specimens with the higher reinforcement ratio, shear cracks were additionally formed as the load was increased.

Almost the same crack formations were observed both in the bonded PC specimens and in the unbonded PC ones as shown in Figs. 19 and 20.

In the cast-in-place concrete joint specimens, cracks were initiated at the upper and the lower sections in the cast-in-place region simultaneously and developed at both joint faces. Subsequently, cracks were formed on the cast-in-place concrete region

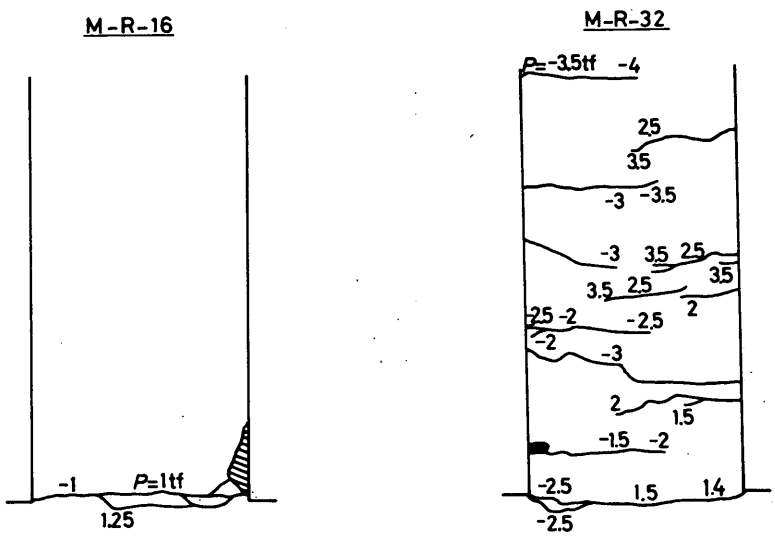

Fig. 18 Crack formation (M-R)

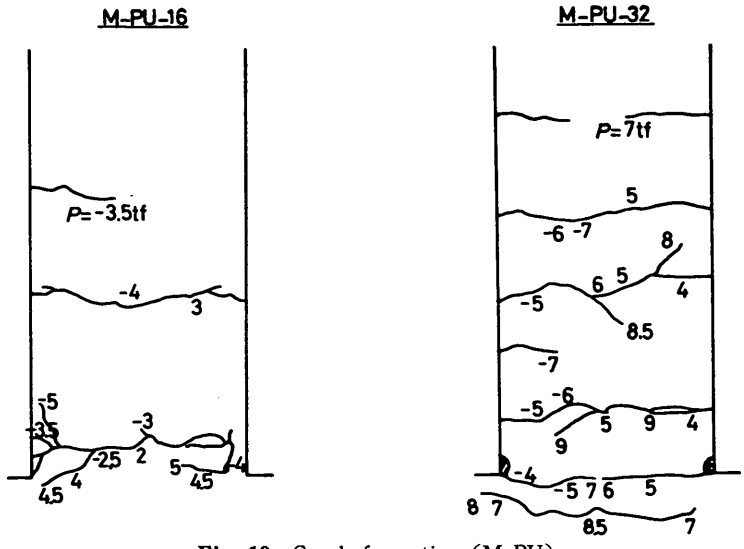

Fig. 19 Crack formation (M-PU)

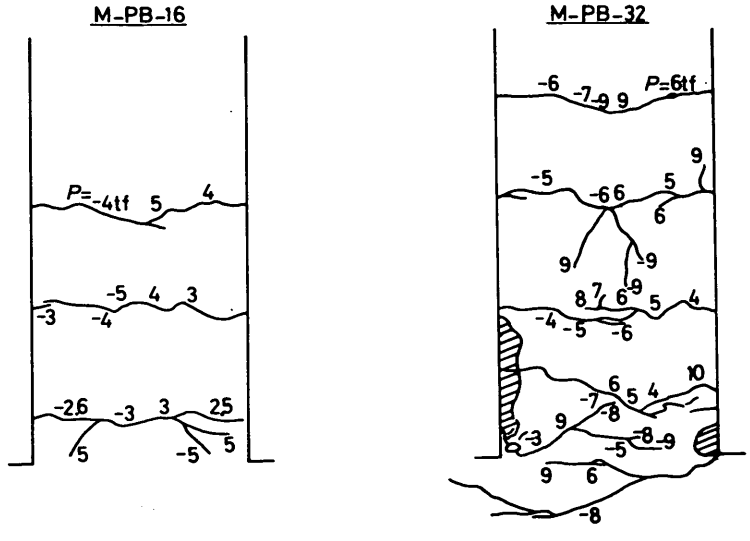

Fig. 20 Crack formation (M-PB)

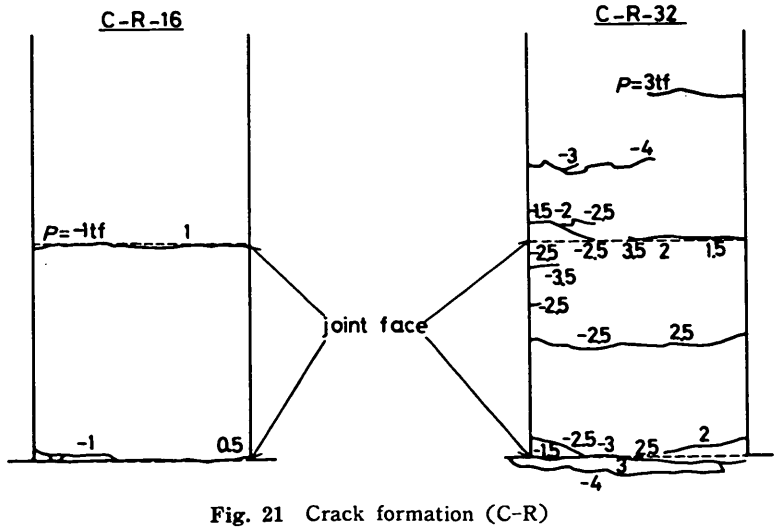

Fig. 21 Crack formation (C-R)

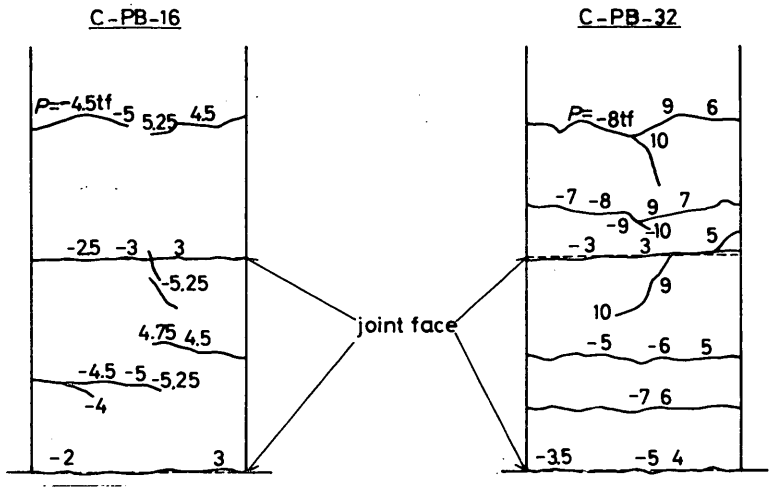

Fig. 22 Crack formation (C-PB)

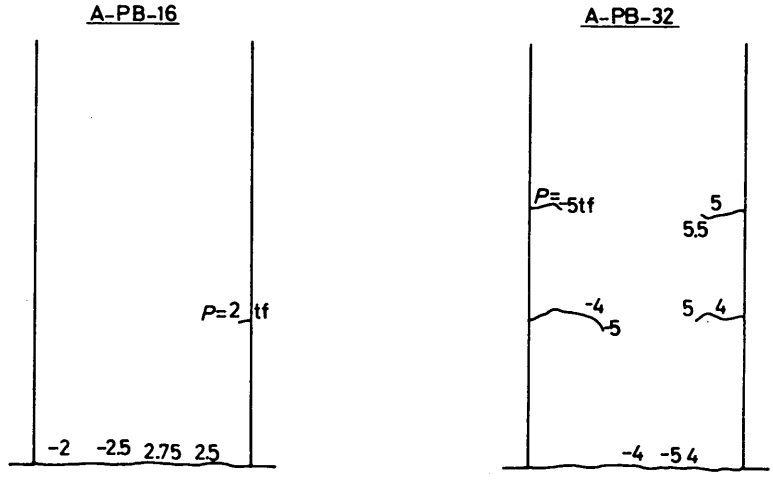

Fig. 23 Crack formation (A-PB)

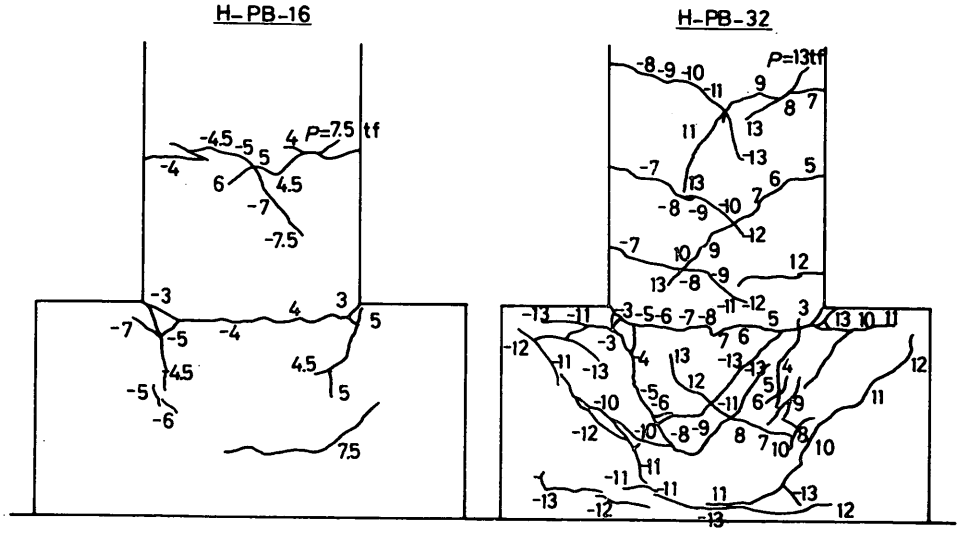

Fig. 24 Crack formation (H-PB)

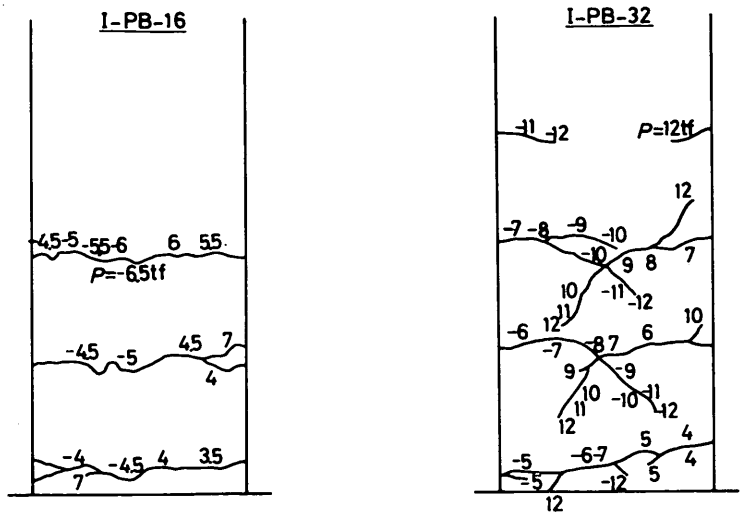

Fig. 25 Crack formation (I-PB)

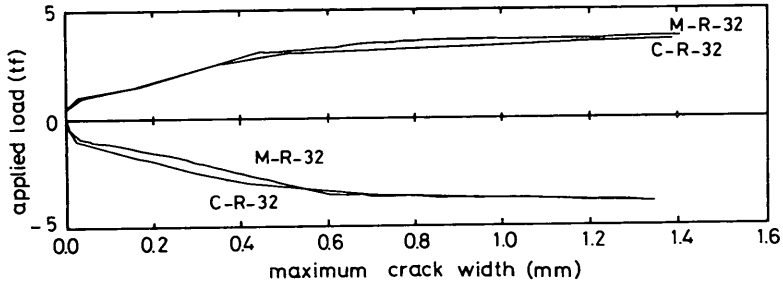

Fig. 26 Variation of crack width (RC)

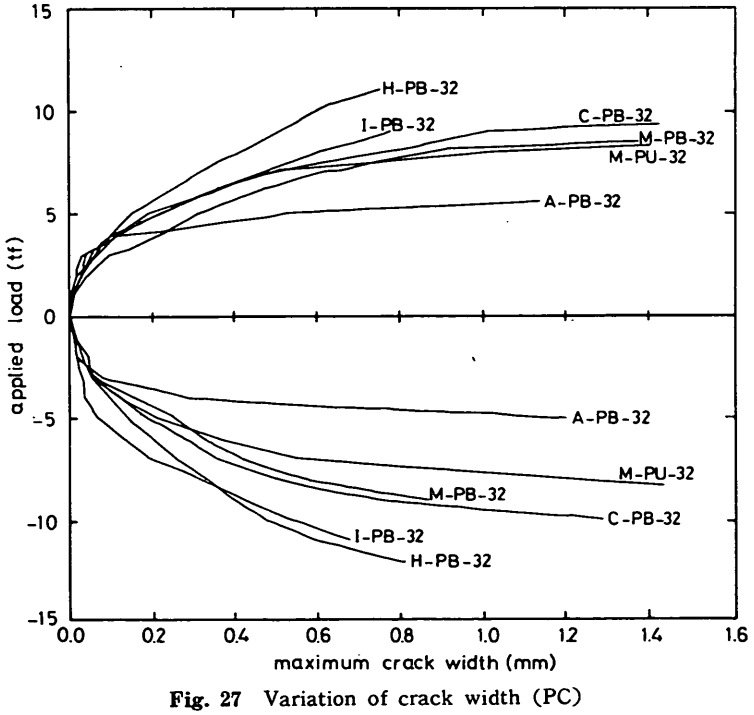

Fig. 27 Variation of crack width (PC)

and on the column. On the other hand in the monolithic specimens, cracks were initiated at the joint section, and subsequently on the other sections of the column. Only a crack was initiated and developed at the joint section in the adhesive joint specimens up to the ultimate. Cracks were not formed at the joint surface in the haunch joint specimens, but initiated on the upper section of the haunch. In particular, many shear cracks were formed in the haunch and the column in H-PB-32 as shown in Fig. 24. There was no remarkable difference of crack formations between the monolithic and the insertion joint specimens.

Figures 26 and 27 show the variations of the crack width measured on the specimens with the higher reinforcement ratio. Those of the other specimens are presented in **Appendix E.** The crack width refers to its maximum value. It was measured at the joint section except for the haunch joint specimens. The maximum crack width was observed at the upper section of the haunch in the haunch joint specimens. The ratio of the applied loads when the maximum crack width was 0.1 mm to the ultimate loads ranged from 0.3 to 0.5. The ratio when the maximum crack width was 0.2 mm ranged 0.4 to 0.6. These ratios of H-PB-32 and I-PB-32 were slightly larger than those of the other specimens.

4.4 Strain of Bars and Concrete

(1) Strain of Longitudinal Reinforcing Bars

The measured strains in longitudinal reinforcing bars in the columns with the higher reinforcement ratio at nearby the joint are shown in Figs. 28 through 31. For the sake of clarity of the figures, only the envelopes are drawn in these figures.

As shown in Fig. 28, strain of the reinforcing bar in the connected specimen was slightly smaller than that in the monolithic specimen. Measured strain of reinforcing bars in the unbonded PC specimen was larger than that in the bonded PC specimen when the applied flexural moment exceeded 5 tf•m as shown in Fig. 29. Strains of reinforcing bars were almost the same among M-PB, C-PB, H-PB, and I-PB. However, strain of the reinforcing bar in the adhesive joint specimen was merely 400×10^{-6} at the ultimate, because no reinforcing bars passed through the joint surface.

The examples of measured strains of reinforcing bars in the columns with the lower reinforcement ratio are shown in Figs. 32 and 33. Being compared of the bonded PC specimen (M-PB-16) with the unbonded one (M-PU-16), strain of the reinforcing

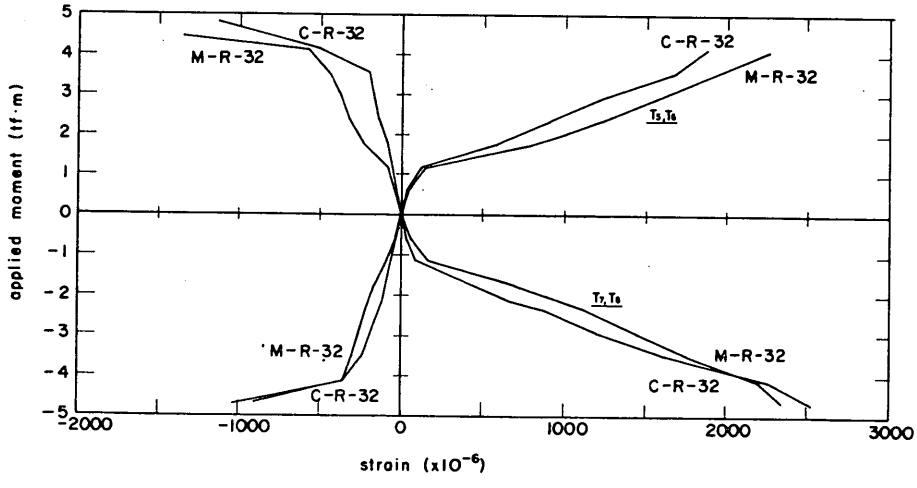

Fig. 28 Variation of strain of reinforcing bars (M-R-32 and C-R-32)

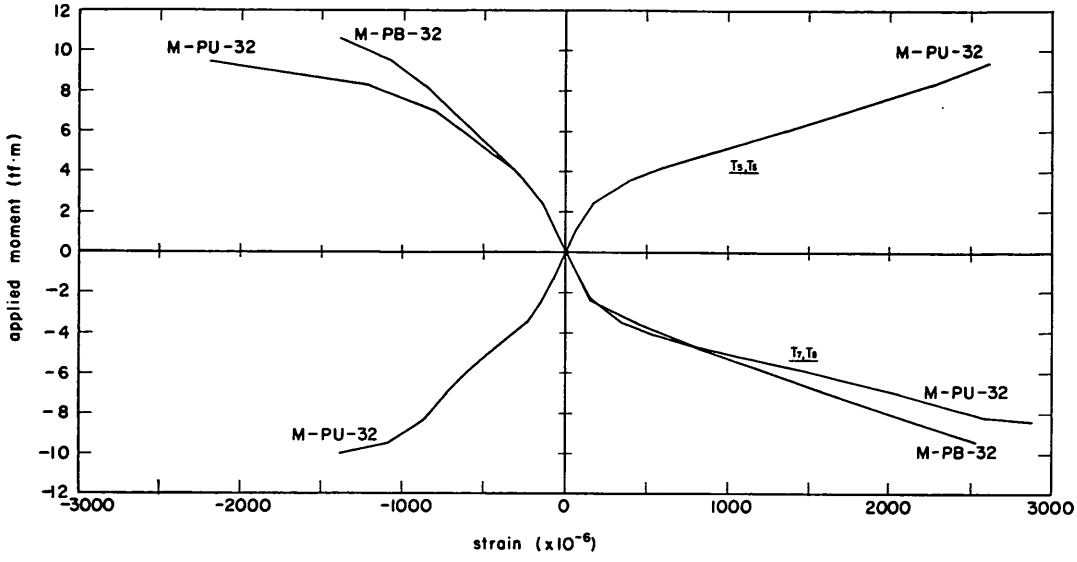

Fig. 29 Variation of strain of reinforcing bars (M-PU-32 and M-PB-32)

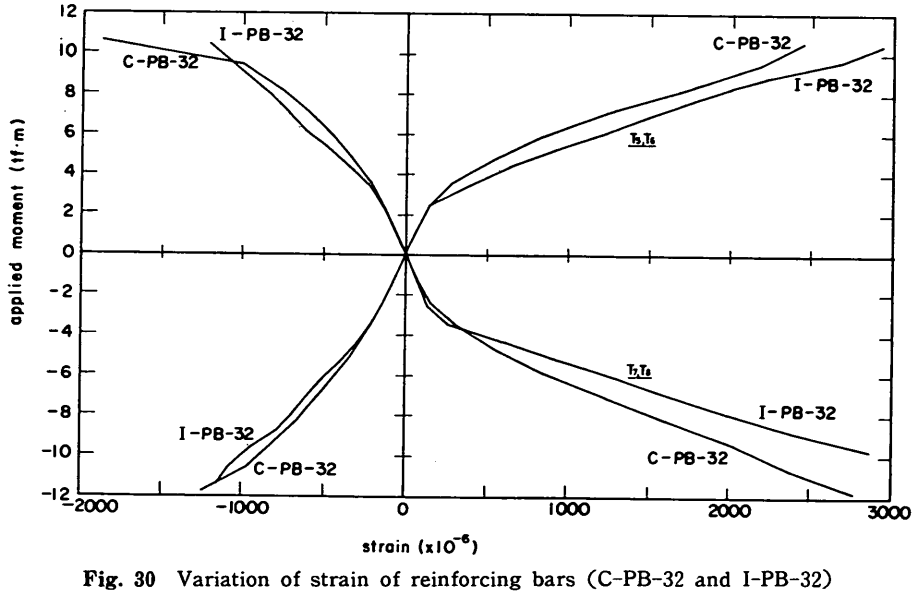

Fig. 30 Variation of strain of reinforcing bars (C-PB-32 and I-PB-32)

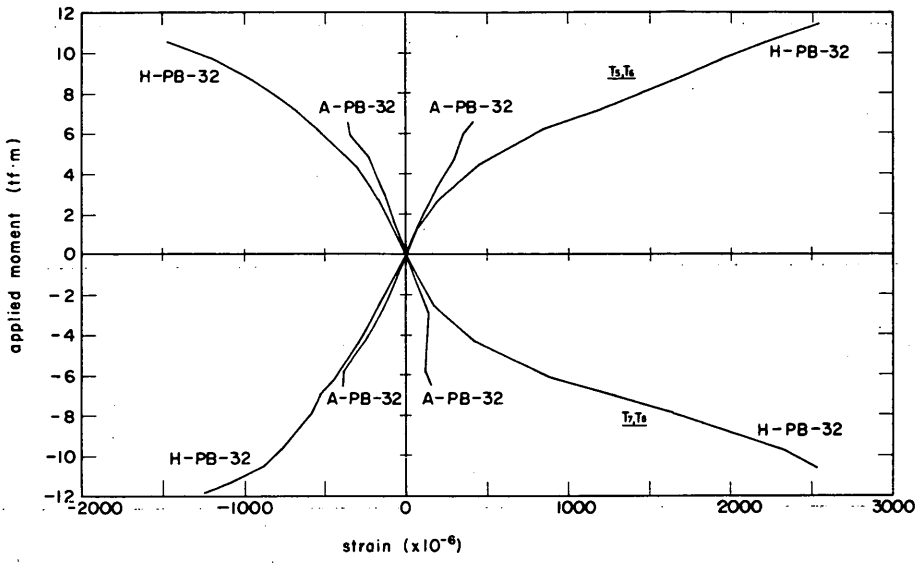

Fig. 31 Variation of strain of reinforcing bars (A-PB-32 and H-PB-32)

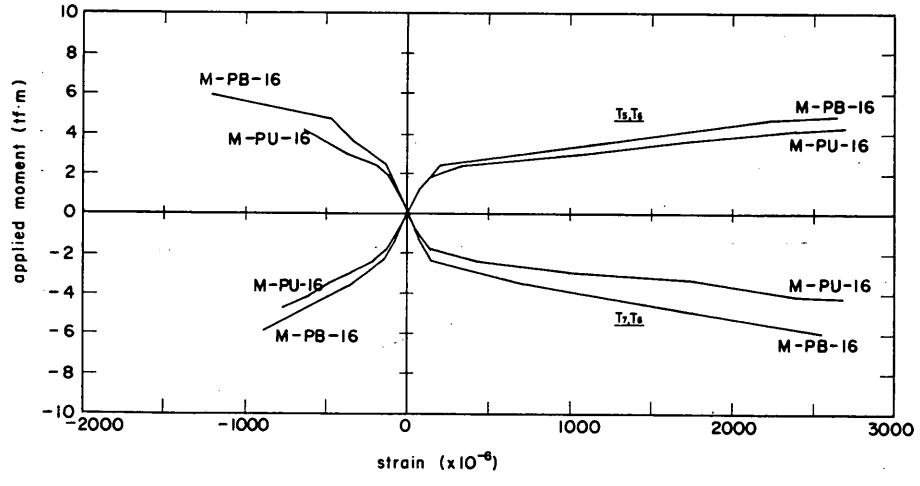

Fig. 32 Variation of strain of reinforcing bars (M-PU-16 and M-PB-16)

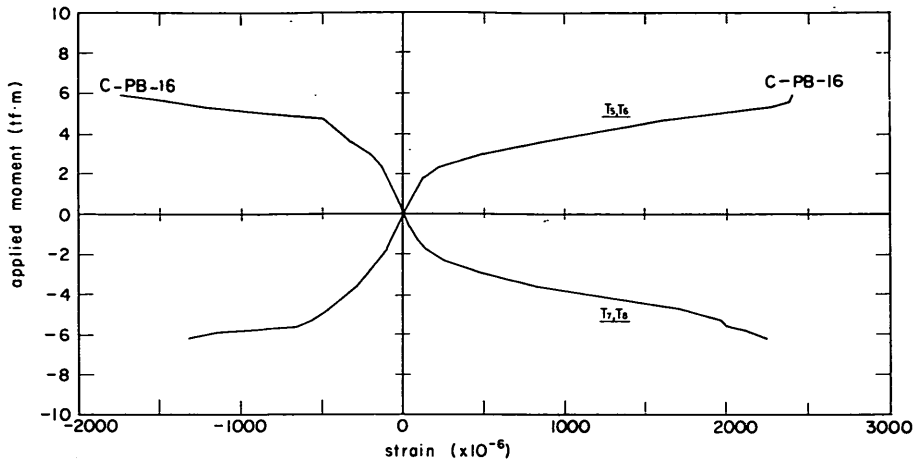

Fig. 33 Variation of strain of reinforcing bars (C-PB-16)

bar in the unbonded specimen was larger than that in the bonded one. This result was the same as that obtained in the specimens with the higher reinforcement ratio.

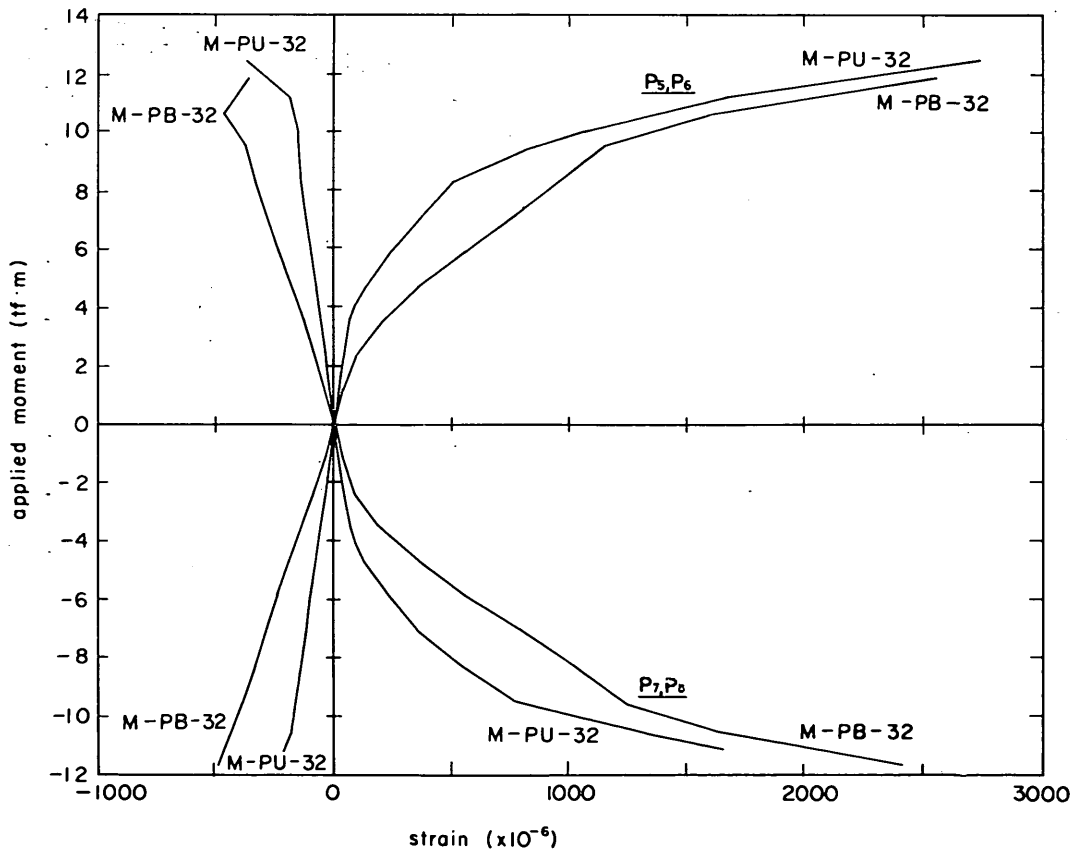

Fig. 34 Variation of strain of prestressing bars (M-PU-32 and M-PB-32)

(2) Strain of Prestressing Bars

Measured strains of the prestressing bars at nearby the joint in the PC specimens are shown in Figs. 34 through 38. Strain of the prestressing bars was set to zero just before the loading, that is, induced strain due to the prestressing force was neglected.

Compressive strain measured of the prestressing bars did not exceed 500×10^{-6}. On the other hand, tensile strain of the prestressing bars became large as the applied moment was increased. Tensile strain of the prestressing bars, however, did not reach the yield strain. Measured strains of the prestressing bars in the bonded PC specimens were larger than those in the unbonded specimens as shown in Figs. 34 and 37. This relationship was reverse to that obtained in the reinforcing bars described in 4.4 (1). The bond force between the prestressing bar and its surrounding concrete is expected in the bonded PC specimens, and therefore, larger stress and strain of the prestressing bar in the bonded specimen than those in the unbonded one was observed. On the other hand, the reinforcing bars in the bonded specimen showed less stress and strain than those in the unbonded one, because the prestressing bars could share the larger forces.

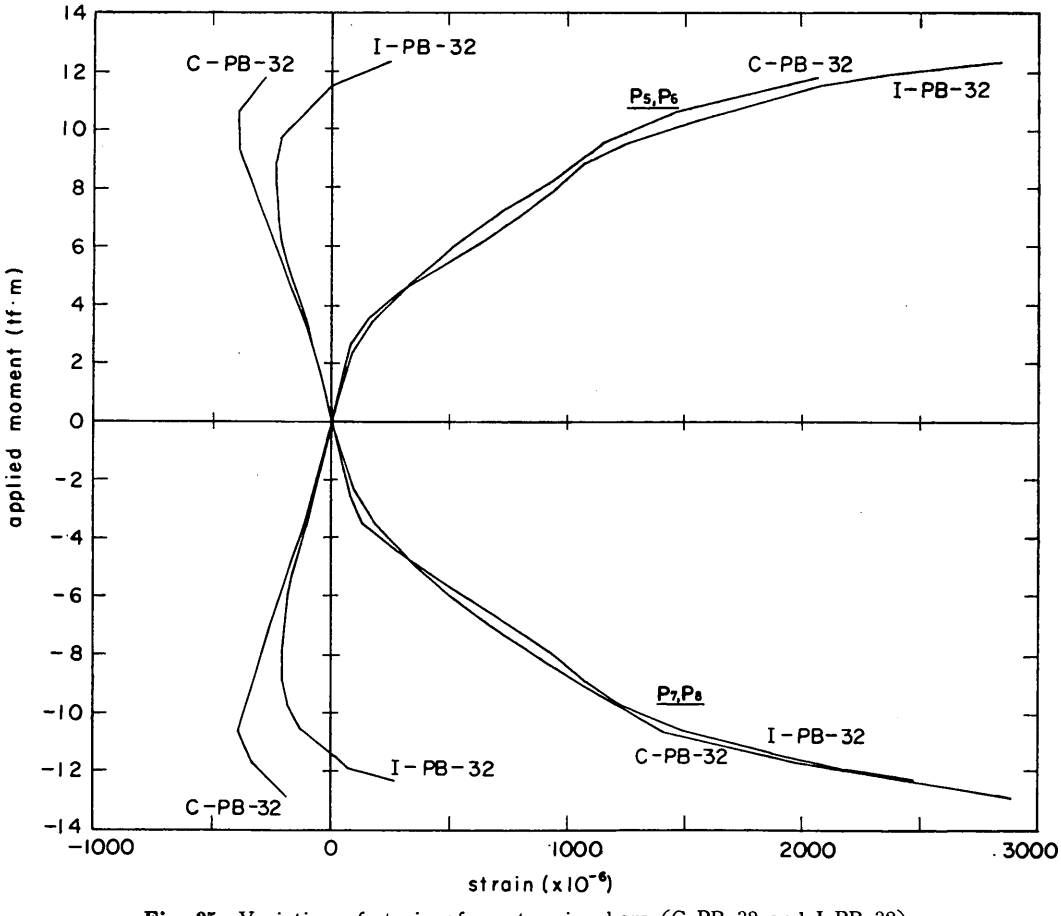

Fig. 35 Variation of strain of prestressing bars (C-PB-32 and I-PB-32)

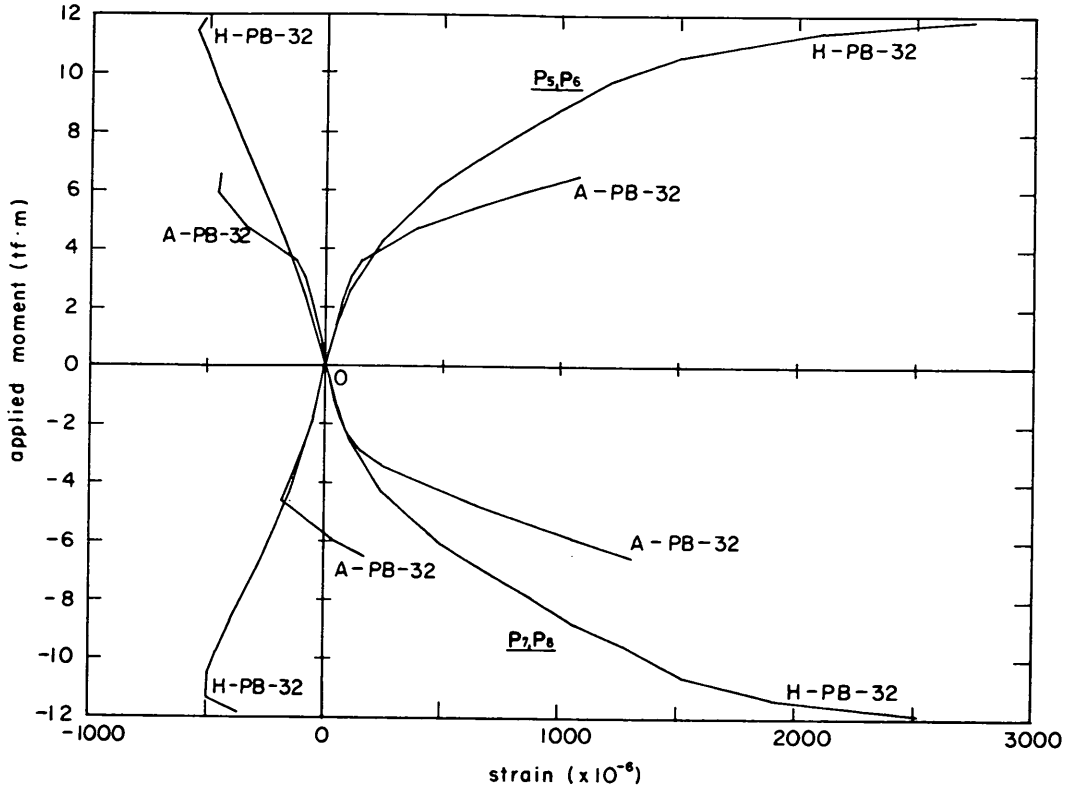

Fig. 36 Variation of strain of prestressing bars (A-PB-32 and H-PB-32)

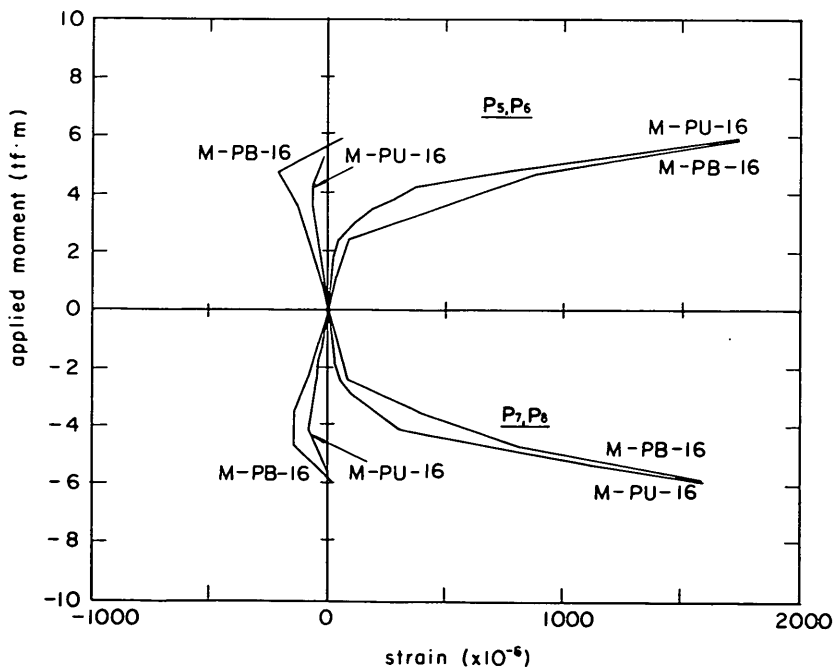

Fig. 37 Variation of strain of prestressing bars (M-PU-16 and M-PB-16)

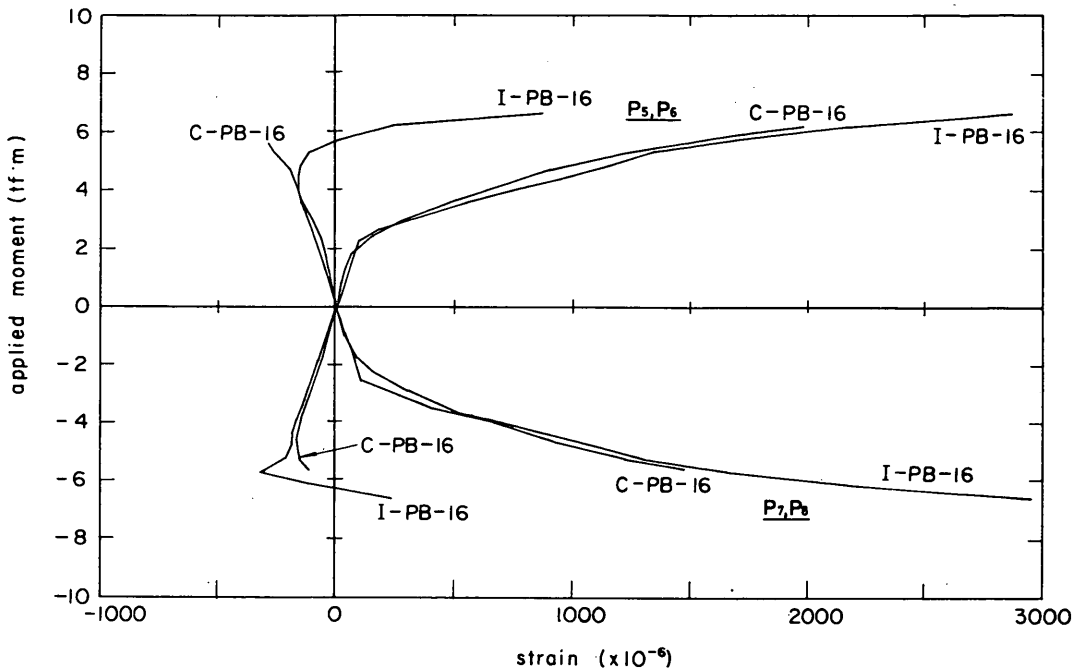

Fig. 38 Variation of strain of prestressing bars (C-PB-16 and I-PB-16)

(3) Strain of Hoop Reinforcing Bars

Strains of the hoop reinforcement at nearby the joint in the column are shown in Figs. 39 through 41. At the ultimate, measured strain was about 120×10^{-6} in the monolithic RC specimens. It was about 50×10^{-6} in the cast-in-place concrete joint RC

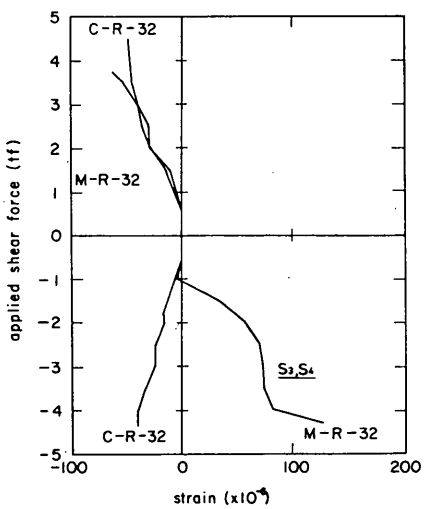

Fig. 39 Variation of strain of hoop reinforcement in the joint region (M-R-32 and C-R-32)

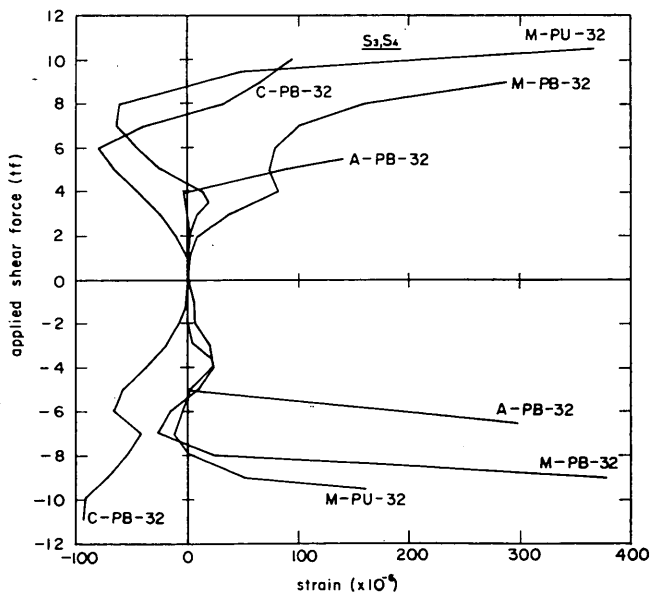

Fig. 40 Variation of strain of hoop reinforcement in the joint region (C-PB-32 and A-PB-32)

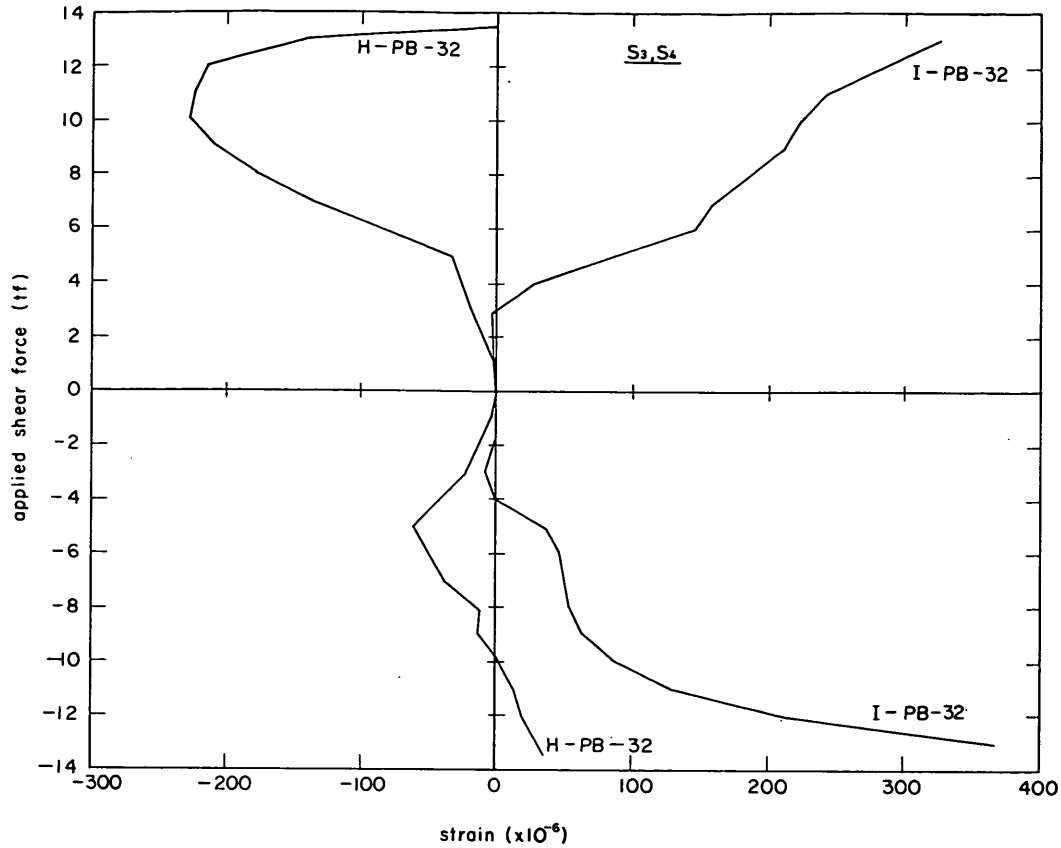

Fig. 41 Variation of strain of hoop reinforcement in the joint region (H-PB-32 and I-PB-32)

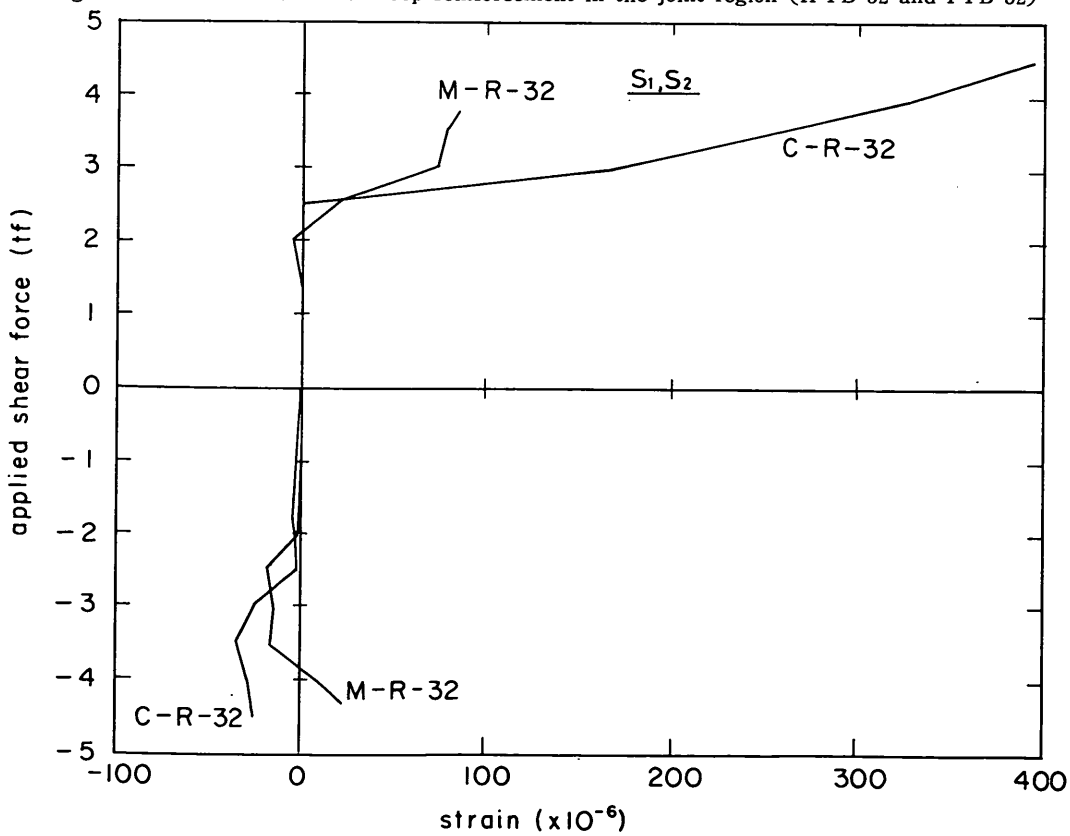

Fig. 42 Variation of strain of hoop reinforcement above the joint region (M-R-32 and C-R-32)

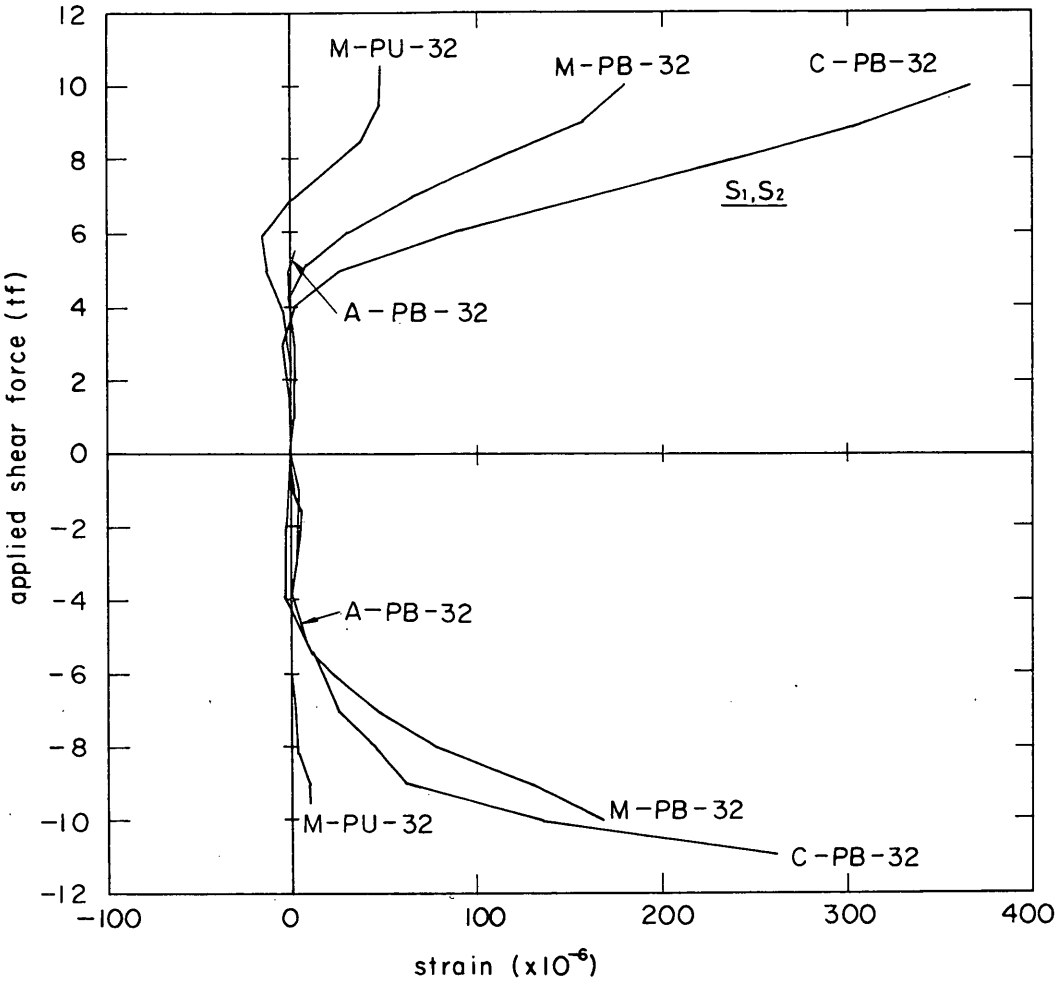

Fig. 43 Variation of strain of hoop reinforcement above the joint region (M-PU-32, M-PB-32, C-PB-32, and A-PB-32)

specimen (C-R-32). Measured strain was about 100×10^{-6} in the cast-in-place concrete PC specimen and the haunch joint specimen. Moreover, measured strain was larger than 300×10^{-6} in the adhesive joint specimen and the insertion joint specimen.

The reason why the smaller strain of the hoop reinforcement occurred in the cast-in-place concrete joint specimens is as follows: Strains of the hoop reinforcement located above the cast-in-place concrete region are shown in Figs. 42 and 43. Measured strain larger than 300×10^{-6} was observed there, and the values were larger than those observed at the joint. Thus, all the applied shear forces did not transfer into the beam through the upper joint section.

(4) Strain of Concrete

Measured concrete strain along the column surface are shown in Figs. 44 through 46. Those of the other specimens are presented in **Appendix F.** These figures show the maximum strain in each cycle of the load applied. The alternate loading provides compressive and tensile strains on the extreme fiber of concrete by turns. As the

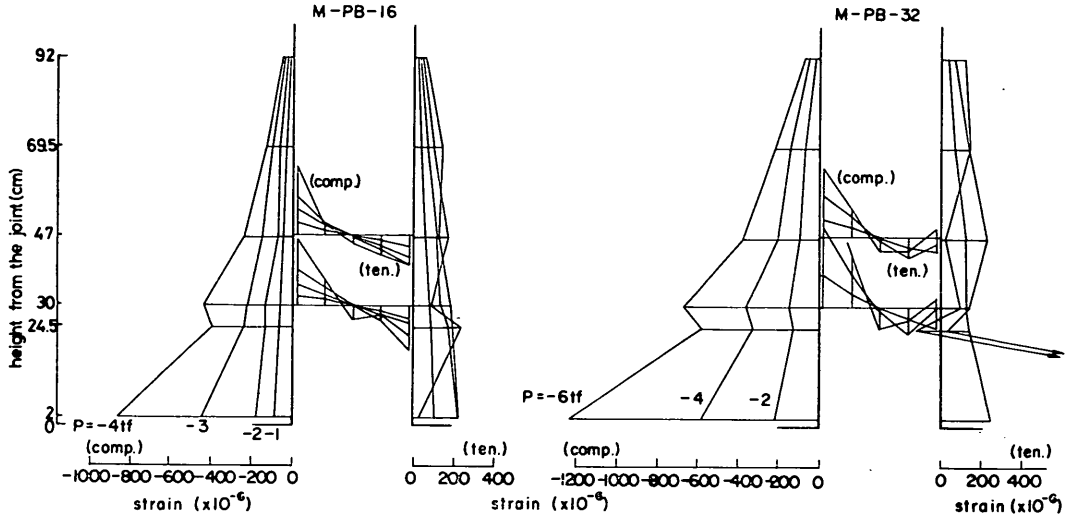

Fig. 44 Distribution of strain on concrete (M-PB)

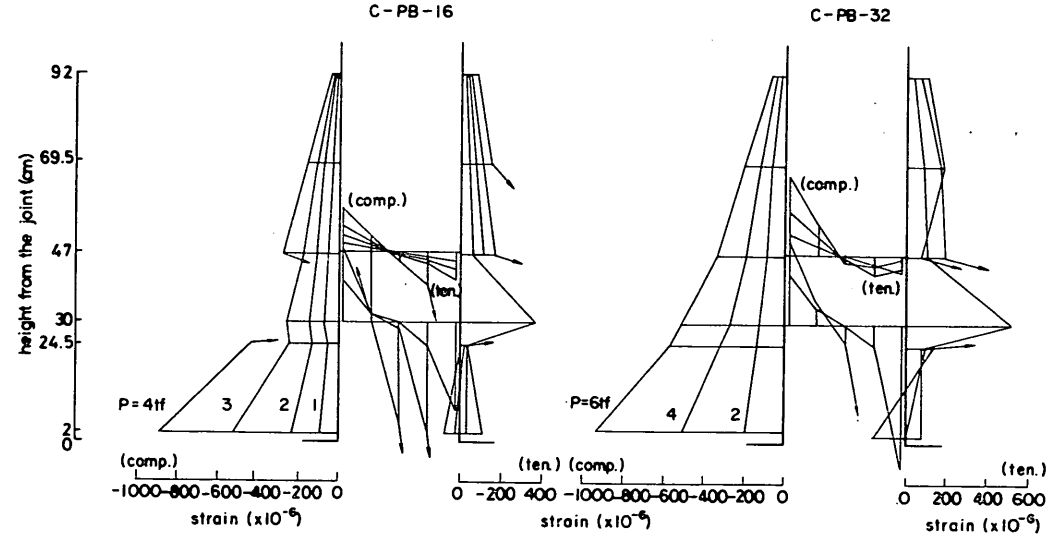

Fig. 45 Distribution of strain on concrete (C-PB)

number of loading cycles was increased, however, remaining tensile strain became large at the extreme fiber of concrete and then compressive strain could not be observed. These results were not plotted in these figures. Furthermore, strain of concrete could not be measured after many concrete cracks occurred. Therefore, the prior state of concrete strain will be discussed.

The distribution of concrete strain along the height of the column in the monolithic specimens was almost linear as shown in Fig. 44. Considerable large tensile strain occurred at the upper joint section in the cast-in-place concrete joint specimens as shown in Fig. 45. However, concrete tensile strain scarcely occurred in the cast-in-place concrete region. Furthermore, considerable large compressive strain occurred

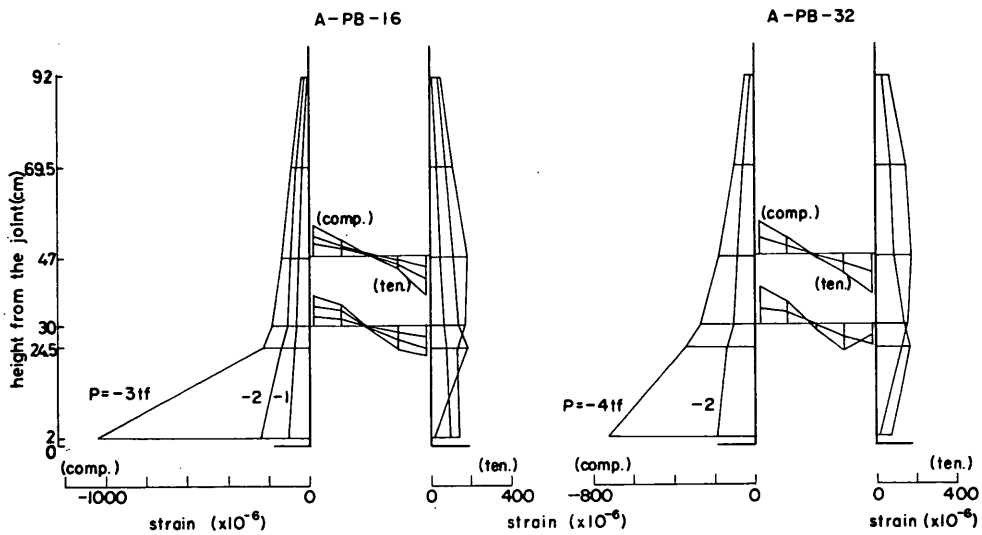

Fig. 46 Distribution of strain on concrete (A-PB)

in both types of the specimen with the lower reinforcement ratio compared with the specimens with the higher reinforcement ratio. Fairly large compressive strain occurred at the joint section in the adhesive joint specimen as shown in Fig. 46. Therefore, concrete in the adhesive joint specimen shared much more forces than that in the monolithic specimen did. This result was the reason that the ultimate flexural moment of the specimen was very small. As to concrete strain, the other specimens showed almost the same results.

4.5 Energy Absorption and Damping Coefficient

The ability of energy absorption and damping within each cycle of loading will be discussed. The energy absorption can be determined as the area of the upper half loading loop A-B-C-A in Fig. 47, and the equivalent viscous damping coefficient (h_e) is expressed as follows:

$$h_e = \text{area (A-B-C-A)} \,/\, \text{area (}\triangle\text{OAD)} \,/\, 2\pi \qquad \cdots\cdots\cdots(2)$$

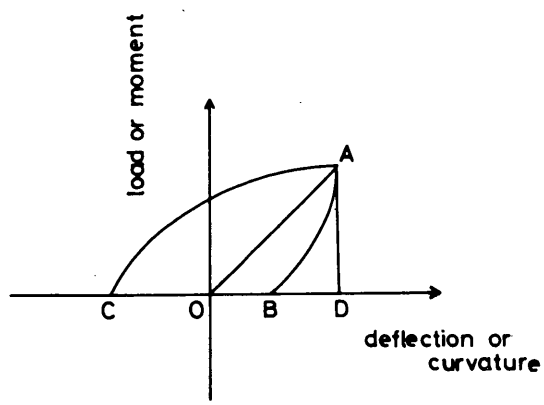

Fig. 47 Definition of energy absorption and h_e

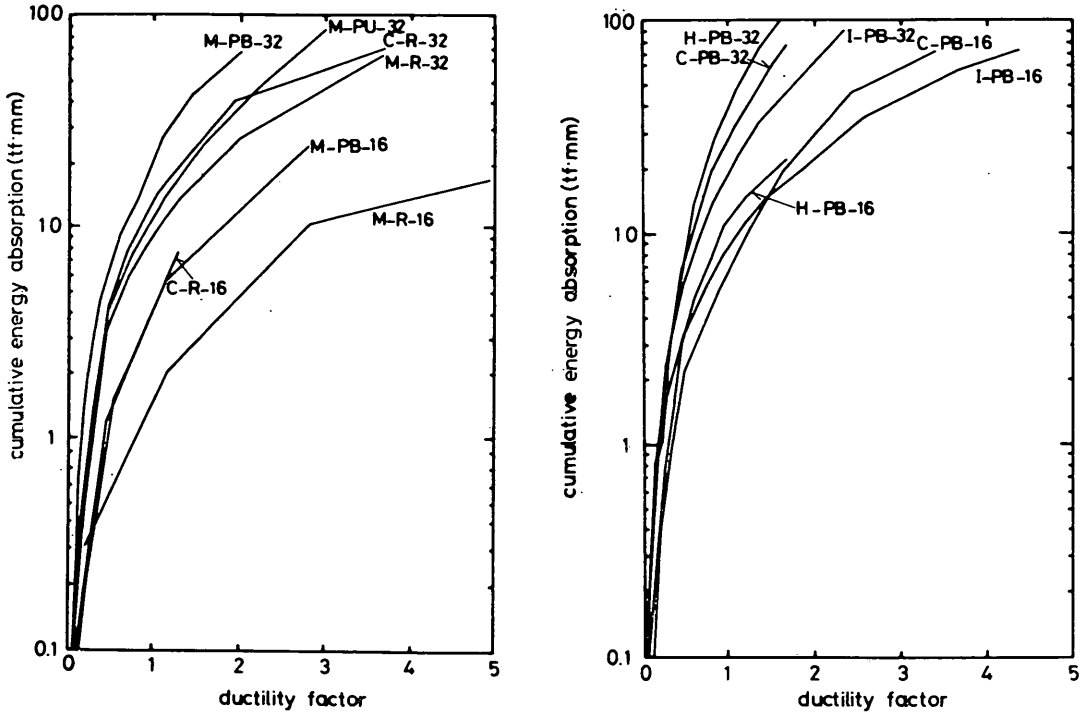

Fig. 48 Cumulative energy absorption

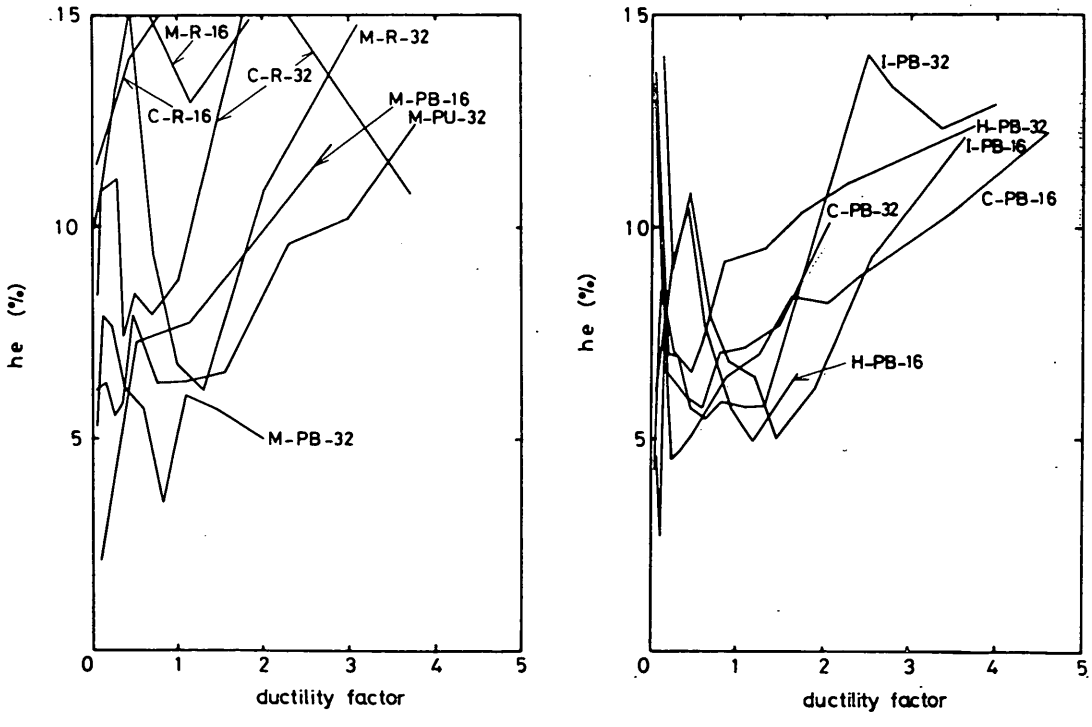

Fig. 49 Equivalent viscous damping coefficient

Figures 48 and 49 show the cumulative absorbed energy and the damping coefficient plotted against the ductility factor. The cumulative absorbed energy naturally increased as the number of cycles. The energy of the connected specimens were larger than that of the monolithic ones. However, the energy of all the PC specimens with the higher reinforcement ratio was almost the same. Moreover, the cumulative energy absorption of the bonded PC specimen was almost the same as that of the unbonded PC one.

The damping coefficient ranged from about 5% to 15% in all the specimens. These values are consistent with those recommended for ordinary PC and/or RC structures [10]. When the ductility factor exceeded 1.0, the damping coefficient became large with the increasing in the ductility factor. In general, the damping coefficient was very small within the elastic range. In this experimental results, however, large values of the damping coefficient were obtained up to the first yield (the ductility factor equals 1.0). The reason is that the procedure obtaining energy absorption up to the first yield was not accurate. In this experiment, a few loading-unloading loops were applied to the specimen up to the first yield.

5. Comparison of the Experimental Results with the Calculated Ones

5.1 Flexure and Shear Strength

Ultimate flexural moment and shear force of the specimens were calculated by the equations proposed in the limit state design method [11, 12, 13]. The outline of the calculation procedure is described below.

Design strength of the specimen subjected to the flexural moment is obtained on the basis of the following assumptions:

(a) Strains in reinforcements and concrete are directly proportional to the distance from the neutral axis.
(b) Tensile stress of concrete is neglected.
(c) The stress-strain diagram for concrete is defined in Fig. 50.
(d) The stress-strain diagram for steel is defined in Fig. 51.

Figure 52 gives stress and strain distributions for a member with a rectangular section subjected to the flexural moment. In the case of predominant bending, a simplified rectangular distribution of stress in concrete as defined in Fig. 52 is used.

The meanings of the symbols used in these figures are as follows:

A_s: area of tension reinforcement
A_s': area of compression reinforcement

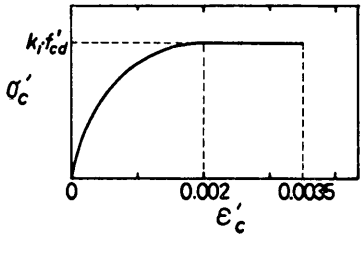

Fig. 50 Stress-strain diagram of concrete

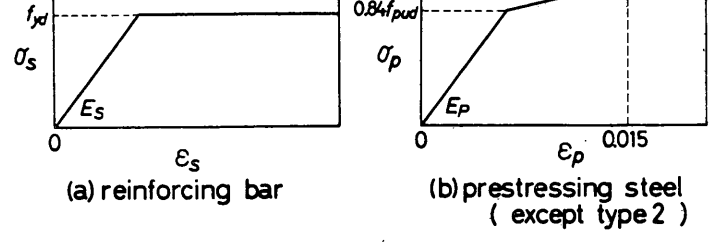

Fig. 51 Stress-strain diagram of steel reinforcement

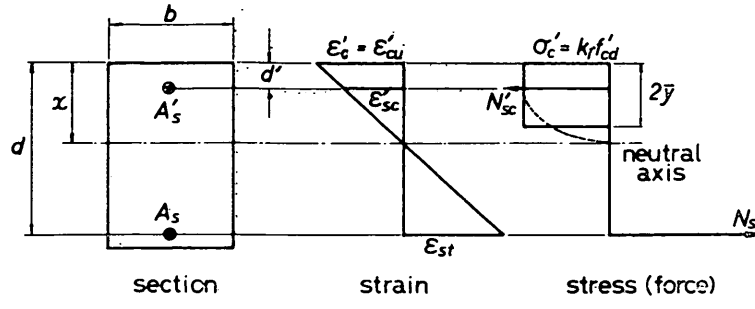

Fig. 52 Strain and stress distributions in the section at the ultimate

b : width of section
d : effective depth of tension reinforcement
d' : distance from extreme compression fiber to centroid of compressive reinforcement
f_{cd}' : design compressive strength of concrete
k_1 : coefficient for reduction in strength due to sustaining load (=0.85)
N_c' : resulting compressive force in the concrete section
N_s : tensile force in reinforcement
N_{sc}' : compressive force in reinforcement
x : neutral axis depth
$\bar{y}$: distance from extreme compression fiber to line of action for resulting compression force
ε_c' : compressive strain of concrete
ε_{cu}' : limiting concrete strain at the ultimate state
ε_{sc}' : compressive strain of compression reinforcement
ε_{st} : tensile strain of tension reinforcement

The equilibrium condition of inner axial forces is expressed as follows:

$$N_c'+N_{sc}'=N_s \qquad \cdots\cdots(3)$$

where, $N_{sc}'=\sum A_s'\sigma_{sc}'$ and $N_s=\sum A_s\sigma_s$. At the ultimate limit state, ε_c' is set equal to ε_{cu}' at the extreme compression fiber, and σ_c' is set equal to $k_1 f_{cd}'$. Therefore, N_c' is calculated by the following equation:

$$N_c'=0.85 f_{cd}' \cdot 0.8x \cdot b=0.68 \cdot b \cdot x \cdot f_{cd}' \qquad \cdots\cdots(4)$$

As the induced flexural moment by internal forces is equal to that by the external forces, the ultimate flexural moment M_u is obtained by the following equation:

$$M_u=N_c'\ (d-\bar{y})\ +N_{sc}'\ (d-d') \qquad \cdots\cdots(5)$$

Equations (3) and (5) can be expressed as functions of x. Therefore, once the value of x was determined, both the internal forces and the ultimate flexural moment can be obtained.

Design shear strength is calculated taking account of concrete strength, cross sectional dimensions of the member, the longitudinal reinforcement, and quantity and arrangement of shear reinforcement. The design shear strength V_{cd} contributed by factors other than shear reinforcement should be obtained by Eq. (6).

$$V_{cd}=f_{vd} \cdot b_w \cdot d/\gamma_b \qquad \cdots\cdots(6)$$
$$f_{vd}=f_{vod}\ (1+\beta_d+\beta_p+\beta_n)$$

$$f_{vod}=0.94f_{ck}'^{1/3}/\gamma_c$$
$$\beta_d=(100/d)^{1/4}-1\geqq 0 \quad (d:\text{cm})$$
$$\beta_p=(100\times p_w)^{1/2}-1\leqq 0.73$$
$$\beta_n=M_o/M_d\leqq 1$$

where,

f_{vd}: design shear strength of concrete
b_w: width of a member
p_w: ratio of reinforcement $(=A_s/b_wd)$
M_o: moment at the limit of inducing tensile stress at the section
M_d: design moment of resistance
γ_b: member factor
γ_c: material factor for concrete

When a crack occurs due to axial tension forces, it should be that $V_{cd}=0$.

Design shear strength V_{yd} contributed to the yield of shear reinforcement should be obtained by Eq. (7).

$$V_{yd}=A_wf_{wyd}z\ (\sin\alpha+\cos\alpha)\ /s/\gamma_b \qquad \cdots\cdots\cdots\cdots(7)$$

where,

A_w: area of shear reinforcement
f_{wyd}: design yield strength of shear reinforcement
z: distance from centroid of applied resulting compressive force to centroid of tension reinforcement (may be regarded as $d/1.15$)
α: angle between inclined stirrups and longitudinal axis of member
s: spacing of shear reinforcement in direction parallel to longitudinal reinforcement

The design shear strength V_d should be obtained by adding the values of V_{cd} and V_{yd}.

The beam-to-column joint in real structures will be subjected to both flexural

Table 10 The calculated ultimate strength

specimen	calculated strength		ultimate applied load ($\times 10^3$kgf)	exp./cal.	
	M_u($\times 10^5$kgf・cm)	V_d($\times 10^3$kgf)		moment	shear
M- R -16	1.60	16.1	2.2	1.63	7.32
M- R -32	4.36	17.3	4.3	1.16	4.02
M-P U-16	6.57	11.3	5.0	0.90	2.26
M-P U-32	11.59	12.2	10.5	1.07	1.16
M-P B-16	6.57	11.4	5.0	0.90	2.28
M-P B-32	11.59	12.3	10.0	1.02	1.23
C- R -16	1.60	16.1	1.7	1.26	9.47
C- R -32	4.36	17.4	4.5	1.22	3.87
C-P B-16	6.45	11.2	6.0	1.10	1.87
C-P B-32	11.34	12.1	10.9	1.14	1.11
A-P B-16	5.23	11.5	3.5	0.79	3.29
A-P B-32	7.84	12.5	5.5	0.83	2.27
H-P B-16	6.55	11.3	7.5	1.01	1.51
H-P B-32	11.30	12.0	13.5	1.05	0.89
I-P B-16	6.54	11.3	7.9	1.06	1.43
I-P B-32	11.88	12.6	14.0	1.04	0.90

and shear forces simultaneously. In the experiment in this study, however, the axial load was not applied to the column. Therefore, the specimens are in the predominant bending situation. Thus, the formulae in the limit state design method can be applied in calculating flexural and shear strengths of the specimens.

The calculated ultimate flexural moment (M_u) and shear force (V_d) are listed in Table 10. The experimental ultimate moments were almost the same as or slightly larger than the calculated ones of all the specimens except for the adhesive joint specimens. The ratio of the experimental ultimate moment to the calculated one ranged from 0.90 to 1.63; however, most of the ratios concentrated around 1.0. Thus the precise flexural moment of resistance could be predicted by the assumption of the limit state design method. On the other hand, the experimental ultimate moment of the adhesive joint specimens were considerably smaller than the calculated one, and their ratios were about 0.80. The absence of reinforcing bars through the joint surfaces in the specimen was taken into consideration into the calculation. That is, the area of reinforcing bars was set equal to zero in Eqs. (3) and (5).

According to the calculation, it was estimated that the load to cause the shear failure at the joint was considerably larger than that to cause the flexural failure. The experimental results were consistent with the estimation. Therefore, as far as experiments of this study cover, the design methods examined here were proved to be adequate. However, it was not possible to examine the adequacy of the calculated shear strength because the shear failure did not occur at the joints in all the specimens.

5.2 Crack Width

Several formulae regarding the crack width have been proposed. The formula proposed by CEB-FIP in 1978 [14] has been widely applied to offshore structures. This formula will be applied to predict the maximum crack width in this study. The applicability of the formula to the specimens with joints is examined.

The formula proposed by CEB-FIP is presented as follows:

$$w_k = 1.7 w_m \qquad \cdots\cdots\cdots\cdots (8)$$

$$w_m = S_{rm} \cdot \varepsilon_{sm}$$

$$S_{rm} = 2\left(c + \frac{c_\phi}{10}\right) + k_1 k_2 \frac{\phi}{\rho_r}$$

$$\rho_r = A_s / A_{c,ef}$$

$$\varepsilon_{sm} = \frac{\Delta\sigma_s}{E_s}\left\{1 - \beta_1\beta_2\left(\frac{\Delta\sigma_{sr}}{\Delta\sigma_s}\right)^2\right\} \geqq 0.4\frac{\Delta\sigma_s}{E_s}$$

where,

w_k: characteristic crack width
c: concrete cover thickness
c_ϕ: spacing of bars
ϕ: diameter of steel
$A_{c,ef}$: effective embedded zone where reinforcing bars can effectively influence the crack widths
$\Delta\sigma_s$: stress increment of reinforcement in the cracked section
E_s: modulus of elasticity of reinforcement
$\Delta\sigma_{sr}$: stress of reinforcement calculated in the cracked section where the maximum tensile stress in concrete (uncracked section) is taken equal to tensile strength of concrete
k_1: coefficient expressing influence of bond behavior of reinforcement

Table 11 The applied load at each crack width

specimen	crack width of 0.1mm			crack width of 0.2mm			crack width of 0.3mm		
	cal. ($\times 10^3$kgf)	exp. ($\times 10^3$kgf)	exp./cal.	cal. ($\times 10^3$kgf)	exp. ($\times 10^3$kgf)	exp./cal.	cal. ($\times 10^3$kgf)	exp. ($\times 10^3$kgf)	exp./cal.
M- R -16	0.2	1.0	5.0	0.3	1.1	3.7	0.3	1.2	4.0
M- R -32	0.6	1.2	2.0	1.1	1.6	1.5	1.6	2.1	1.3
M-P U-16	1.9	2.1	1.1	2.1	2.5	1.2	2.3	2.8	1.2
M-P U-32	4.1	3.6	0.9	4.9	4.8	1.0	5.8	5.6	1.0
M-P B-16	2.1	2.4	1.1	2.5	3.0	1.2	2.9	3.3	1.1
M-P B-32	4.3	3.4	0.8	5.4	4.4	0.8	6.5	5.6	0.9
C- R -16	0.2	0.7	3.5	0.3	0.8	2.7	0.3	1.0	3.3
C- R -32	0.6	1.4	2.3	1.1	1.9	1.7	1.6	2.5	1.6
C-P B-16	2.1	2.3	1.1	2.5	3.2	1.3	2.8	3.6	1.3
C-P B-32	4.3	3.6	0.8	5.4	5.0	0.9	6.5	6.2	1.0
P-P B-16	1.5	2.2	1.5	1.6	2.5	1.6	1.7	2.7	1.6
A-P B-32	2.8	3.1	1.1	2.9	3.6	1.2	3.2	4.0	1.3
H-P B-16	2.8	3.1	1.1	3.3	3.9	1.2	3.8	4.4	1.2
H-P B-32	5.7	4.0	0.7	7.1	6.0	0.8	8.6	7.6	0.9
I-P B-16	2.8	4.8	1.7	3.3	5.4	1.6	3.8	6.2	1.6
I-P B-32	5.9	7.0	1.2	7.4	8.8	1.2	8.9	10.4	1.2

k_2: coefficient expressing influence of the form of stress diagrams
β_1: coefficient related to bond properties of bars ($=1/2.5\ k_1$)
β_2: coefficient related to the influence of the duration of the application or repetition of the loads

This formula is applicable to calculate crack widths under the pure flexural state.

The comparison between the calculated crack width and the experimental one was made in the following procedure: By Eq. (8), the bar stress increments ($\Delta\sigma_s$) corresponding to the crack widths 0.1, 0.2, and 0.3 mm were calculated. Then the forces which causes those bar stress increments were obtained. Those calculated forces were compared with the applied loads in the experiment. When the calculated force is smaller than the applied load at the same crack width, it is considered that the calculated crack width is conservatively estimated at the same loads.

The calculated forces corresponding to crack widths 0.1, 0.2, and 0.3 mm are listed in Table 11. At the same crack width, the applied loads to almost all the specimens were larger than the calculated forces. However, the reverse results were observed in some specimens with the higher reinforcement ratio. In this experiment, shear stress occurred as well as flexural stresses. Although this formula had been developed under the pure-bending situation, the safe side values of crack widths at joint was obtained by this formula.

5.3 Cracking Moment

The experimental cracking moments and the calculated ones are listed in Table 12. The cracking moment was calculated by the following equation. This equation was proposed for flexural cracks.

$$M_c=(f_{ct}+\sigma_{pe})\cdot I_{cc}/h/2 \qquad \cdots\cdots\cdots(9)$$

where, f_{ct}: modulus of rapture of concrete
σ_{pe}: stress at the centroid of the concrete section due to the final prestress-

Table 12 Cracking moment

specimen	I_{cc} (cm⁴)	f_{ct} (kgf/cm²)	M_c (×10⁵kgf·cm)		exp./cal.
			cal.	exp.	
M- R -16	71650	40.8	1.95	1.18	0.61
M- R -32	76261	40.8	2.07	1.77	0.86
M-P U-16	70910	48.7	3.25	2.95	0.91
M-P U-32	75393	48.7	4.46	3.54	0.79
M-P B-16	73502	48.7	3.37	2.95	0.88
M-P B-32	79443	48.7	4.70	3.54	0.75
C- R -16	71650	40.8	1.95	0.59	0.30
C- R -32	79261	40.8	2.07	1.77	0.86
C-P B-16	74093	46.8	3.30	1.77	0.54
C-P B-32	80617	46.8	4.67	3.54	0.76
A-P B-16	74161	49.4	3.43	2.36	0.69
A-P B-32	80584	46.8	4.66	4.72	1.01
H-P B-16	74167	49.4	3.43	2.64	0.77
H-P B-32	79589	47.6	4.65	2.64	0.57
I-P B-16	74241	45.2	3.23	3.08	0.95
I-P B-32	80030	44.4	4.50	3.52	0.78

ing force

I_{cc}: moment of inertia of uncracked composite section

h: overall thickness or depth of member

The experimental cracking moment was the applied one when a crack was initiated. The calculated moments were considerably larger than the experimental ones in all the specimens. The cause is considered that the loss of the prestressing force was more than that had been expected and so on.

Table 13 Calculated stiffness at the fractured section

specimen	E_c (×10⁵kgf/cm²)	stiffness (×10⁷kgf/cm)		
		initial	at the first yield	at the ultimate
M- R -16	2.08	1490	17	1
M- R -32	2.08	1586	369	8
M-P U-16	2.53	1860	249	30
M-P U-32	2.53	2010	526	122
M-P B-16	2.53	1860	249	30
M-P B-32	2.53	2010	526	122
C- R -16	2.08	1490	17	1
C- R -32	2.08	1586	369	8
C-P B-16	2.31	1712	254	33
C-P B-32	2.31	1862	524	134
A-P B-16	2.28	—	—	—
A-P B-32	2.31	—	—	—
H-P B-16	2.28	1691	239	29
H-P B-32	2.51	1998	559	149
I-P B-16	2.25	1670	239	29
I-P B-32	2.41	1929	485	97

5.4 Stiffness and Neutral Axis

The stiffness was defined as the product of the effective moment of inertia and the modulus of elasticity of concrete. The modulus of elasticity of concrete was measured in the preliminary experiment. The calculated flexural stiffness is listed in Table 13. In the calculation, the effective moment of inertia was obtained under the same assumptions as those in the limit state design method described in **5.1.** Namely, the location of the neutral axis due to the external load was calculated, and then the effective moment of inertia about the neutral axis was computed.

The experimental initial stiffnesses (see Fig. 17) of all the specimens were about 1.1 to 1.2 times as large as the calculated ones. Furthermore, the experimental stiffness at the first yield was also considerably larger than the calculated one.

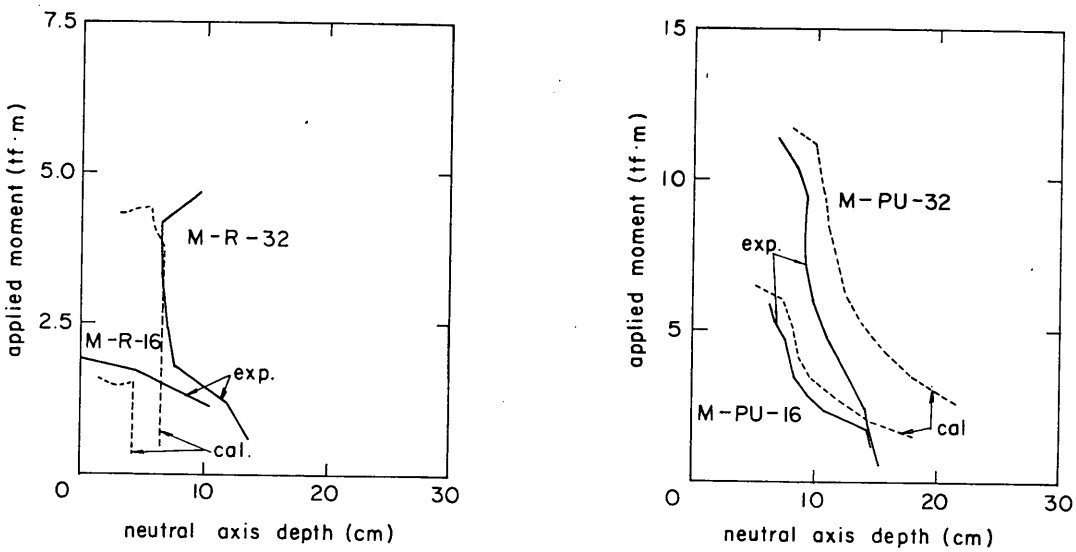

Fig. 53 Variation of neutral axis depth (M-R and M-PU)

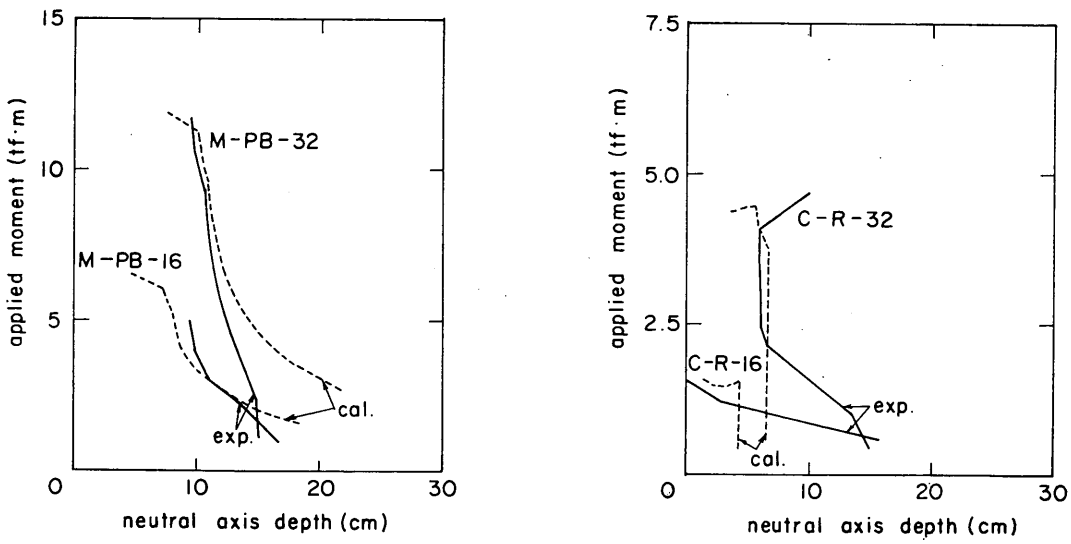

Fig. 54 Variation of neutral axis depth (M-PB an C-R)

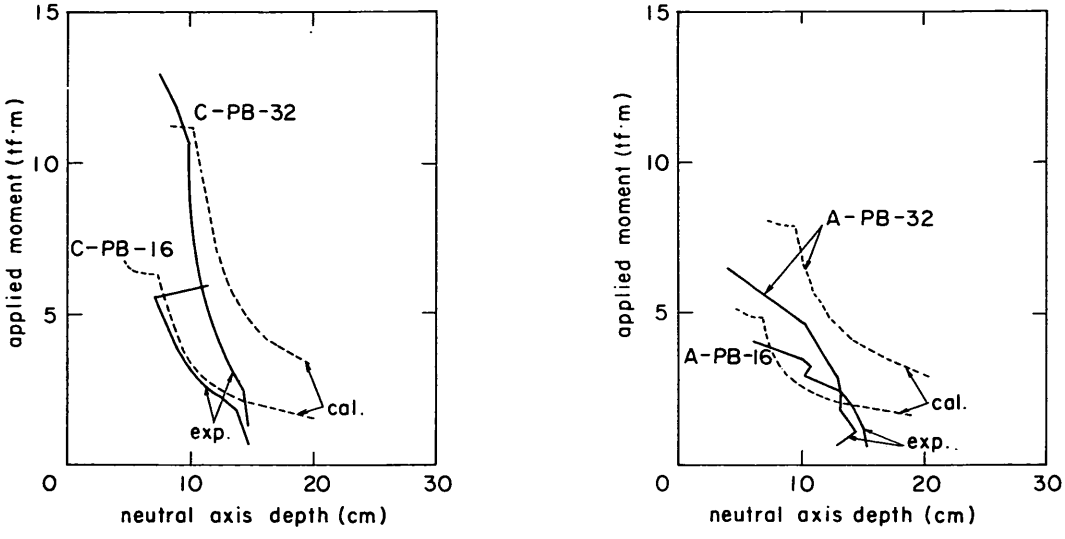

Fig. 55 Variation of neutral axis depth (C-PB and A-PB)

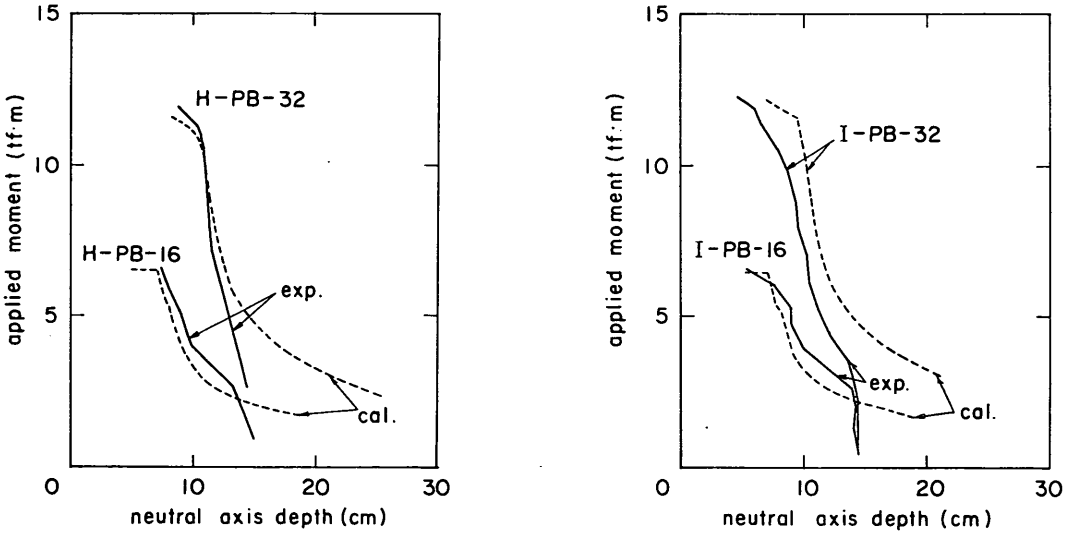

Fig. 56 Variation of neutral axis depth (H-PB and I-PB)

The location of a neutral axis has an effect on the stiffness of the specimen. The neutral axis depth refers to the distance from the extremely compressive fiber of concrete to the neutral axis. The variation of the depth of the experimental and the calculated neutral axes at the joint are shown in Figs. 53 through 56. The experimental neutral axis depth was obtained by measured strains in bars and concrete. The initial values of the neutral axis depth obtained in the PC specimens were much different from those obtained by the calculation. Regarding the prestressing force as the axial compressive force of the specimen caused these differences. The difference of the experimental results and the calculated ones of the neutral axis depth became smaller as the applied load was increased. Therefore, all the specimens showed the larger experimental stiffness than the computed one, and the differences between the

two values became smaller as the applied load was increased.

6. Conclusions

This paper describes the results of the static loading tests of the five kinds of beam (or slab)-to-column joints in offshore structures and the examination on the applicability of the limit state design method to those joints. The fundamental mechanical properties of the joints were made clear. The following conclusions were obtained from the research work:

1) There was not much difference between the monolithic specimens and the connected specimens with the cast-in-place joint, the haunch joint or the insertion joint with regard to the ultimate flexural moment. However, the ultimate flexural moment of the connected specimen with the adhesive joint was lower than those of the other specimens.
2) Flexural cracks occurred at the joints in all the specimens. However, the location of the crack formation is the joint differed among the specimens. The outline of the crack formation was as follows: Cracks concentrated at the two joint faces of the cast-in-place concrete region. Cracks concentrated only the joint face of the adhesive joint specimens. Shear cracks occurred in the haunch region of the haunch joint specimens after the formation of flexural cracks.
3) Flexural stiffness deterioration and equivalent damping coefficient were obtained from the load-deflection relationships. The stiffness became 20 to 30% of the initial stiffness at the first yield of reinforcing bars. The equivalent damping ratio ranged from 5 to 7% at the first yield. The ductility factors at the ultimate of all the specimens except for the adhesive joint specimens were almost the same.
4) The width of cracks in the adhesive joint specimens was larger than that in other joints at the same flexural moment. Consequently, the application of the adhesive joint to offshore structures should be made after careful consideration on the durability.
5) The ultimate strength of the joints obtained by the loading tests was 0.8 to 1.6 times as large as those calculated by the limit state design method. Therefore, it could be said that the joints mentioned in this paper had the safety in respect to the ultimate strength.
6) The crack widths in the joints obtained from the experiment were generally smaller than those obtained from the formula suggested in "CEB-FIP Model Code for Concrete Structures." The applicability of the limit state design method to the design of the joints was confirmed on the crack width under the static loading.

(Received on June 18, 1986)

Acknowledgements

The tests reported herein were conducted as a part of researches on the "Utilization of Marine Space by Coastal and Offshore Structures," and made possible by the support of the Special Coordination Funds for Promoting of the Science and Technology Agency of Japanese Government.

The tests were carried out in cooperation with the Japan Prestressing Concrete Engineering Association (PCEA). The members of PCEA who shared in the tests; Messrs. Muneto Abe, Osamu Kohriyama, Koichi Minamikawa, and Kunihiro Mukai are fully acknowledged for their assistance.

References

[1] OGURA, K. and SEKINE, M: The State of the Art of the Studies on the Reinforced Concrete Beam to Column Joint, *Concrete Journal,* Vol. 19, No. 9, September 1981, pp. 3-15 (in Japanese).

[2] AIHARA, T: Connections of Prefabricated Structures, Prestressed Concrete Connections, *Kenchiku Gijutsu,* July 1976, pp. 294-302 (in Japanese).

[3] SHINAGAWA, T.: Connections of Prefabricated Reinforced Concrete Structures, *Concrete Journal,* Vol. 11, No. 11, November 1973, pp. 75-81 (in Japanese).

[4] FIP: *Recommendations for the Design and Construction of Concrete Sea Structures,* 4th Edition, 1983, 125p.

[5] Ports and Harbours Bureau, and Port and Harbour Research Institute, Ministry of Transport: *Technical Standards for Port and Harbour Facilities in Japan,* April 1980, p. 3-22.

[6] JSCE: *Standard for Prestressed Concrete Structures,* January 1979, 210p. (in Japanese).

[7] NAAMAN, A. E.: *Prestressed Concrete Analysis and Design, Fundamentals,* McGraw-Hill Book Company, 1982, pp. 275-316.

[8] YOKOI, T. et al.: Strength and Deformation Behaviors of Beam-Column Joints in Offshore Structures, *Transactions of the JCI,* Vol. 6, 1984, pp. 605-612.

[9] KIYOMIYA, O., YOKOTA, H., and YOKOI, T.: Strength Evaluation of Beam-Column Joints in Offshore Structures, *Proc. of the JSCE 10th Symposium on Ocean Development,* June 1985, pp. 184-189 (in Japanese).

[10] Committee on Reinforced Concrete Column, Building Center of Japan: Synthetic Experimental Research on Improving Ductility of Reinforced Concrete Columns under Cyclic Lateral Loads, *Concrete Journal,* Vol. 13, No. 1, January 1975, pp. 2-18 (in Japanese).

[11] JSCE Concrete Committee on Limit State Design: Recommendations for Limit State Design of Concrete Structures, *Concrete Library of JSCE,* No. 4, December 1984, pp. 1-102.

[12] OKAMURA, H.: *Limit State Design Method for Concrete Structures,* Second Edition, Kyoritsu Shuppan, 1984, 183p. (in Japanese)

[13] FIP: *Practical Design of Reinforced and Prestressed Concrete Structures,* Thomas Telford Limited, 1984, 36p.

[14] CEB and FIP: *Model Code for Concrete Structures,* CEB-FIP International Recommendations 3rd Edition, 1978, pp. 156-160.

List of Symbols

$A_{c,ef}$: effective embedded zone where reinforcing bars can effectively influence the crack width
A_s: area of tension reinforcement
A_s': area of compression reinforcement
A_w: area of shear reinforcement
b: width of section
b_w: width of member
c: concrete cover for embedded reinforcing bars

c_ϕ: spacing of bars
d: effective depth of tension reinforcement
d': distance from extreme compression fiber to centroid of compressive reinforcement
E_c: modulus of elasticity of concrete
E_s: modulus of elasticity of reinforcement
f_c': specified compressive strength of concrete
f_{cd}': design compressive strength of concrete
f_{ck}': characteristic compressive strength of concrete
f_{ct}: bending-tensile strength of concrete
f_{pud}: design tensile strength of prestressing steel
f_{vd}: design shear strength of concrete
f_{vod}: apparent design shear strength of concrete
f_{wyd}: design yield strength of shear reinforcement
f_{yd}: design yield strength of reinforcement
h: overall thickness or depth of member
h_e: equivalent viscous damping coefficient
I_{cc}: moment of inertia of uncracked composite section
i: used as a subscript to describe ith loading cycle
K: flexural stiffness
k_1: coefficient for reduction in strength due to sustaining load (**Chap. 5**)
k_1: coefficient expressing influence of bond behavior of reinforcement
k_2: coefficient expressing influence of the form of the stress diagram
M: applied moment in general
M_o: moment at the limit of inducing tensile stress at a section considered
M_c: first cracking moment
M_d: design moment of resistance
M_u: ultimate flexural moment
M_y: first yielding moment
N_c': resulting compressive force in the concrete section
N_s: resulting tensile force of tension reinforcement
N_{sc}': resulting compressive force of compression reinforcement
p_w: ratio of longitudinal reinforcement to area of web concrete
s: spacing of shear reinforcement in direction parallel to longitudinal reinforcement
S_{rm}: average distance between cracks
V_{cd}: resistant shear force without shear reinforcement
V_d: design shear strength
V_{yd}: resistant shear force when shear reinforcement yields
w_k: characteristic crack width
w_m: mean crack width
x: neutral axis depth
$\bar{y}$: distance from extreme compression fiber to line of action for resulting compression force
z: distance from centroid of applied resulting compressive force to centroid of tension reinforcement
α: angle between inclined stirrups and longitudinal axis of member
β_1: coefficient related to bond properties of bars
β_2: coefficfent related to the influence of the duration of the application or repetition of the loads
β_d: coefficient to take account of influence of effective depth on shear strength

β_n: coefficient to take account of influence of axial force on shear strength
β_p: coefficient to take account of influence of longitudinal reinforcement on shear strength
γ_b: member factor
γ_c: material factor for concrete
δ_y: deflection at the first yield
δ_u: deflection at the ultimate
μ: ductility factor at the ultimate
π: circular constant
$\Delta\sigma_s$: stress increment of reinforcement in cracked section
$\Delta\sigma_{sr}$: stress of reinforcement calculated in the cracked section where the maximum tensile stress of concrete (uncracked section) is taken equal to tensile strength of concrete
ε_c': concrete compressive strain
ε_{cu}': limiting concrete strain at the ultimate state
ε_p: strain of prestressing bar
ε_s: strain of reinforcement
ε_{sc}': compressive strain of compression reinforcement
ε_{sm}: mean elongation
ε_{st}: tensile strain of tension reinforcement
σ_c': concrete compressive stress
σ_p: stress of prestressing bar
σ_{pe}: effective prestressing stress
σ_s: stress of tension reinforcement
σ_{sc}': stress of compression reinforcement
ϕ: diameter of steel or curvature of section
ρ_r: reinforcement ratio

Abbreviations
A : adhesive joint specimen
C : cast-in-place concrete joint specimen
H : haunch joint specimen
I : insertion joint specimen
M : monolithic joint specimen
PB : bonded prestressed concrete specimen
PC : prestressed concrete in general
PU : unbonded prestressed concrete specimen
R : reinforced concrete specimen
RC : reinforced concrete in general

Abbreviations for Professional Organizations and Standard
CEB : Comité Européen du Béton
FIP : Fédération Internationale de la Précontrainte
JCI : Japan Concrete Institute
JIS : Japanese Industrial Standard
JSCE : Japan Society of Civil Engineers

Appendix A. Details of the Specimen

The details of the specimens are shown in Figs. A1 through A7.

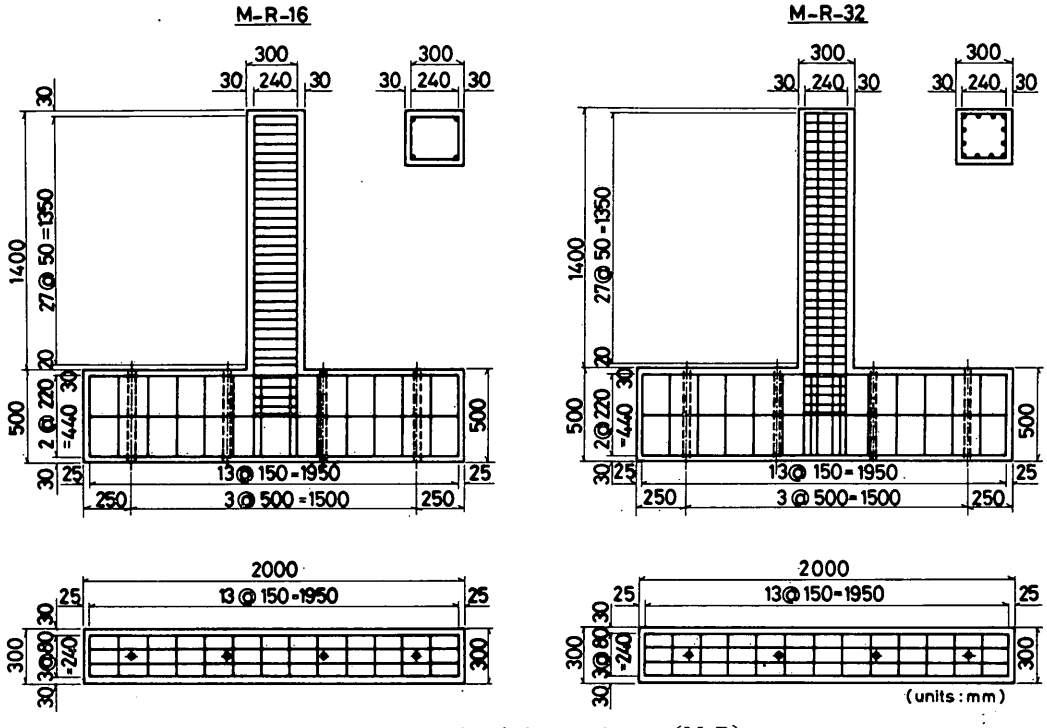

Fig. A1 Details of the specimens (M-R)

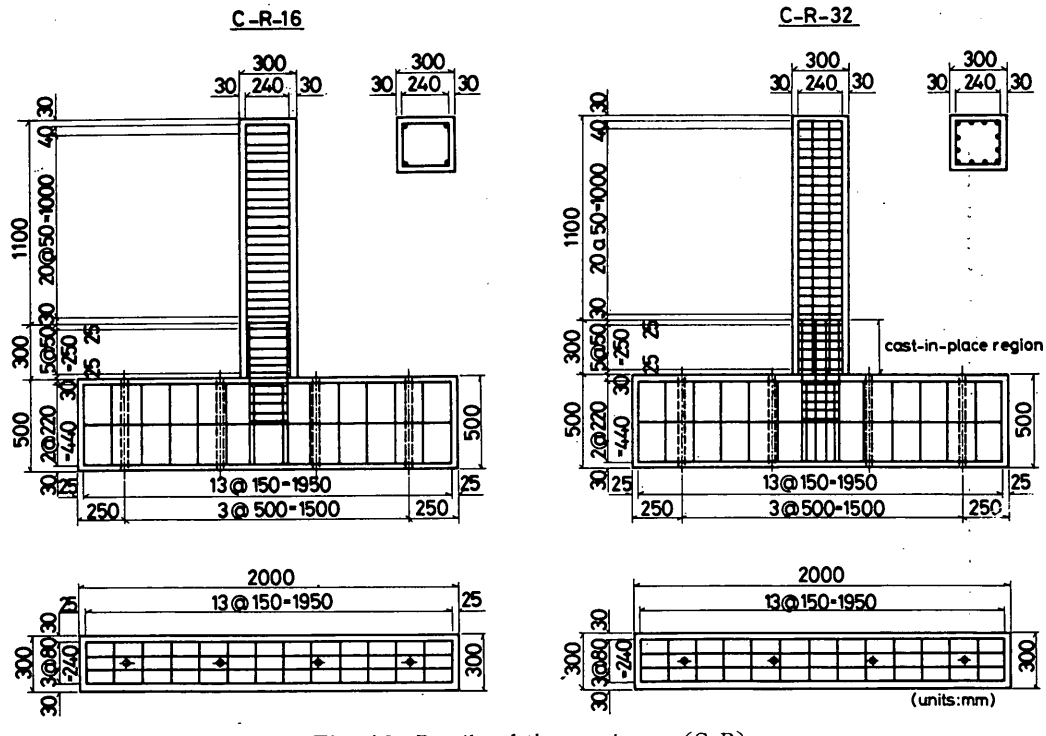

Fig. A2 Details of the specimens (C-R)

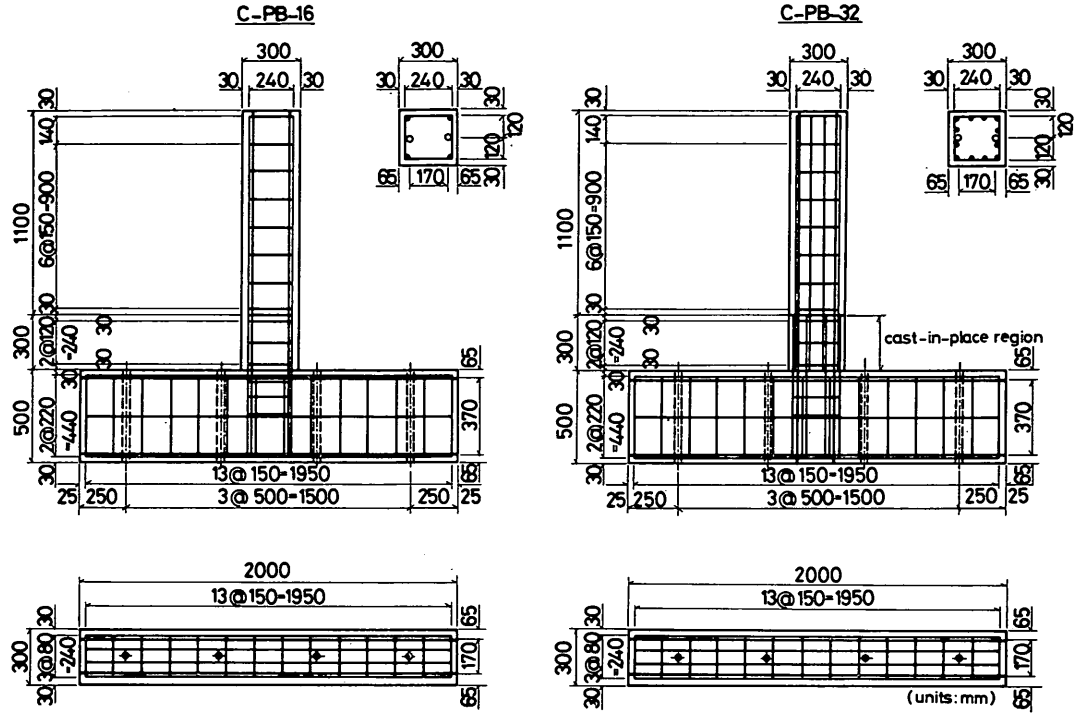

Fig. A3 Details of the specimens (C-PB)

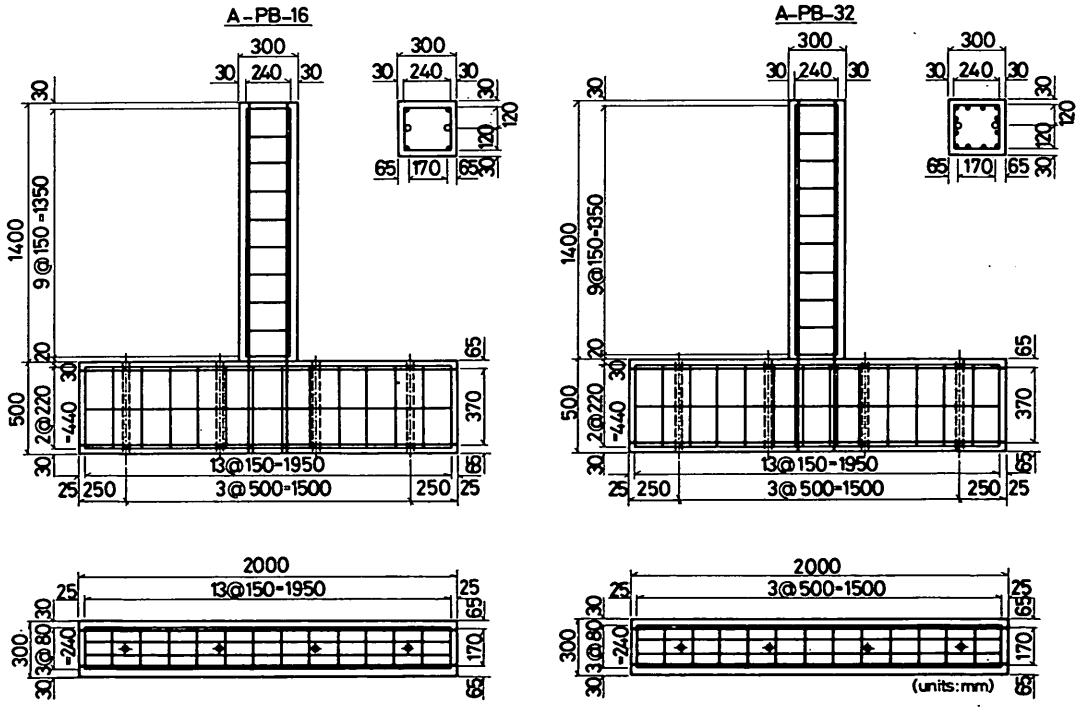

Fig. A4 Details of the specimens (A-PB)

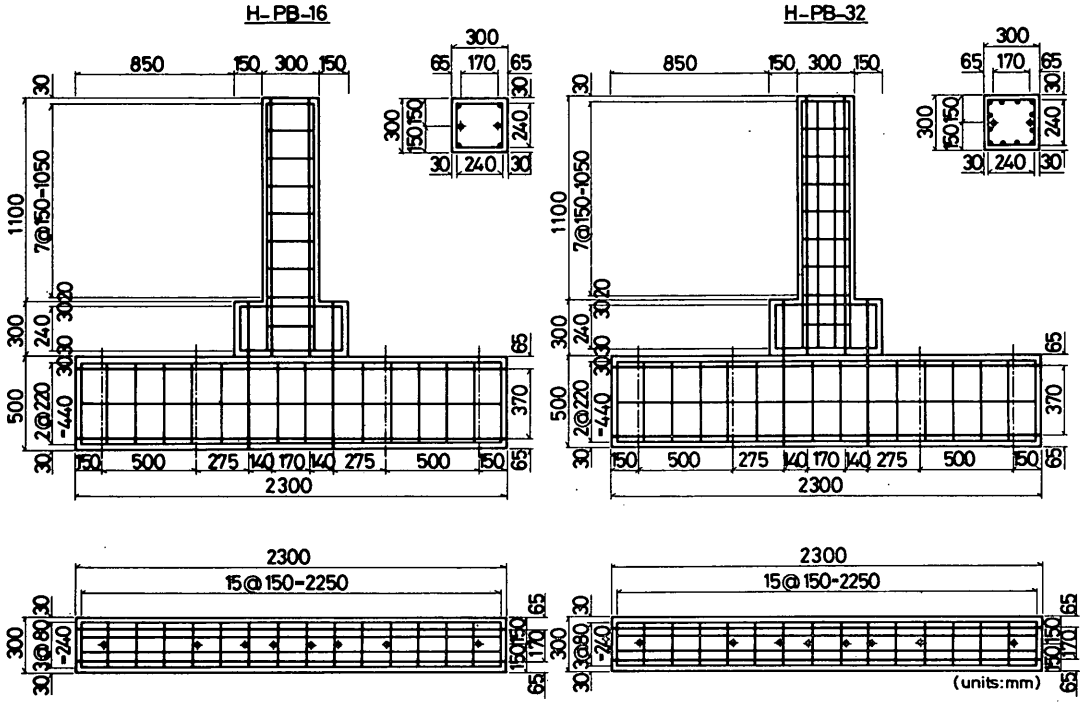

Fig. A5 Details of the specimens (H-PB)

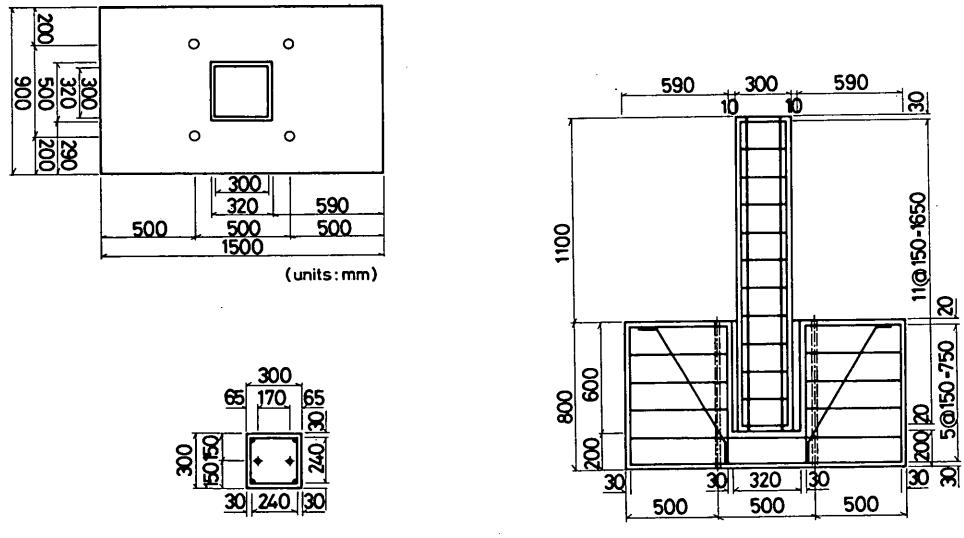

Fig. A6 Details of the specimen (I-PB-16)

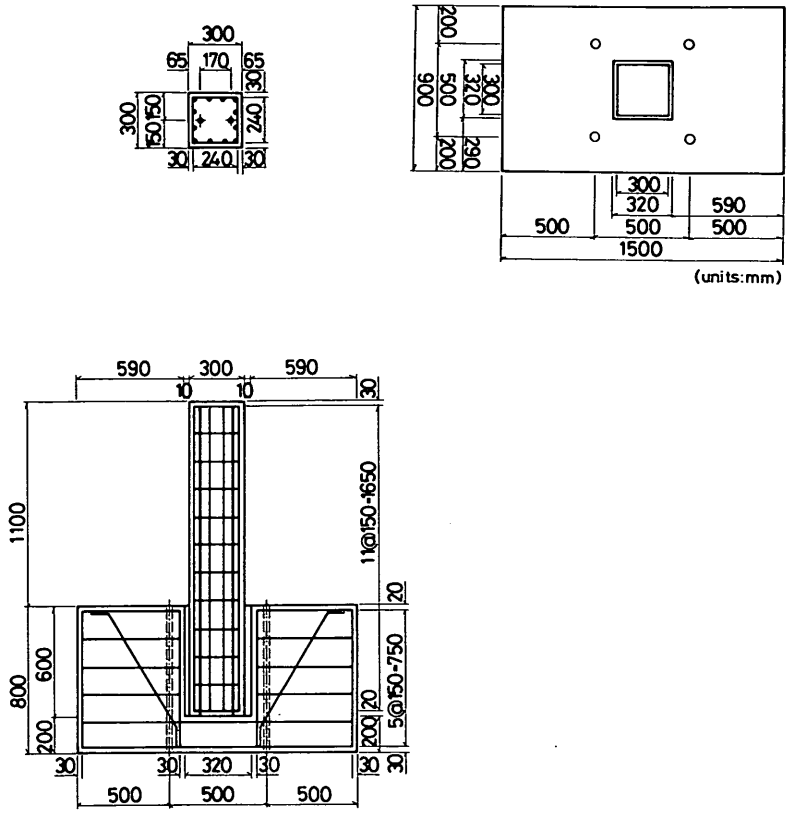

Fig. A7 Details of the specimen (I-PB-32)

Appendix B. The Location of Instrumentation

The location of electrical resistant strain gauges attached in bars and on the concrete surface are shown in Figs. B1 through B5.

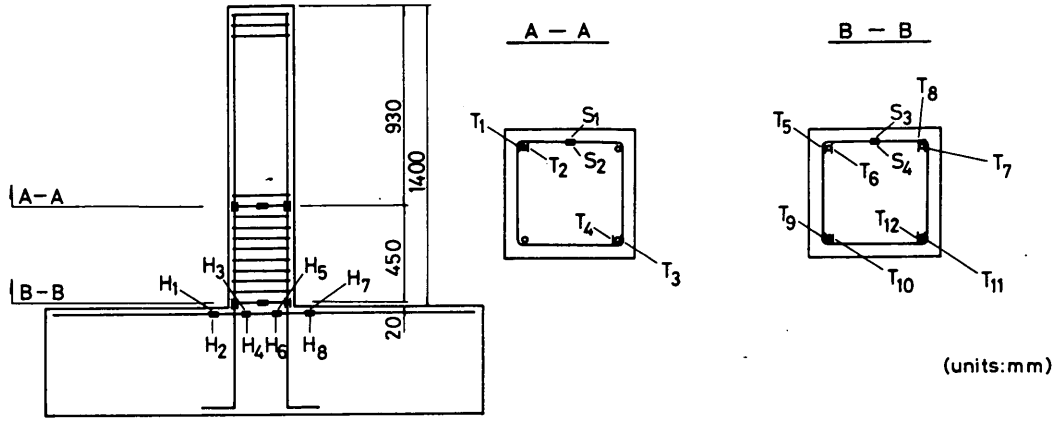

Fig. B1 Location of strain gauges in steel bars (M-R and C-R)

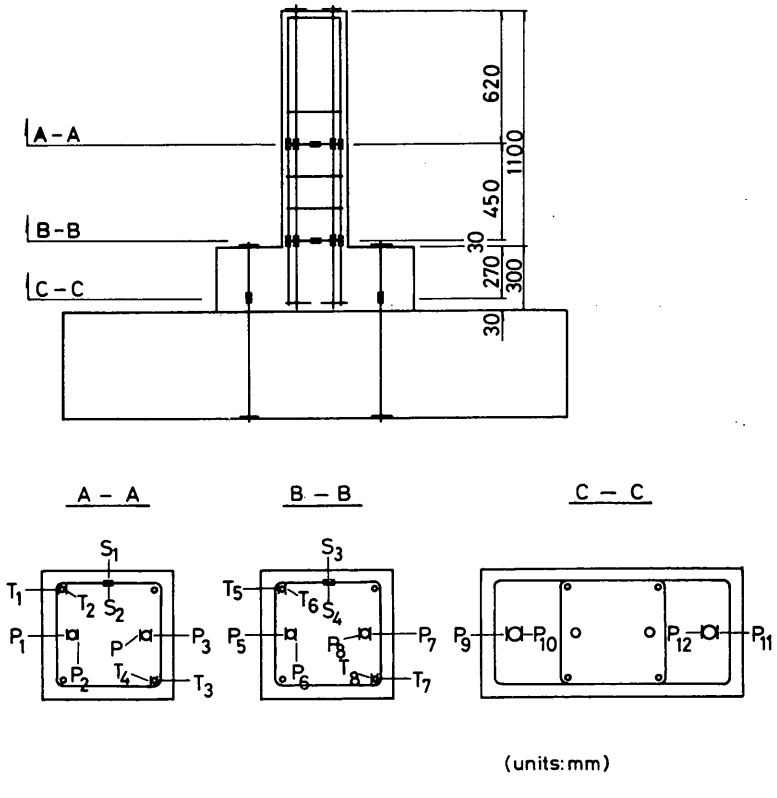

Fig. B2 Location of strain gauges in steel bars (H-PB)

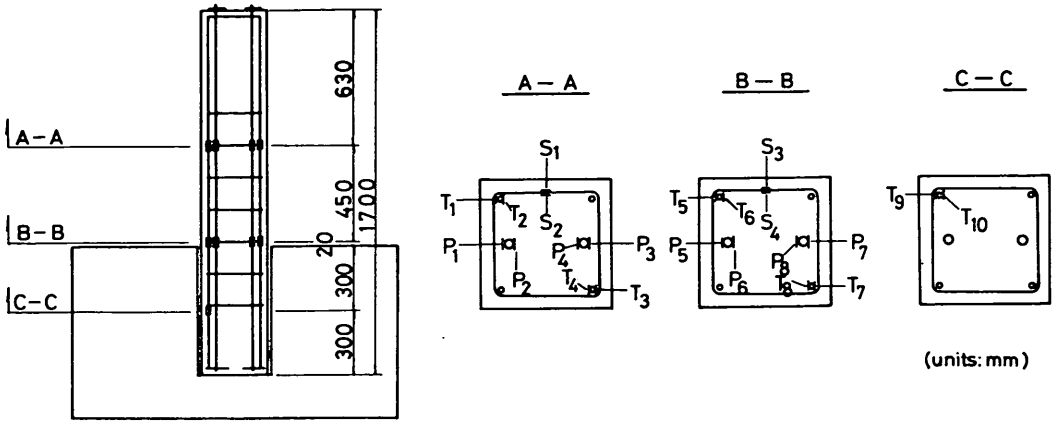

Fig. B3 Location of strain gauges in steel bars (I-PB)

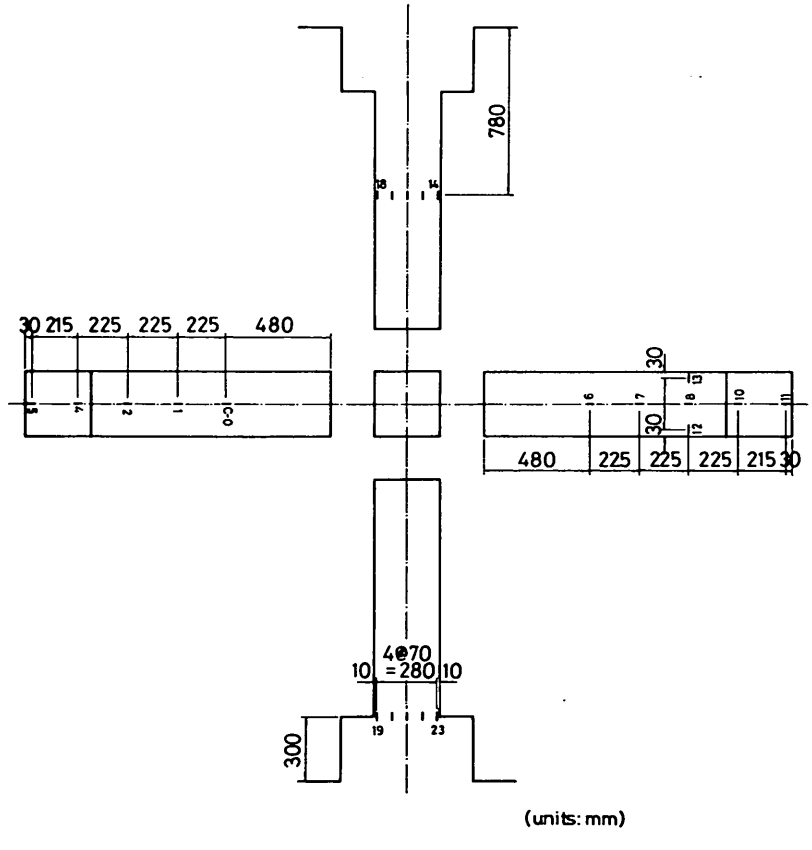

Fig. B4 Location of strain gauges on the concrete surface (H-PB)

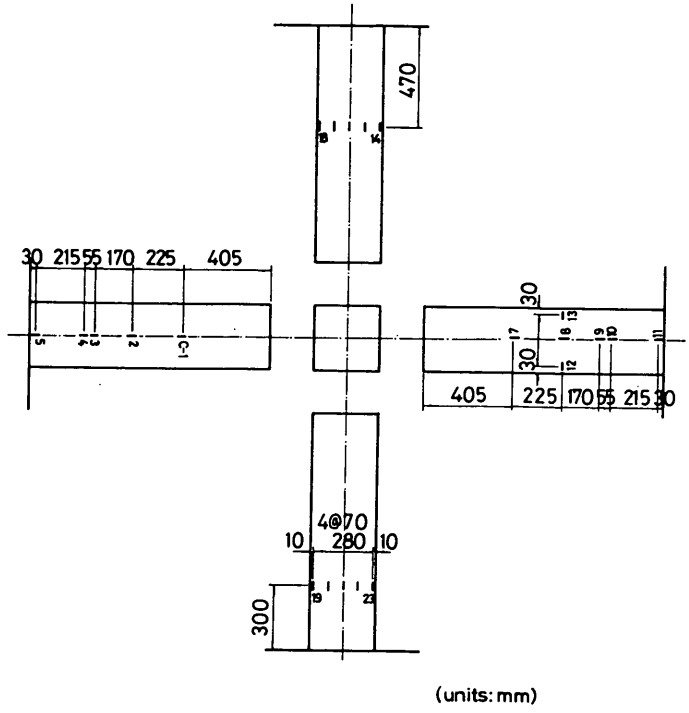

Fig. B5 Location of strain gauges on the concrete surface (I-PB)

Appendix C. The Load-Deflection Relationship

The measured actual load-deflection curves of all the specimens are shown in Figs. C1 through C16. The deflection was measured at the loading point. The load was applied towards its negative value at first. Then the load was decreased and increased to the positive value. In the experiment, this loading pattern was repeated up to the ultimate.

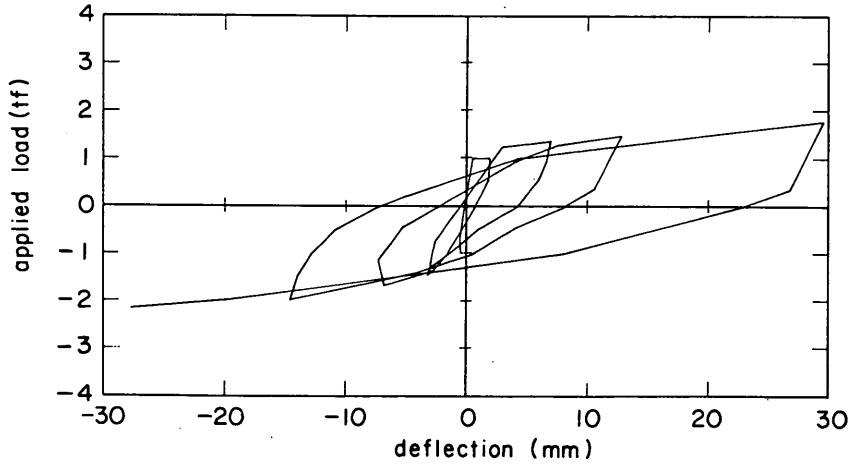

Fig. C1 Load-deflection curve (M-R-16)

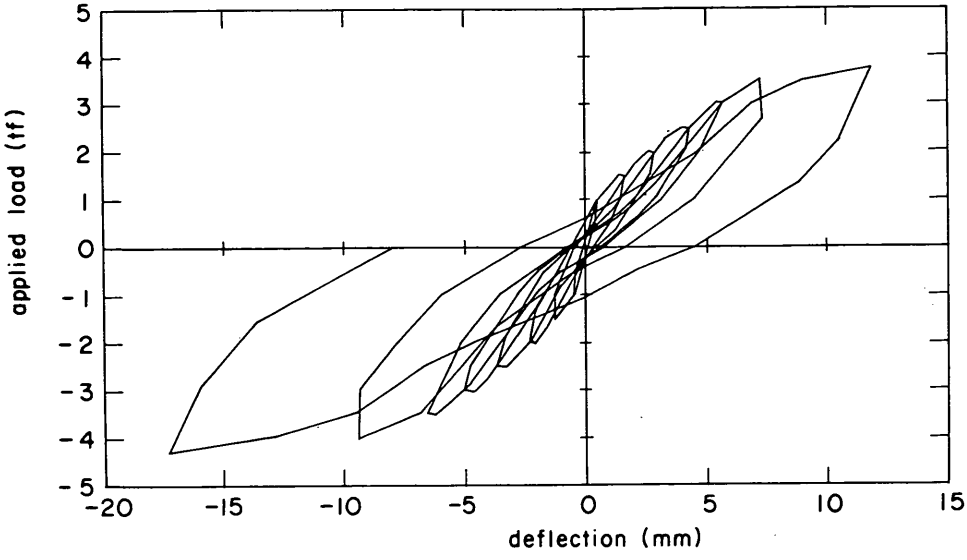

Fig. C2 Load-deflection curve (M-R-32)

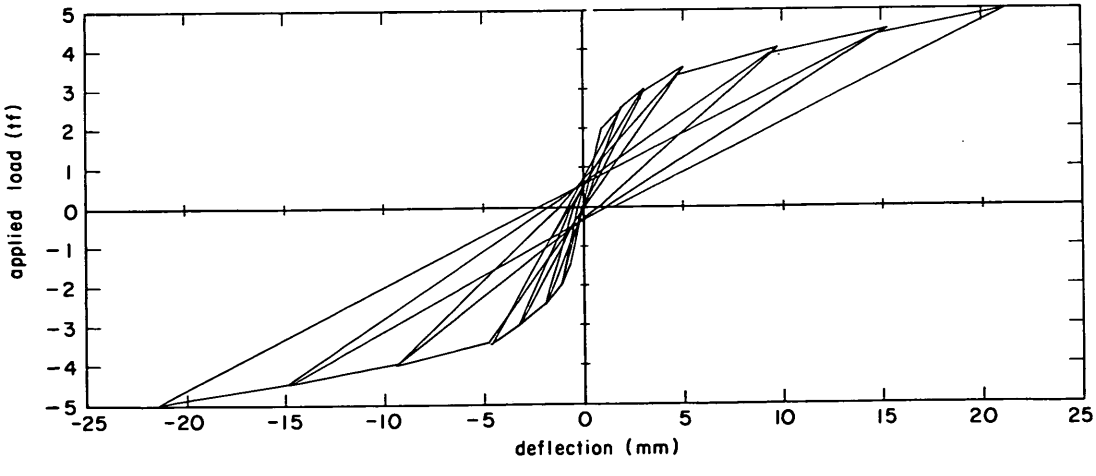

Fig. C3 Load-deflection curve (M-PU-16)

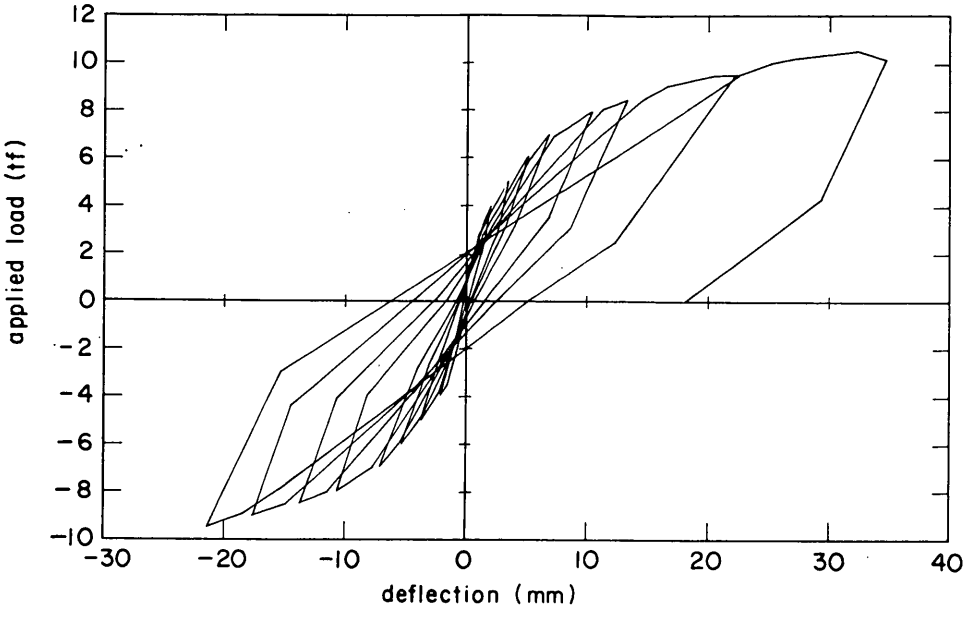

Fig. C4 Load-deflection curve (M-PU-32)

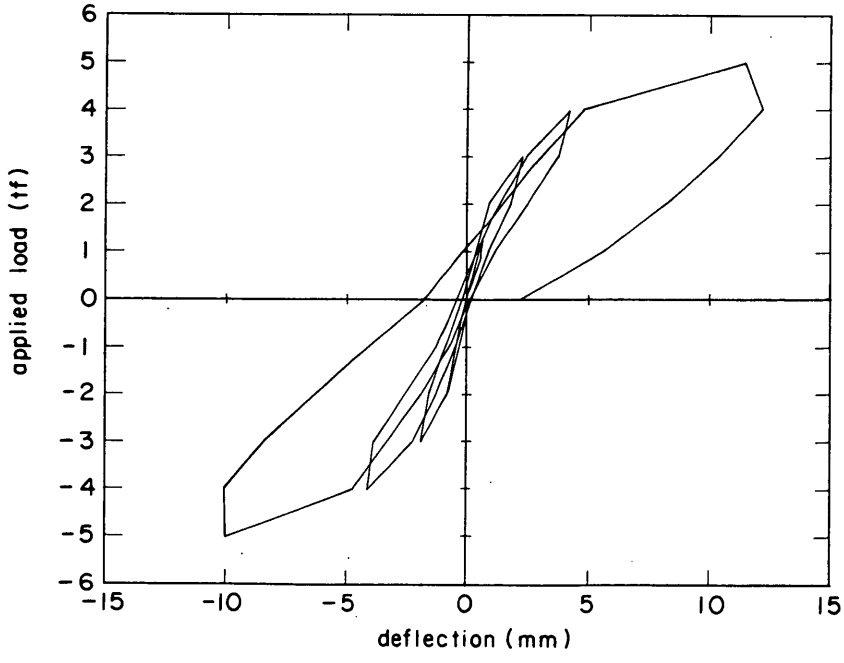

Fig. C5 Load-deflection curve (M-PB-16)

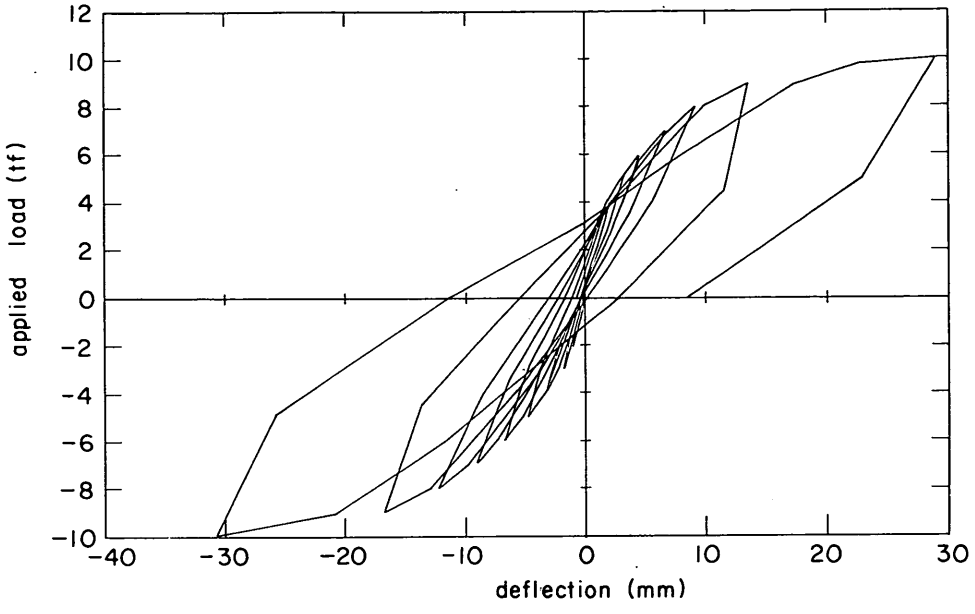

Fig. C6 Load-deflection curve (M-PB-32)

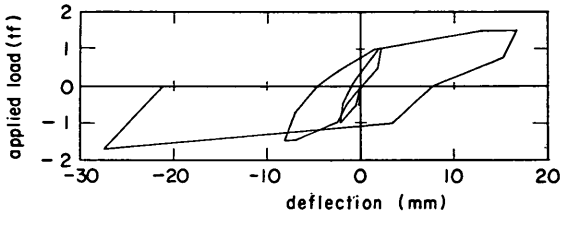

Fig. C7 Load-deflection curve (C-R-16)

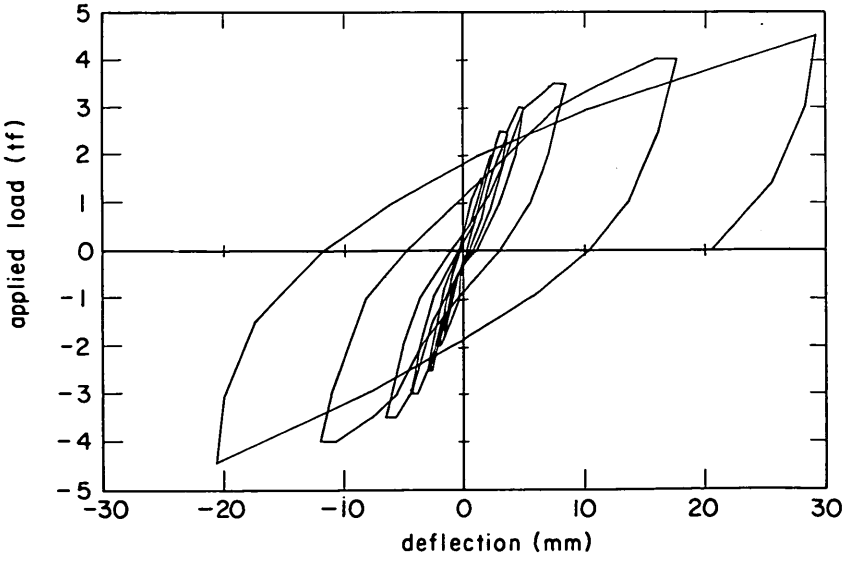

Fig. C8 Load-deflection curve (C-R-32)

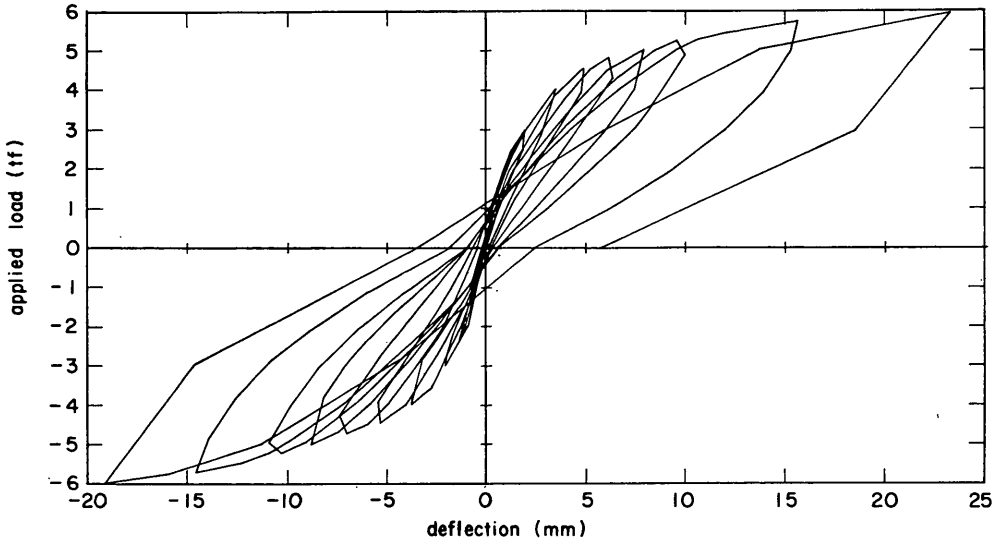

Fig. C9 Load-deflection curve (C-PB-16)

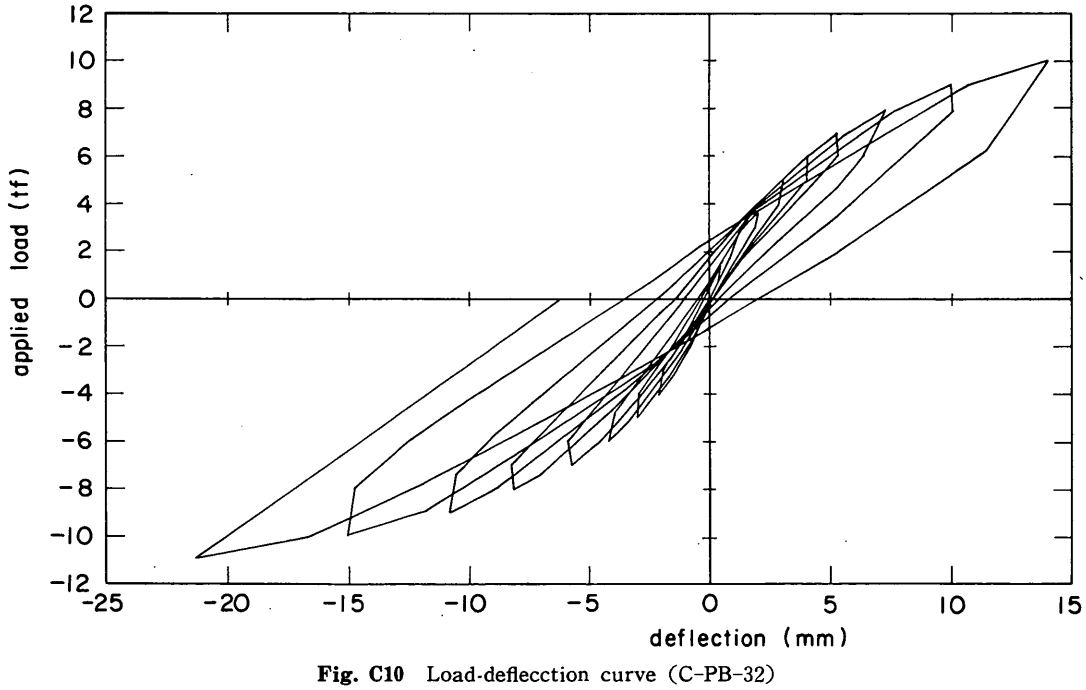

Fig. C10 Load-deflecction curve (C-PB-32)

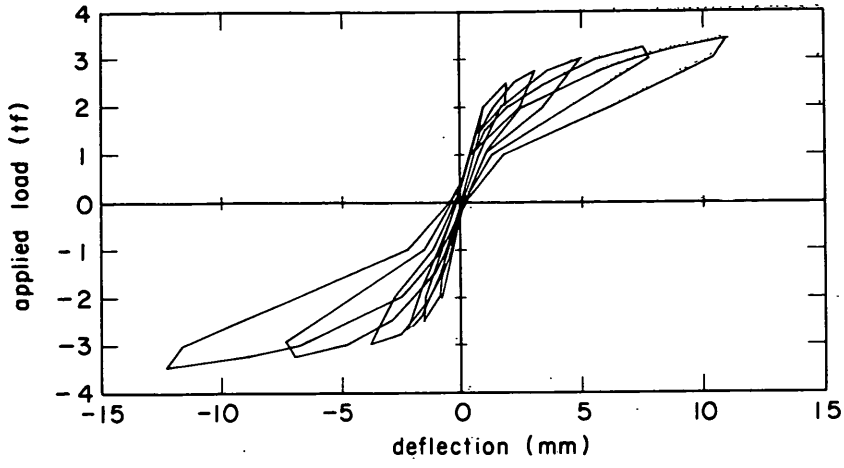

Fig. C11 Load-deflection curve (A-PB-16)

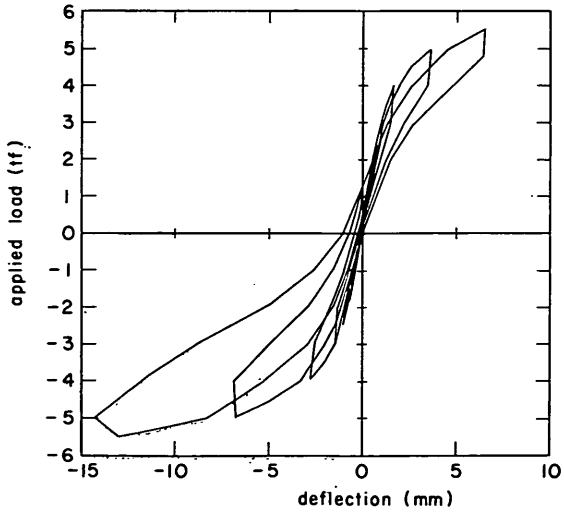

Fig. C12 Load-deflection curve (A-PB-32)

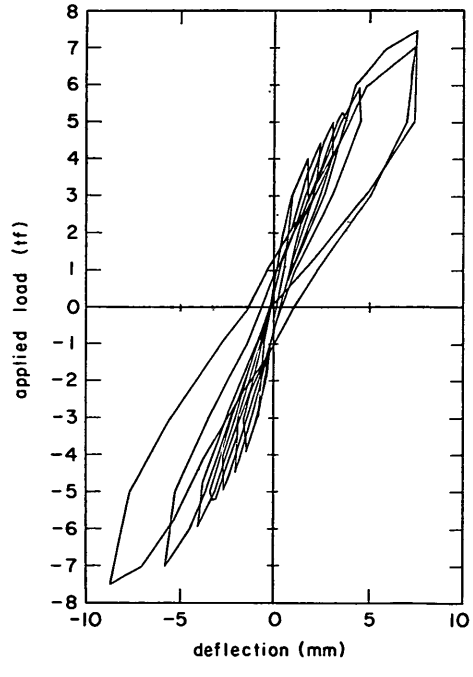

Fig. C13 Load-deflection curve (H-PB-16)

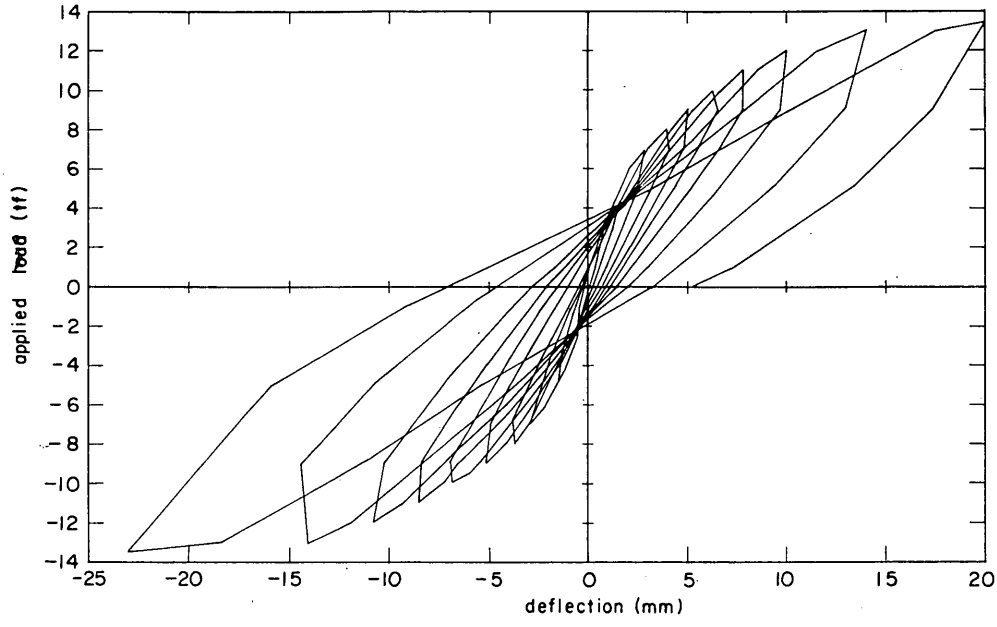

Fig. C14 Load-deflection curve (H-PB-32)

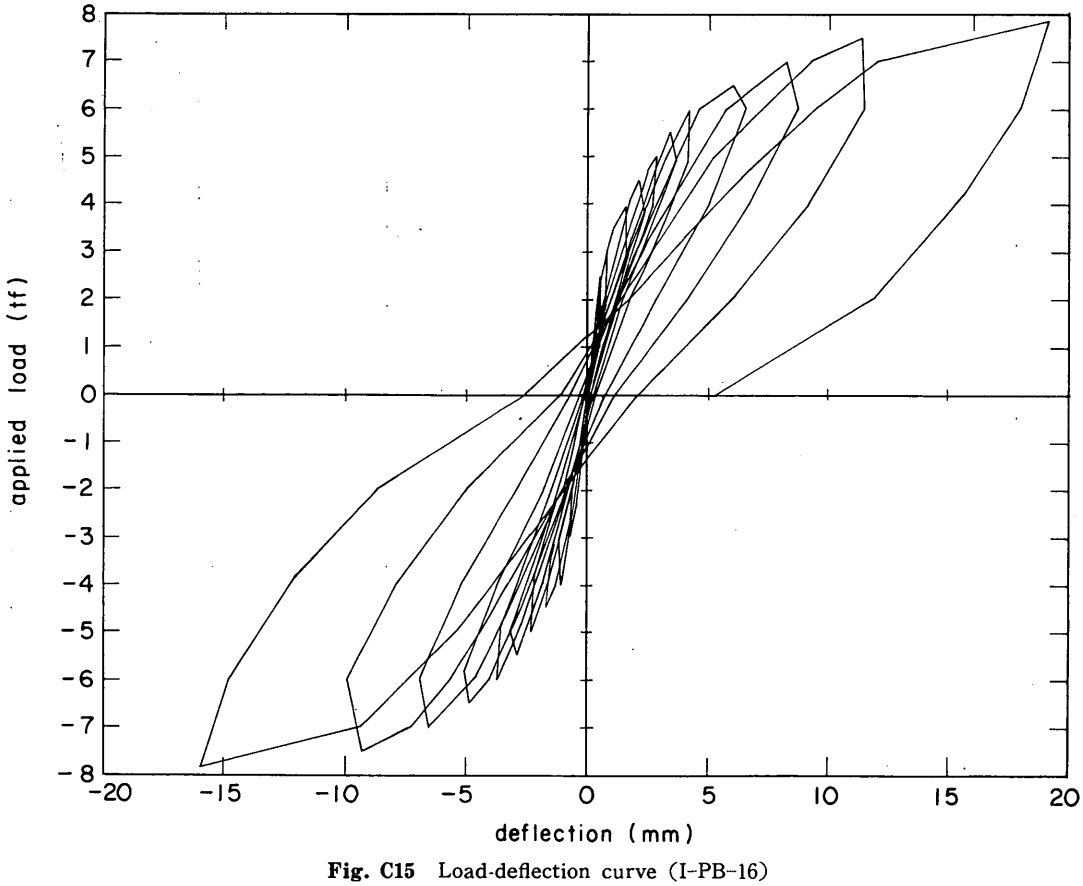

Fig. C15 Load-deflection curve (I-PB-16)

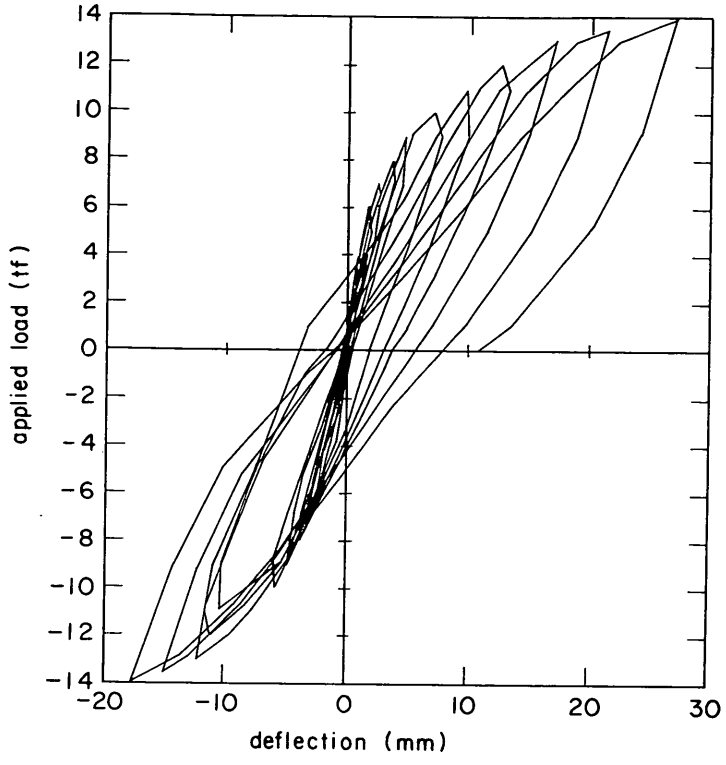

Fig. C16 Load-deflection curve (I-PB-32)

Appendix D. Deflected Shapes of the Specimen

Figures D1 through D6 show the deflected shapes of the column at the each applied load.

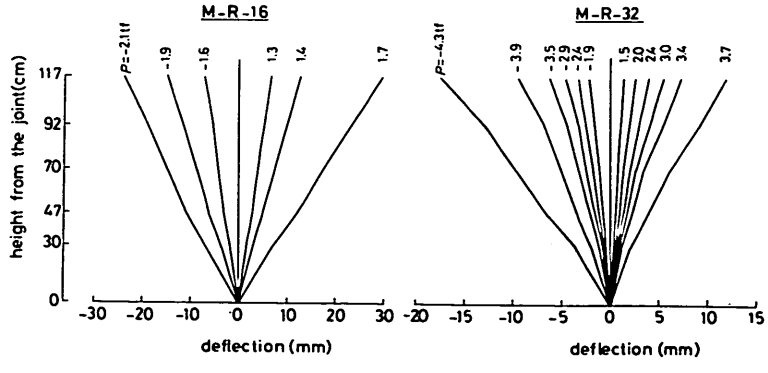

Fig. D1 Deflected shapes (M-R)

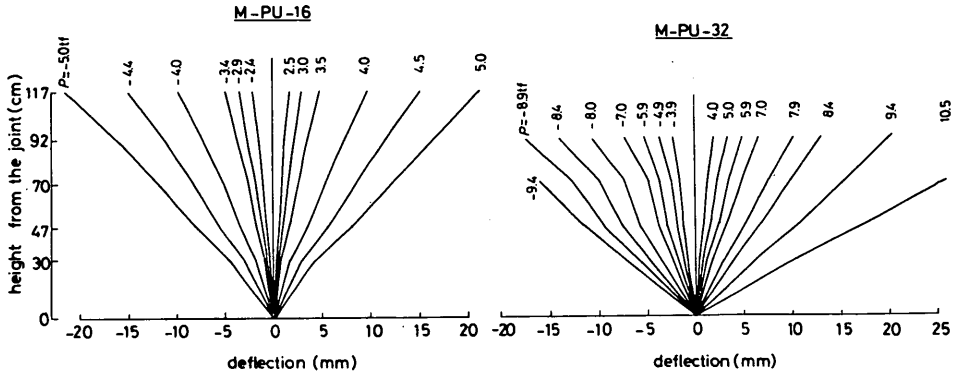

Fig. D2 Deflected shapes (M-PU)

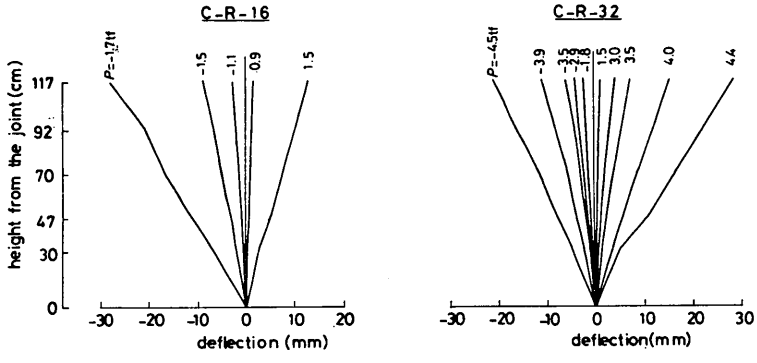

Fig. D3 Deflected shapes (C-R)

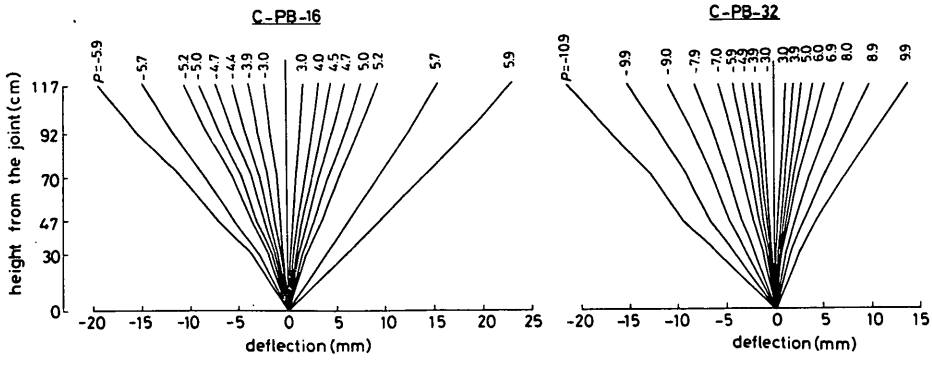

Fig. D4 Deflected shapes (C-PB)

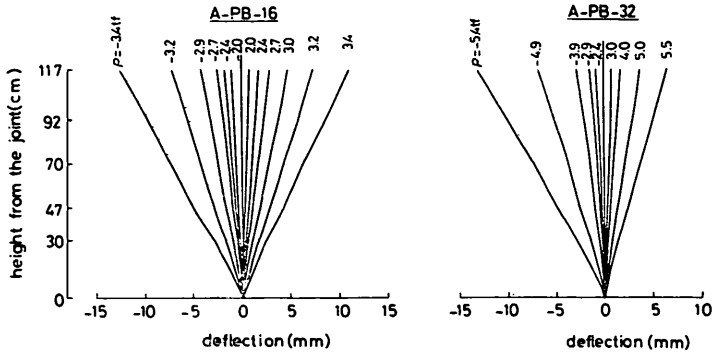

Fig. D5 Deflected shapes (A-PB)

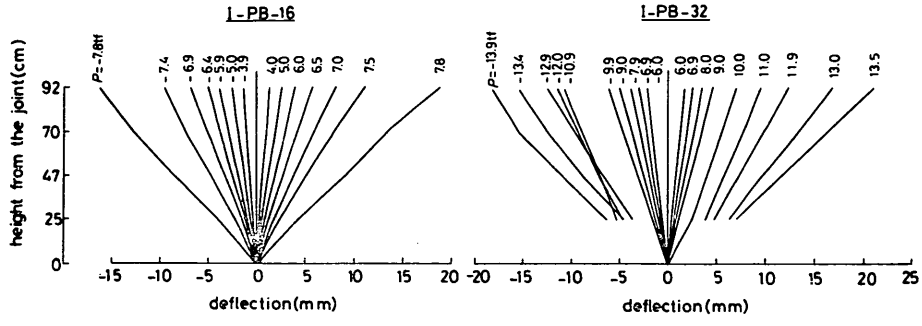

Fig. D6 Deflected shapes (I-PB)

Appendix E. Variation of Crack Width

The variations of crack widths of the specimens with the lower reinforcement ratio are shown in Figs. E1 and E2.

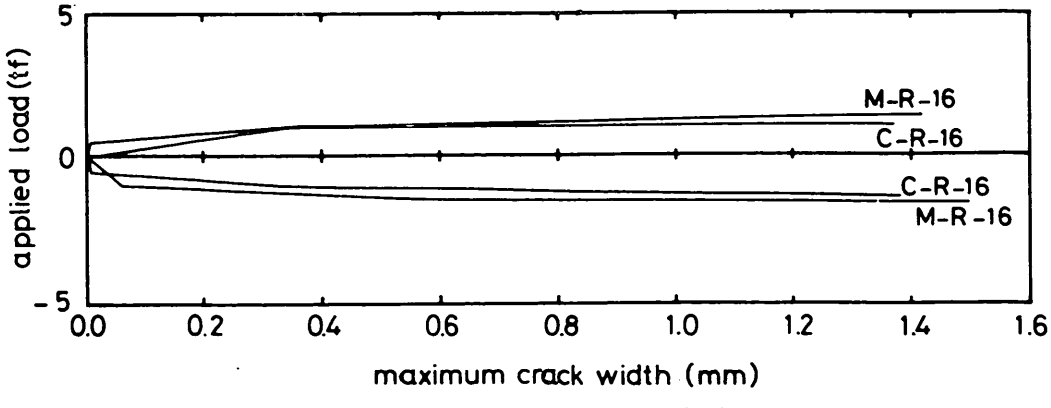

Fig. E1 Variation of crack width (RC)

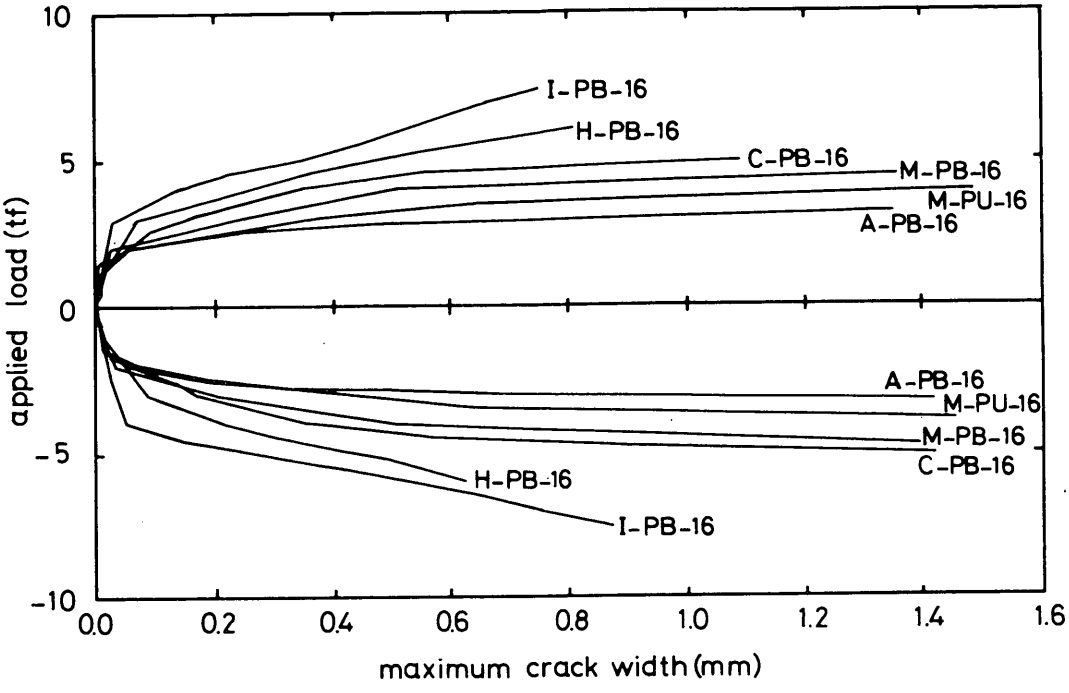

Fig. E2 Variation of crack width (PC)

Appendix F. Distribution of Concrete Strain

The distributions of concrete strain on the column are shown in Fig. F1 through F5.

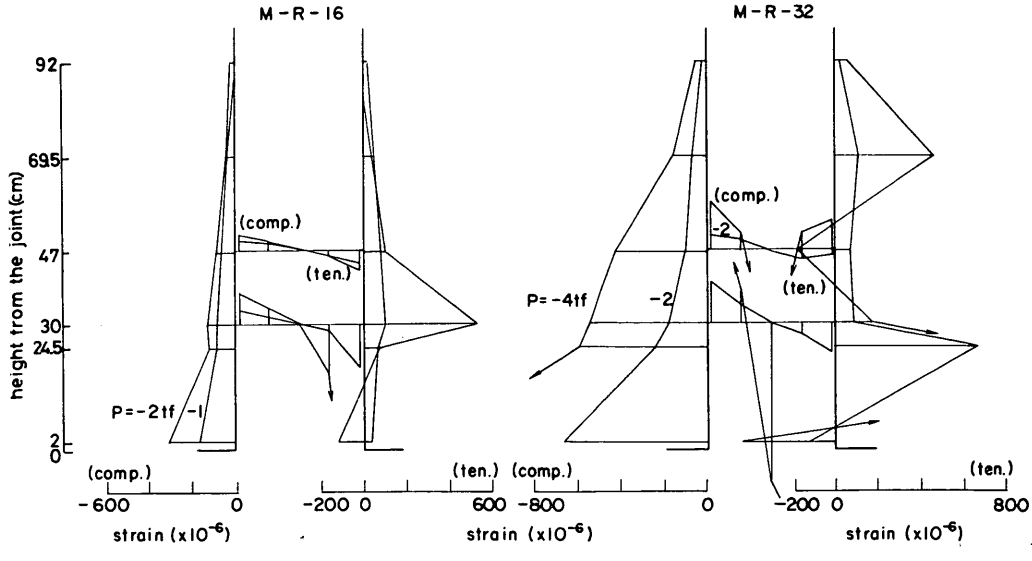

Fig. F1 Distribution of strain on concrete (M-R)

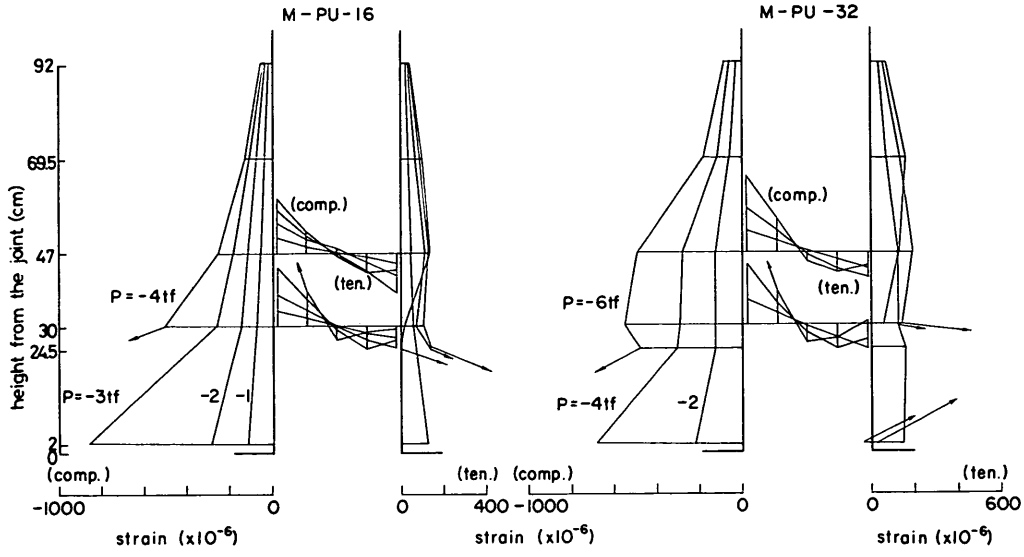

Fig. F2 Distribution of strain on concrete (M-PU)

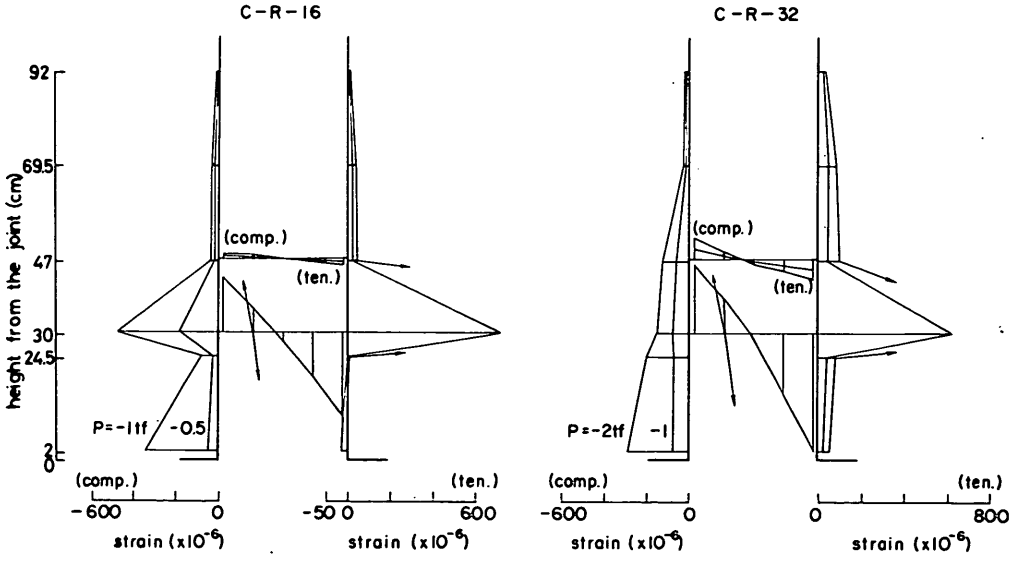

Fig. F3 Distribution of strain on concrete (C-R)

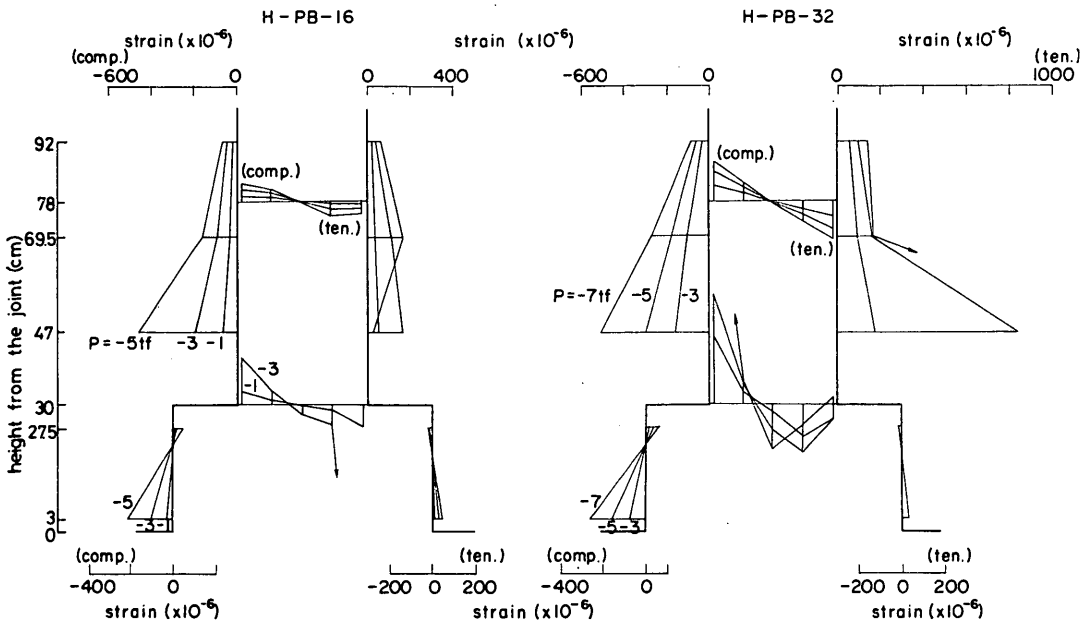

Fig. F4 Distribution of strain on concrete (H-PB)

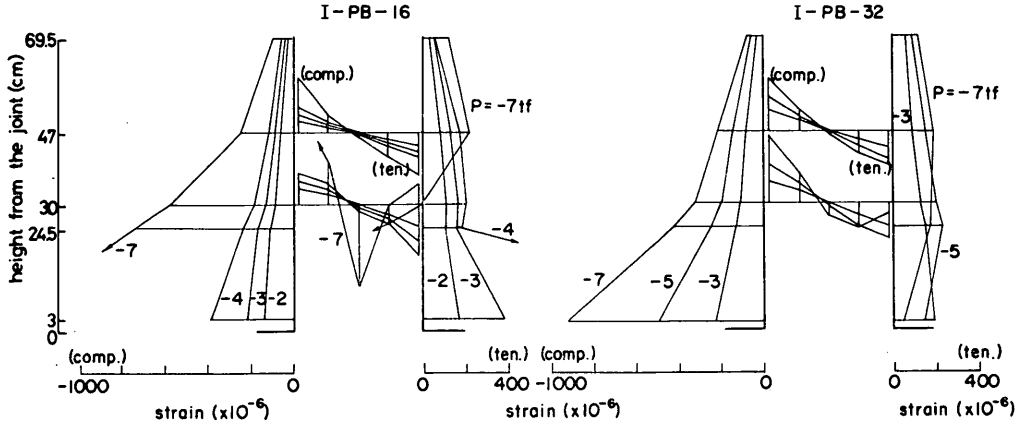

Fig. F5 Distribution of strain on concrete (I-PB)